NASA TECHNICAL MEMORANDUM

NASA TM X-1789

TRANSONIC AERODYNAMIC CHARACTERISTICS OF HYPERSONIC LOW-WAVE-DRAG ELLIPTICAL-BODY—TAIL COMBINATIONS AS AFFECTED BY CHANGES IN STABILIZER CONFIGURATION

by Charles H. Fox, Jr., and Bernard Spencer, Jr.

Langley Research Center

Langley Station, Hampton, Va.

NATIONAL AERONAUTICS AND SPACE ADMINISTRATION • WASHINGTON, D. C. • MAY 1969

NASA TM X-1789

TRANSONIC AERODYNAMIC CHARACTERISTICS OF HYPERSONIC LOW-WAVE-DRAG ELLIPTICAL-BODY—TAIL COMBINATIONS AS AFFECTED BY CHANGES IN STABILIZER CONFIGURATION

By Charles H. Fox, Jr., and Bernard Spencer, Jr.

Langley Research Center
Langley Station, Hampton, Va.

NATIONAL AERONAUTICS AND SPACE ADMINISTRATION

For sale by the Clearinghouse for Federal Scientific and Technical Information
Springfield, Virginia 22151 – CFSTI price $3.00

TRANSONIC AERODYNAMIC CHARACTERISTICS OF HYPERSONIC LOW-WAVE-DRAG ELLIPTICAL-BODY—TAIL COMBINATIONS AS AFFECTED BY CHANGES IN STABILIZER CONFIGURATION

By Charles H. Fox, Jr., and Bernard Spencer, Jr.
Langley Research Center

SUMMARY

The present investigation represents part of a generalized study to determine parametrically the effects of the addition of stabilizing surfaces on both stability and performance in the range from hypersonic to subsonic speeds for a certain class of lifting bodies which have exhibited hypersonic lift-drag ratios in excess of 3.0.

An investigation has been made in the Langley high-speed 7- by 10-foot tunnel at Mach numbers of 0.89, 0.95, and 1.17 to determine systematically the effects of various combinations of outboard-stabilizer and vertical-tail configurations on the longitudinal and lateral-directional stability and the aerodynamic performance of an elliptical hypersonic low-wave-drag body. The longitudinal area distribution of the body conformed to the theoretical shape required to minimize the zero-lift hypersonic pressure drag under the geometric constraints of given length and volume. The body had an elliptical cross section with a semiaxis ratio of 2 (major axis horizontal) and had an equivalent fineness ratio of 6.14. Base-mounted outboard stabilizers were tested at various dihedral angles alone and in combination with either a single center-line vertical tail or with a vee-tail. The angle of attack was varied from approximately -4° to 18° at sideslip angles of 0° and -5°.

The results of the study indicate that the maximum untrimmed lift-drag ratio is improved considerably by the addition of the outboard stabilizers. The resultant performance is, however, sensitive to changes in the stabilizer dihedral for a given tail configuration. With the moment reference center at 55 percent of the body length, the stabilizers at positive dihedral angles provide a more positive pitching moment at zero angle of attack, less stability, and less out-of-trim moment at maximum lift-drag ratio than the stabilizers at negative dihedral angles. In addition, the directional-stability parameter at maximum lift-drag ratio varies nonlinearly with stabilizer dihedral angle.

INTRODUCTION

In recent experimental investigations, methods of improving the hypersonic aerodynamic performance of a certain class of lifting-body shapes have been studied by examining the effects of variations in both longitudinal contour and cross-sectional shape. (See refs. 1 and 2.) Results of these parametric studies have indicated that bodies with elliptical cross sections designed to minimize pressure drag at hypersonic speeds can yield significantly better hypersonic aerodynamic performance than conical bodies with circular cross sections (ref. 1). In addition, results of systematic studies made on these body shapes from hypersonic to low subsonic speeds indicate that in the speed range below hypersonic the optimum hypersonic bodies exhibit performance characteristics higher than or as high as those of any other configuration tested. (See refs. 3 and 4.) These studies, however, were primarily concerned with the aerodynamic performance of lifting bodies and no attempt was made to examine methods of providing stability or to investigate the effects of adding stabilizing surfaces on the overall aerodynamic characteristics of these configurations. Therefore, a systematic study has been initiated to examine the effects of the addition and location of stabilizing surfaces on the overall aerodynamic characteristics of a particular member of the family of bodies studied in references 1 to 4. The body selected has a fineness ratio of 6.14 and an elliptical cross section with a semiaxis ratio of 2 and the major axis horizontal.

The present investigation was made in the Langley high-speed 7- by 10-foot tunnel at Mach numbers of 0.89, 0.95, and 1.17. The hypersonic aerodynamic characteristics of the same configurations are given in reference 5.

SYMBOLS

Longitudinal data are referred to the stability-axis system and lateral-directional data are referred to the body-axis system. All coefficients are normalized with respect to the projected planform area, length, and span of the body. The moment reference point was on the body center line at 55 percent body length.

A_b base area of body, ft^2 (m^2)

a semimajor axis of ellipse at base of body (semispan of body), ft (m)

b semiminor axis of ellipse at base of body (one-half the base height of body), ft (m)

C_D drag coefficient, Drag/qS

$C_{D,min}$ minimum drag coefficient

C_L lift coefficient, Lift/qS

C_{L_α} lift-curve slope, $\partial C_L / \partial \alpha$ at $\alpha \approx 0^o$, per degree

C_l rolling-moment coefficient, $\frac{\text{Rolling moment}}{2aqS}$

C_{l_β} lateral-stability parameter, $\Delta C_l / \Delta \beta$ at $\beta = 0^o$ and -5^o, per degree

C_m pitching-moment coefficient, $\frac{\text{Pitching moment}}{qSl}$

$C_{m,o}$ pitching-moment coefficient at $\alpha = 0^o$

C_N normal-force coefficient, $\frac{\text{Normal force}}{qS}$

C_n yawing-moment coefficient, $\frac{\text{Yawing moment}}{2aqS}$

C_{n_β} directional-stability parameter, $\Delta C_n / \Delta \beta$ at $\beta = 0^o$ and -5^o, per degree

C_Y side-force coefficient, $\frac{\text{Side force}}{qS}$

C_{Y_β} side-force parameter, $\Delta C_Y / \Delta \beta$ at $\beta = 0^o$ and -5^o, per degree

f equivalent fineness ratio, $\frac{l}{2\sqrt{ab}}$

L/D lift-drag ratio

$(L/D)_{max}$ maximum lift-drag ratio

l length of body, ft (m)

M Mach number

$\Delta p/q$ pressure coefficient at model base, $\frac{p - p_\infty}{q}$

p_∞ free-stream static pressure, lb/ft^2 (N/m^2)

p base pressure, lb/ft^2 (N/m^2)

q dynamic pressure, lb/ft^2 (N/m^2)

S projected planform area of body, ft^2 (m^2)

S_t exposed planform area of stabilizers or tails normal to the surface, ft^2 (m^2)

S_{wet} wetted area of body, ft^2 (m^2)

x_{cp}/l center-of-pressure location as fraction of body length, $0.55 - \left(\frac{\partial C_m}{\partial C_N}\right)_{\alpha \approx 0^o}$

α angle of attack, deg

β angle of sideslip, deg

Γ_s stabilizer dihedral angle, deg; the axis of rotation is a line parallel to the body longitudinal axis and passing through the semimajor axis at the point defined as the semispan of the body minus one-half of the root base thickness of the stabilizer (fig. 1)

θ_v tail dihedral angle, deg; the axis of rotation is the body longitudinal axis (fig. 1)

Subscript:

$(L/D)_{max}$ at maximum lift-drag ratio

MODELS

The longitudinal area distribution of the body used in the present investigation conformed to the theoretical shape required to minimize the zero-lift hypersonic pressure drag under the geometric constraints of given length and volume (ref. 1). The body had an elliptical cross section with a semiaxis ratio of 2 (major axis horizontal) and had an equivalent fineness ratio of 6.14.

The following configurations were investigated:

(a) Body alone (data were obtained from ref. 3)

(b) Body in combination with outboard stabilizers in the dihedral range Γ_s from -90^o to 90^o

(c) Body in combination with center-line vertical tail ($\theta_V = 90^o$) and the outboard stabilizers in the dihedral range Γ_S from -90^o to 90^o

(d) Body in combination with vee-tail ($\theta_V = 30^o$) and the outboard stabilizers in the dihedral range Γ_S from -90^o to 0^o

The pertinent geometric constants are given in the following table:

a/l	0.115
f	6.14
l	1.666 ft (0.5080 m)
S/l^2	0.1504
S_{wet}/l^2	0.362
A_b/l^2	0.0208
S_t/S for $\theta_V = 90^o$	0.0715
S_t/S for $\theta_V = 30^o$	0.143
S_t/S for any value of Γ_S	0.143

APPARATUS, TESTS, AND CORRECTIONS

The present investigation was made in the Langley high-speed 7- by 10-foot tunnel at Mach numbers of 0.89, 0.95, and 1.17, corresponding to average test Reynolds numbers (based on body length) of 7.17, 7.18, and 6.92×10^6, respectively. Forces and moments were measured with a sting-supported internally mounted six-component strain-gage balance. The angle of attack was varied from approximately -4^o to 18^o at sideslip angles of 0^o and -5^o. The angle of attack has been corrected for sting and balance deflections under load. Base pressure measurements were taken and are presented in the form of $\Delta p/q$ as a function of angle of attack in figure 2. However, the drag data presented represent gross drag in that no correction for the effects of base pressure have been made. The base of the model was made concave in an effort to obtain a uniform pressure over the base. No attempt has been made to correct the drag data for the effects of the sting support; however, the ratio of sting diameter to equivalent base diameter was made small (0.08) in an effort to minimize these effects. Support interference effects on various types of base configurations are shown in references 6, 7, and 8.

A strip of No. 60 grit 0.1 inch (2.5 mm) wide was located in a circumferential band around the body 1.25 inches (31.7 mm) from the body apex. In addition, a strip of No. 60 grit 0.1 inch (2.5 mm) wide was located 0.15 inch (3.8 mm) from the leading edge of all tail and stabilizer surfaces.

The lateral and directional stability parameters C_{l_β}, C_{n_β}, and C_{Y_β} have been computed from data obtained at sideslip angles of 0^o and -5^o, and therefore do not account for any nonlinearities which may exist in the intermediate sideslip range.

RESULTS

The basic longitudinal aerodynamic characteristics and summary lateral-directional results obtained for each configuration and Mach number are presented in the following figures:

DISCUSSION

Performance Characteristics

Figure 3 presents a comparison of the longitudinal characteristics for configurations of the present investigation having $\Gamma_S = 0^o$, with and without vertical tails, and data for the body alone obtained from reference 3. The addition of the outboard stabilizers at $\Gamma_S = 0^o$ resulted in considerable improvement in untrimmed $(L/D)_{max}$ at these transonic Mach numbers. This result is in contrast to the loss in $(L/D)_{max}$ due to the addition of the outboard stabilizers at $M = 10.03$. (See ref. 5.) Figure 9 shows that untrimmed $(L/D)_{max}$ values for the configurations with the outboard stabilizers at $\Gamma_S = 0^o$ generally are as high as, or higher than, those for the configurations with stabilizers at other angles. This value of Γ_S represents the greatest span for a given wetted area. The configurations with $\Gamma_S = -30^o$ had $(L/D)_{max}$ values equal to those for the configurations with $\Gamma_S = 0^o$, but a general loss in $(L/D)_{max}$ occurred with increasing

magnitude of Γ_S (Γ_S positive or negative) due to a loss in lift-curve slope which resulted primarily from a decrease in span.

As expected, the addition of the vertical tail ($\theta_V = 90^o$) resulted in a constant incremental loss in $(L/D)_{max}$ at all Mach numbers and for all configurations tested, because of the increased drag. (See figs. 6, 7, and 9.) The addition of the vee-tails ($\theta_V = 30^o$), while increasing the lift-curve slope for the $\Gamma_S = 0^o$ configuration, also resulted in losses in $(L/D)_{max}$ due to the large increases in drag. For the configuration with vee-tails, as Γ_S was increased from 0^o to -90^o the loss in $(L/D)_{max}$ was considerably less than that noted for the configuration without vee-tails. This results from the improved lift of the vee-tail configuration. (See figs. 8 and 9.)

Longitudinal Stability

For the selected moment reference, the body alone is approximately neutrally stable at all Mach numbers (fig. 3). The addition of the outboard stabilizers ($\Gamma_S = 0^o$) resulted in considerable aft movement of the longitudinal center of pressure and rather high values of stability.

Increasing the magnitude of the dihedral angle decreased the stability of the configuration. (See figs. 4 and 5.) The stabilizers at positive dihedral angles result in more positive $C_{m,o}$ and less out-of-trim moment at angles of attack near $(L/D)_{max}$ than the stabilizers at negative dihedral angles. (See figs. 4, 5, and 9.) In addition, increasing the Mach number results in large increases in the stability of a configuration with negative Γ_S. For positive Γ_S, the increases in stability with increasing Mach number are considerably less.

The addition of the vertical tail ($\theta_V = 90^o$) to the body-stabilizer configurations had little or no effect on the longitudinal stability trends associated with variation in stabilizer dihedral angle, as would be expected, and the drag of the vertical tail acting above the moment reference had a small favorable effect in that it increased $C_{m,o}$ as compared with the configurations with vertical tail off. (See figs. 6 and 7.) The addition of the vee-tail resulted in large increases in stability (fig. 8), and varying the dihedral angle of the outboard stabilizers from $\Gamma_S = 0^o$ to $\Gamma_S = -60^o$ (for $\theta_V = 30^o$) had little effect on stability level. The stabilizers at $\Gamma_S = -90^o$ did, however, show a significant destabilizing effect. (See fig. 8.)

The $(L/D)_{max}$ and $C_{m_{(L/D)_{max}}}$ values are summarized in figure 9. The values of $C_{m_{(L/D)_{max}}}$ are presented to show the variation of out-of-trim moments with dihedral angle. The values of $(L/D)_{max}$ are not shown for those configurations for which the maximum test angle of attack did not permit the accurate determination of $(L/D)_{max}$.

With the selected moment reference point, at 55 percent body length, the maximum out-of-trim moment $C_{m_{(L/D)_{max}}}$ occurs in the region of $\Gamma_s = -30^o$ to $\Gamma_s = 0^o$. As the dihedral angle increases from $\Gamma_s = 0^o$ to $\Gamma_s = 90^o$, the out-of-trim moment decreases until the configuration with $\Gamma_s = 90^o$ is trimmed but unstable. (See fig. 9.) Because of their lower out-of-trim moments, the configurations with positive Γ_s would have much lower trim drag penalties than the corresponding configurations with negative Γ_s. For a given moment reference point the variation of C_m with α must be considered, as unstable tendencies may occur in the region of $(L/D)_{max}$ for a given dihedral angle.

Lateral-Directional Stability

The configuration with the outboard stabilizers at $\Gamma_s = 0^o$ and no vertical or vee-tails is directionally unstable at all Mach numbers. (See figs. 10 and 11.) Increasing the dihedral angle negatively results in a directionally stable configuration at the low to moderate angles of attack, but the configurations still show directional instability at the higher angles of attack. (See fig. 10.) The use of the outboard stabilizers at positive dihedral angles provides directional stability up to the highest test angles of attack. (See fig. 11.) The configurations without tails and with negative Γ_s are laterally unstable at low angles of attack (fig. 10); however, with positive Γ_s they have positive effective dihedral throughout the test angle-of-attack range (fig. 11). The latter configurations also show superior directional stability throughout the angle-of-attack range.

The lateral and directional stability characteristics after addition of the vertical tail, $\theta_v = 90^o$, are shown in figures 12 and 13. Increases in C_{n_β} are seen at low angles of attack, and the outboard stabilizers with positive dihedral angles provide higher values of C_{n_β} than those with negative dihedral angles. The addition of the vertical tail also increased positive effective dihedral $\left(-C_{l_\beta}\right)$ throughout the test angle-of-attack range for both the positive- and negative-dihedral stabilizers and reduced somewhat the region of lateral instability for the negative-dihedral stabilizers. With the vertical tail on or off, however, a rapid loss in directional stability occurred at the higher angles of attack for all configurations. Increasing the Mach number resulted in increased losses in directional stability at the highest test angles of attack for all configurations.

All configurations with $\theta_v = 30^o$ were directionally stable at all Mach numbers throughout the test angle-of-attack range. (See fig. 14.) In addition, these configurations exhibited positive effective dihedral $\left(-C_{l_\beta}\right)$ at positive angles of attack.

A summary of the lateral-directional stability characteristics at $(L/D)_{max}$ is presented in figure 15. All the configurations exhibited positive effective dihedral at $(L/D)_{max}$. Of the configurations without tails, those with $\Gamma_s = 0^o$ and -30^o are

directionally unstable at $(L/D)_{max}$ at all Mach numbers, and those with $\Gamma_s = -60^o$ and -90^o have approximately neutral stability at $M = 1.17$. The configurations with either the vertical tail or the vee-tail on are directionally stable for all stabilizer dihedral angles and test Mach numbers in the region of $(L/D)_{max}$. However, the directional-stability parameter $C_{n_{\beta(L/D)_{max}}}$ varies nonlinearly with Γ_s.

SUMMARY OF RESULTS

An investigation has been made in the Langley high-speed 7- by 10-foot tunnel at Mach numbers of 0.89, 0.95, and 1.17 to determine systematically the effects of various combinations of outboard stabilizer and vertical-tail configurations on the longitudinal and lateral-directional stability and the aerodynamic performance of an elliptical hypersonic low-wave-drag body. The results of the study are summarized as follows:

1. The addition of the outboard stabilizers at positive or negative dihedral angles from 0^o to 60^o improved the untrimmed maximum lift-drag ratio of the body, the largest increases being for 0^o or $\pm 30^o$ dihedral. Progressively increasing the dihedral from 0^o to $\pm 90^o$ resulted in losses in untrimmed maximum lift-drag ratio, as would be expected.

2. With the selected moment reference point of 55-percent body length, the configurations having outboard stabilizers at positive dihedral angles exhibited considerably less out-of-trim moment in the region of maximum lift-drag ratio than the configurations having stabilizers at corresponding negative dihedral angles.

3. In the region of maximum untrimmed lift-drag ratio, directional instabilities were present at all test Mach numbers for the configurations without tails and with stabilizers at dihedral angles of 0^o and -30^o. Addition of either the vertical tail or vee-tails results in directionally stable configurations for all outboard stabilizer dihedral angles. Positive effective dihedral was noted for all configurations in the region of maximum lift-drag ratio.

Langley Research Center,
National Aeronautics and Space Administration,
Langley Station, Hampton, Va., February 18, 1969,
722-01-00-02-23.

REFERENCES

1. Spencer, Bernard, Jr.; and Fox, Charles H., Jr.: Hypersonic Aerodynamic Performance of Minimum-Wave-Drag Bodies. NASA TR R-250, 1966.

2. Spencer, Bernard, Jr.: Hypersonic Aerodynamic Characteristics of Minimum-Wave-Drag Bodies Having Variations in Cross-Sectional Shape. NASA TN D-4079, 1967.

3. Spencer, Bernard, Jr.: Transonic Aerodynamic Characteristics of a Series of Related Bodies With Cross-Sectional Ellipticity. NASA TN D-3203, 1966.

4. Fournier, Roger H.; Spencer, Bernard, Jr.; and Corlett, William A.: Supersonic Aerodynamic Characteristics of a Series of Related Bodies With Cross-Sectional Ellipticity. NASA TN D-3539, 1966.

5. Fox, Charles H., Jr.; and Spencer, Bernard, Jr.: Hypersonic Aerodynamic Characteristics of Low-Wave-Drag Elliptical-Body—Tail Combinations as Affected by Changes in Stabilizer Configuration. NASA TM X-1620, 1968.

6. Love, Eugene S.: A Summary of Information on Support Interference at Transonic and Supersonic Speeds. NACA RM L53K12, 1954.

7. Cahn, Maurice S.: An Experimental Investigation of Sting-Support Effects on Drag and a Comparison With Jet Effects at Transonic Speeds. NACA Rep. 1353, 1958. (Supersedes NACA RM L56F18a.)

8. Stivers, Louis S., Jr.; and Levy, Lionel L., Jr.: Effects of Sting-Support Diameter on the Base Pressures of an Elliptic Cone at Mach Numbers From 0.60 to 1.40. NASA TN D-354, 1961.

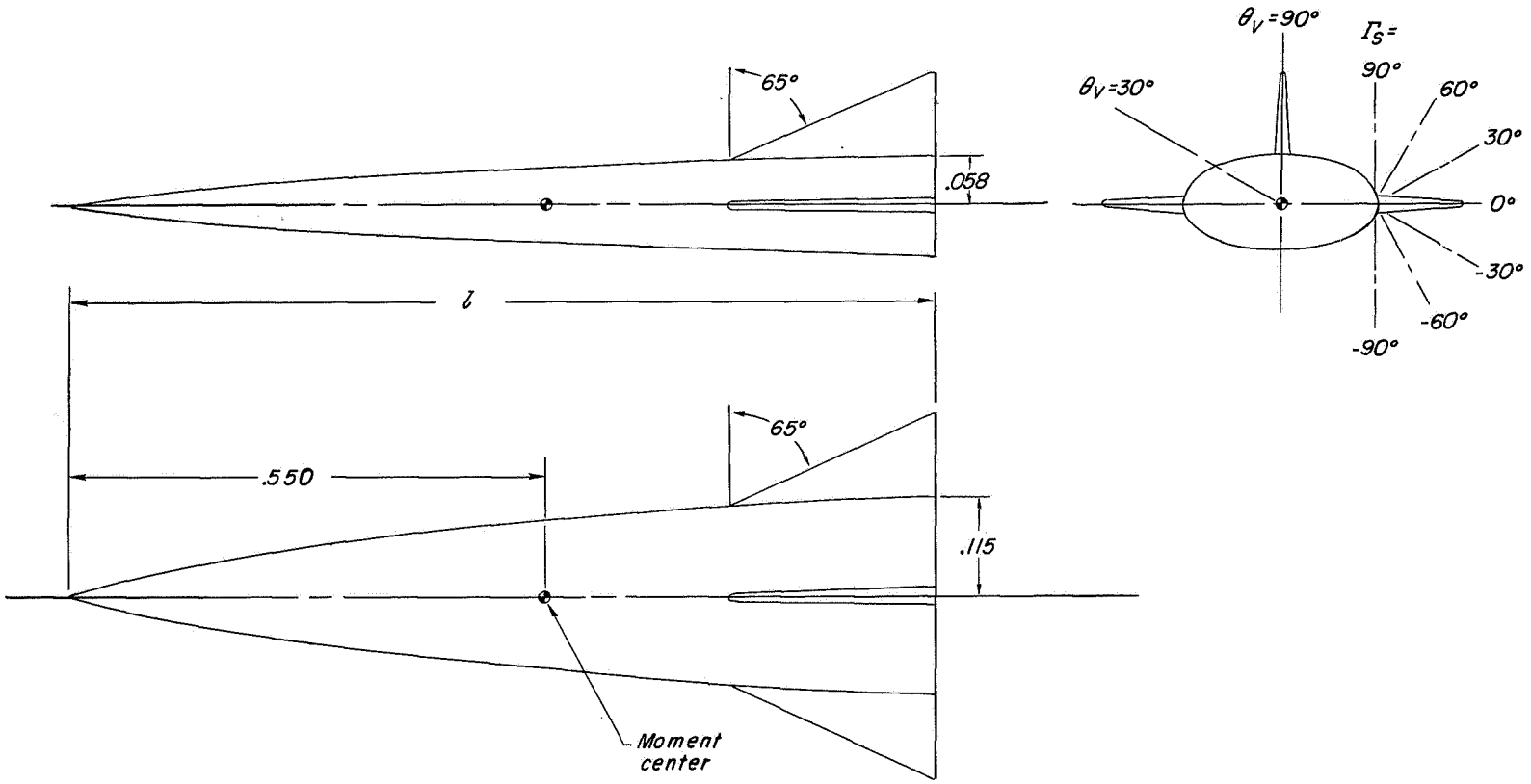

(a) General arrangement.

Figure 1.- Views of the models investigated. All dimensions are nondimensionalized with respect to body length.

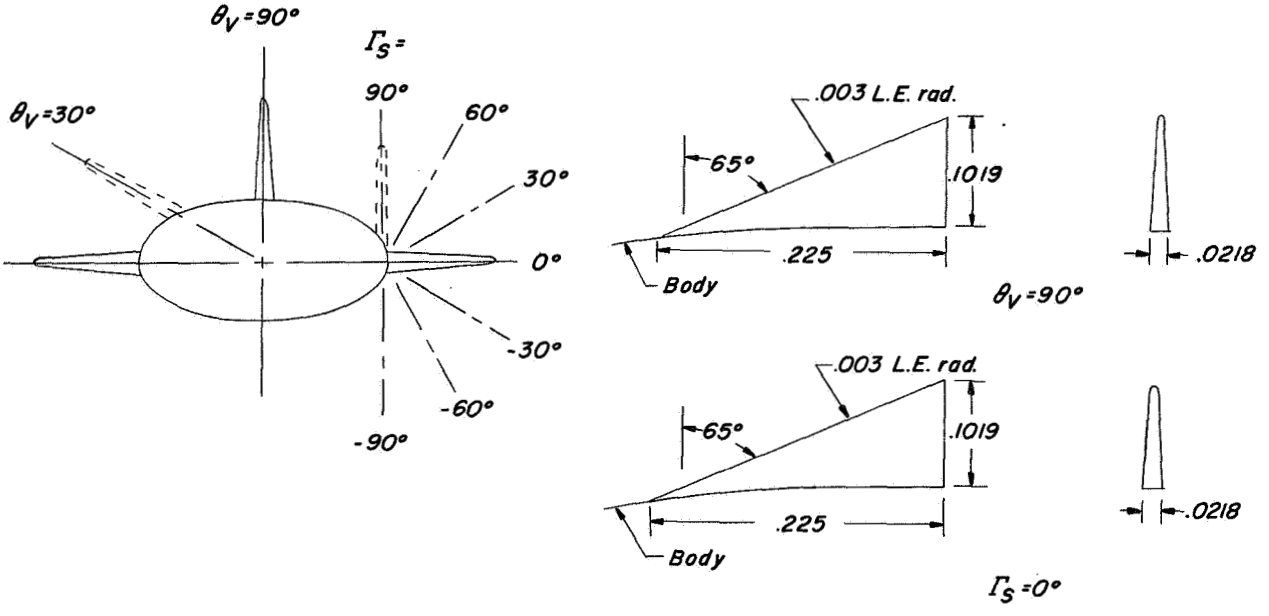

(b) Details of tails and stabilizers.

Figure 1.- Continued.

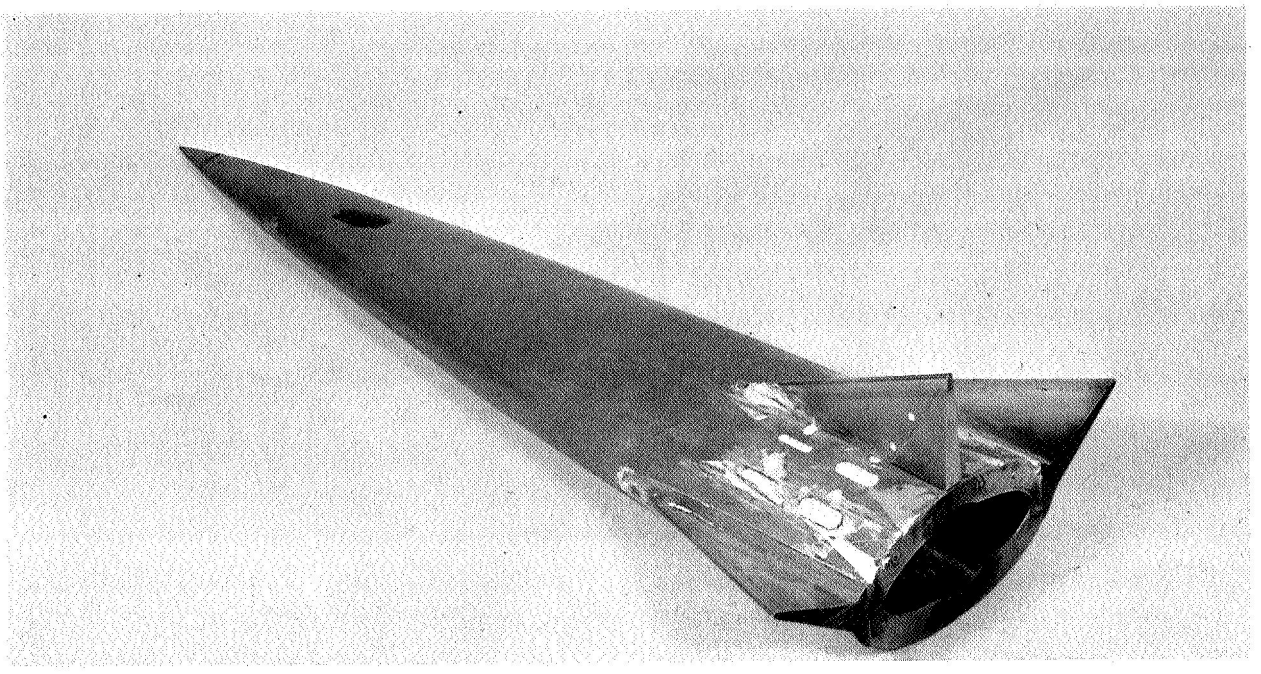

(c) One-quarter rear view of configuration with $\theta_V = 90^0$ and $\Gamma_S = 30^0$. L-67-4313

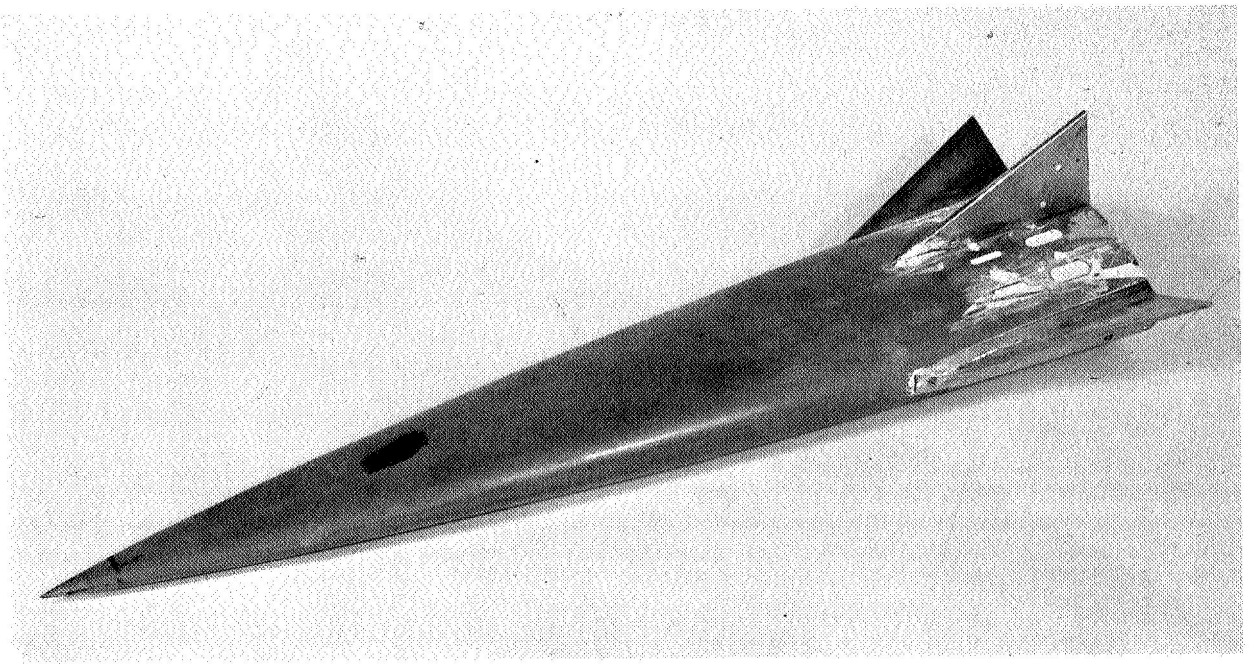

(d) Three-quarter front view of configuration with $\theta_V = 90^0$ and $\Gamma_S = 30^0$. L-67-4316

Figure 1.- Continued.

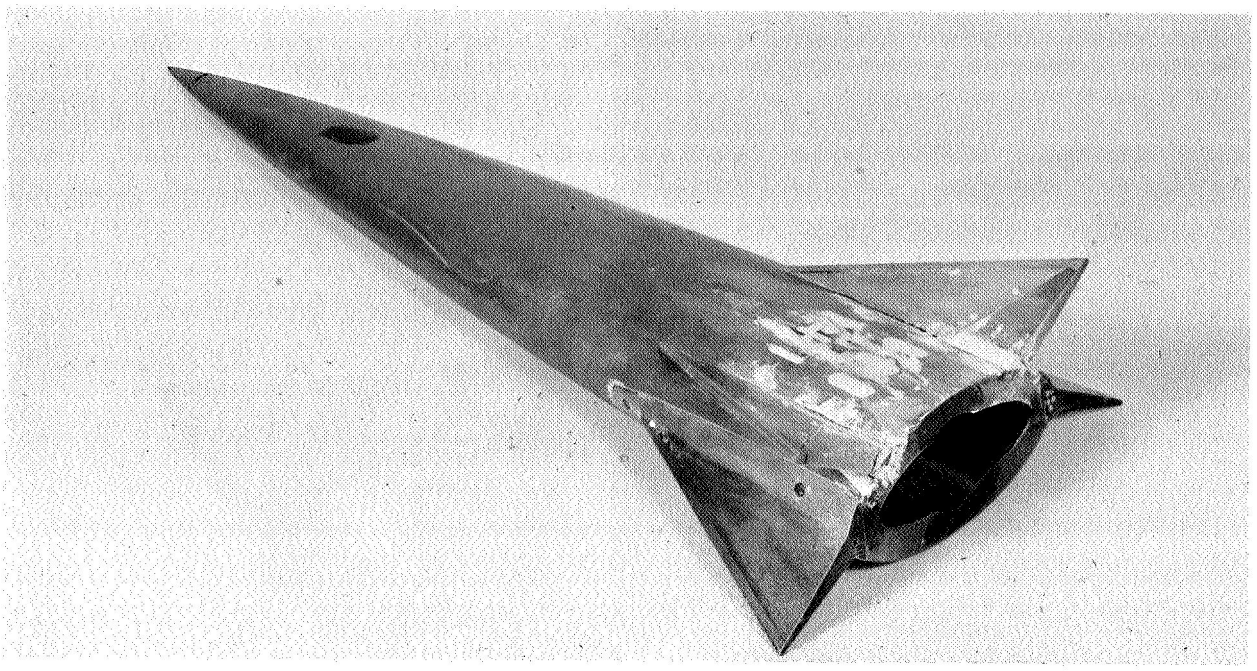

(e) One-quarter rear view of configuration with $\theta_v = 30^0$ and $\Gamma_s = -30^0$. L-67-4315

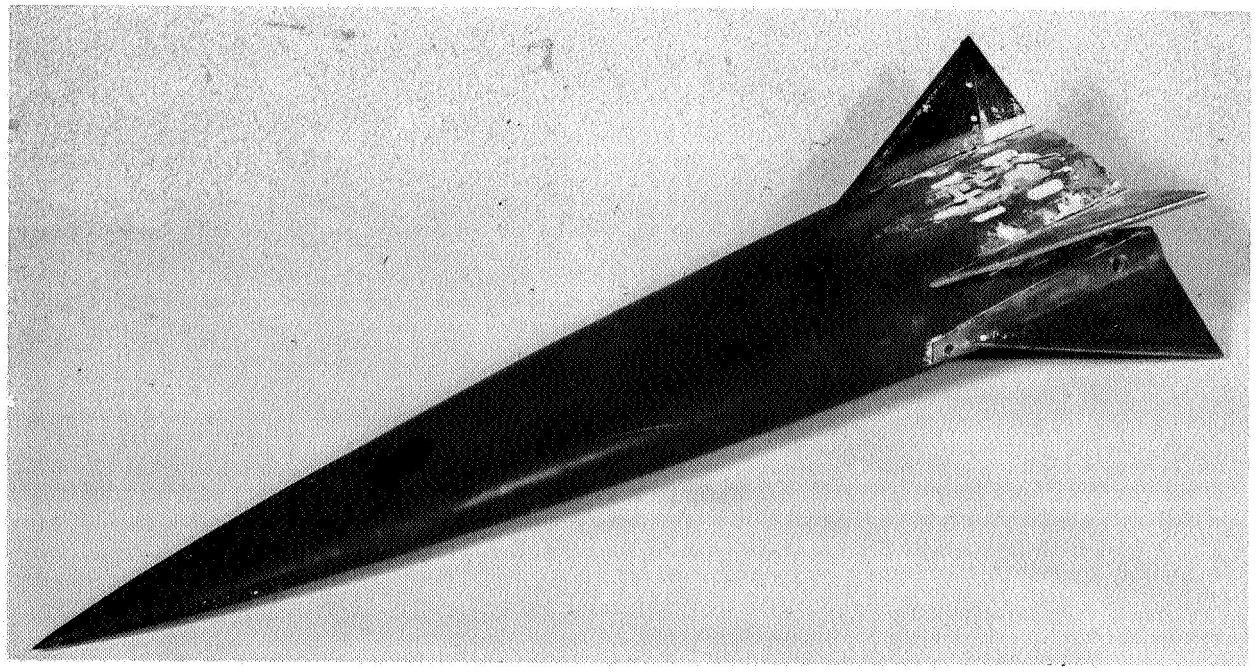

(f) Three-quarter front view of configuration with $\theta_v = 30^0$ and $\Gamma_s = -30^0$. L-67-4314

Figure 1.- Concluded.

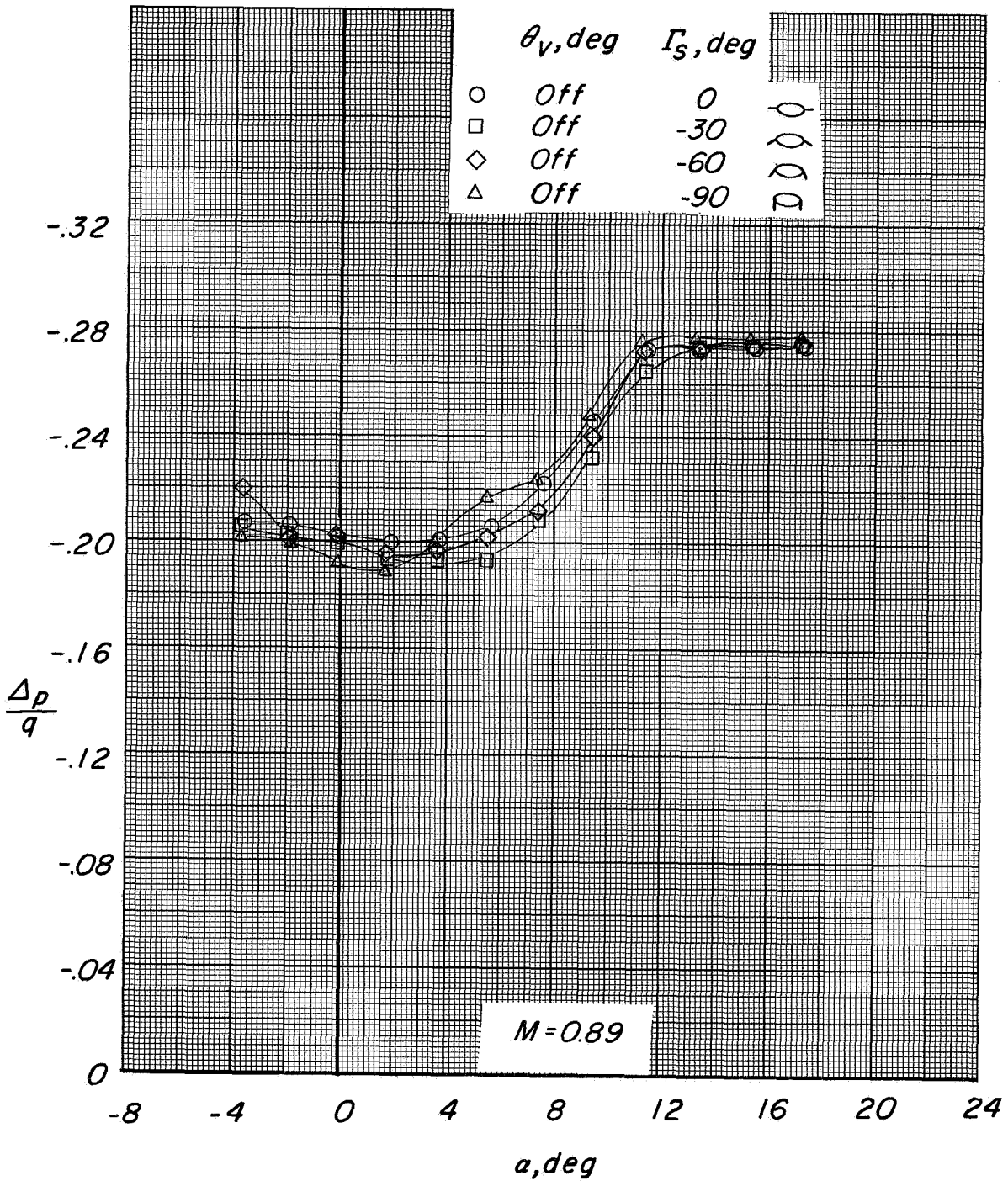

(a) Tails off; negative Γ_S.

Figure 2.- Base pressure characteristics of the various configurations at the three Mach numbers of the investigation.

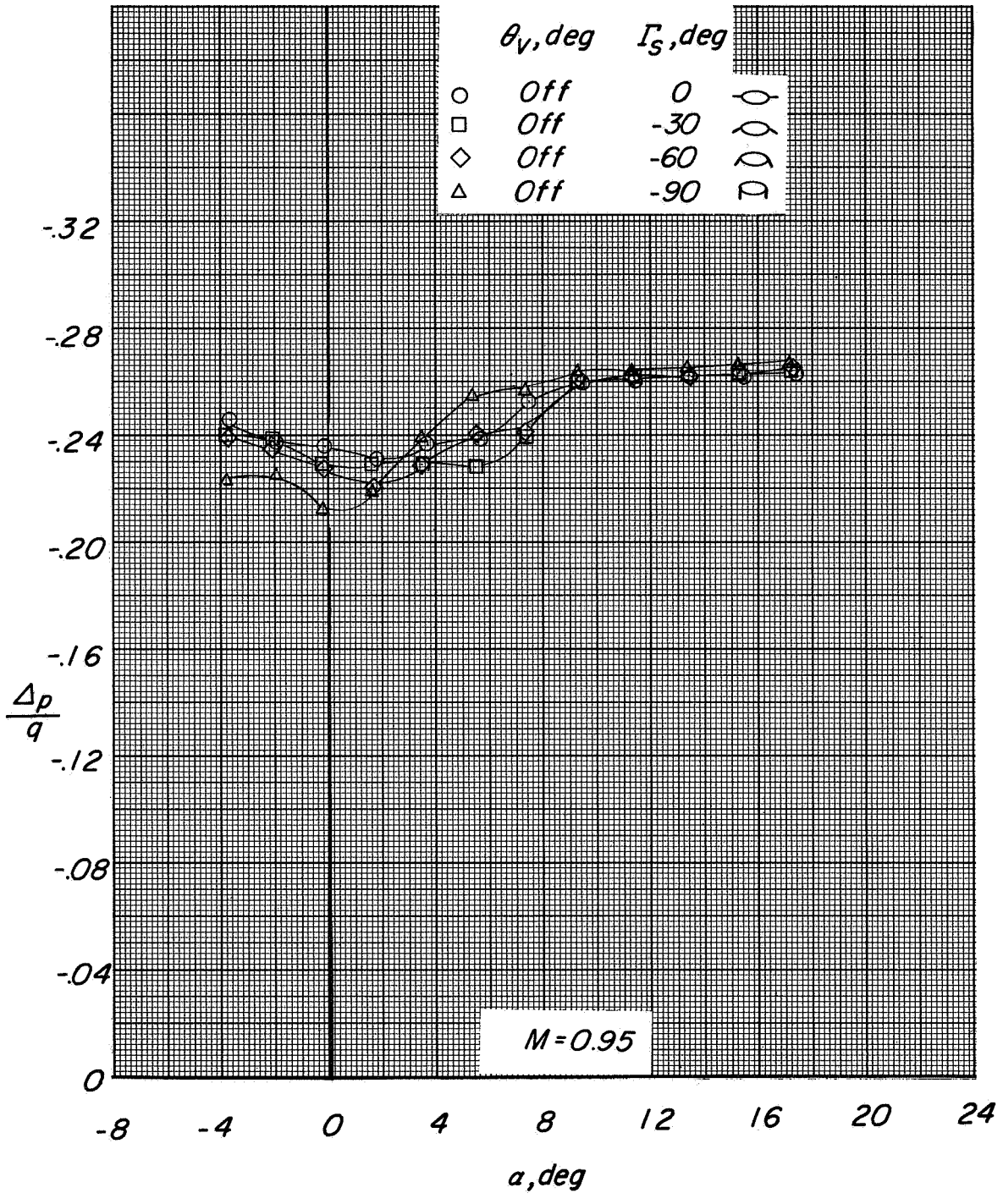

(a) Continued.

Figure 2.- Continued.

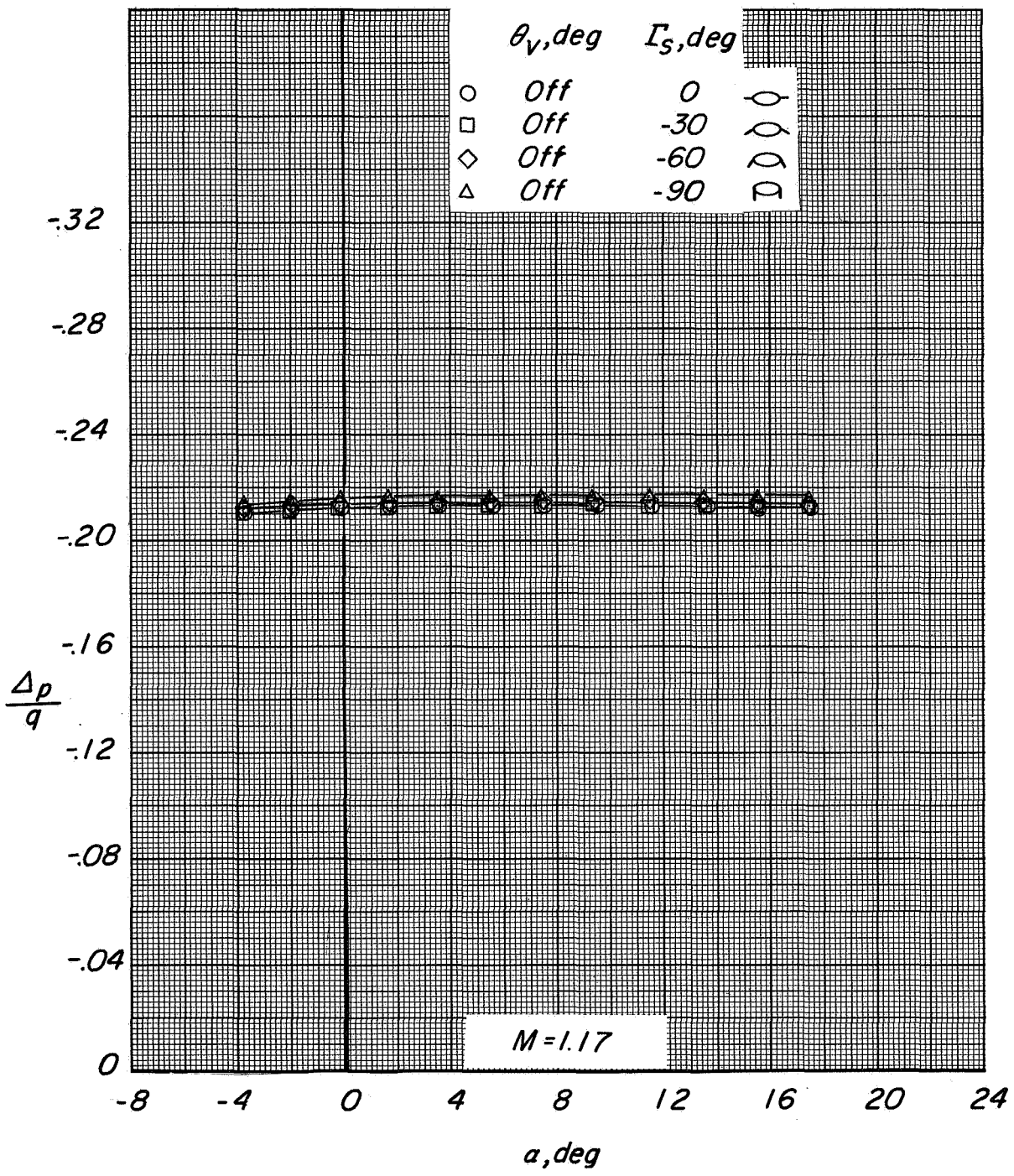

(a) Concluded.

Figure 2.- Continued.

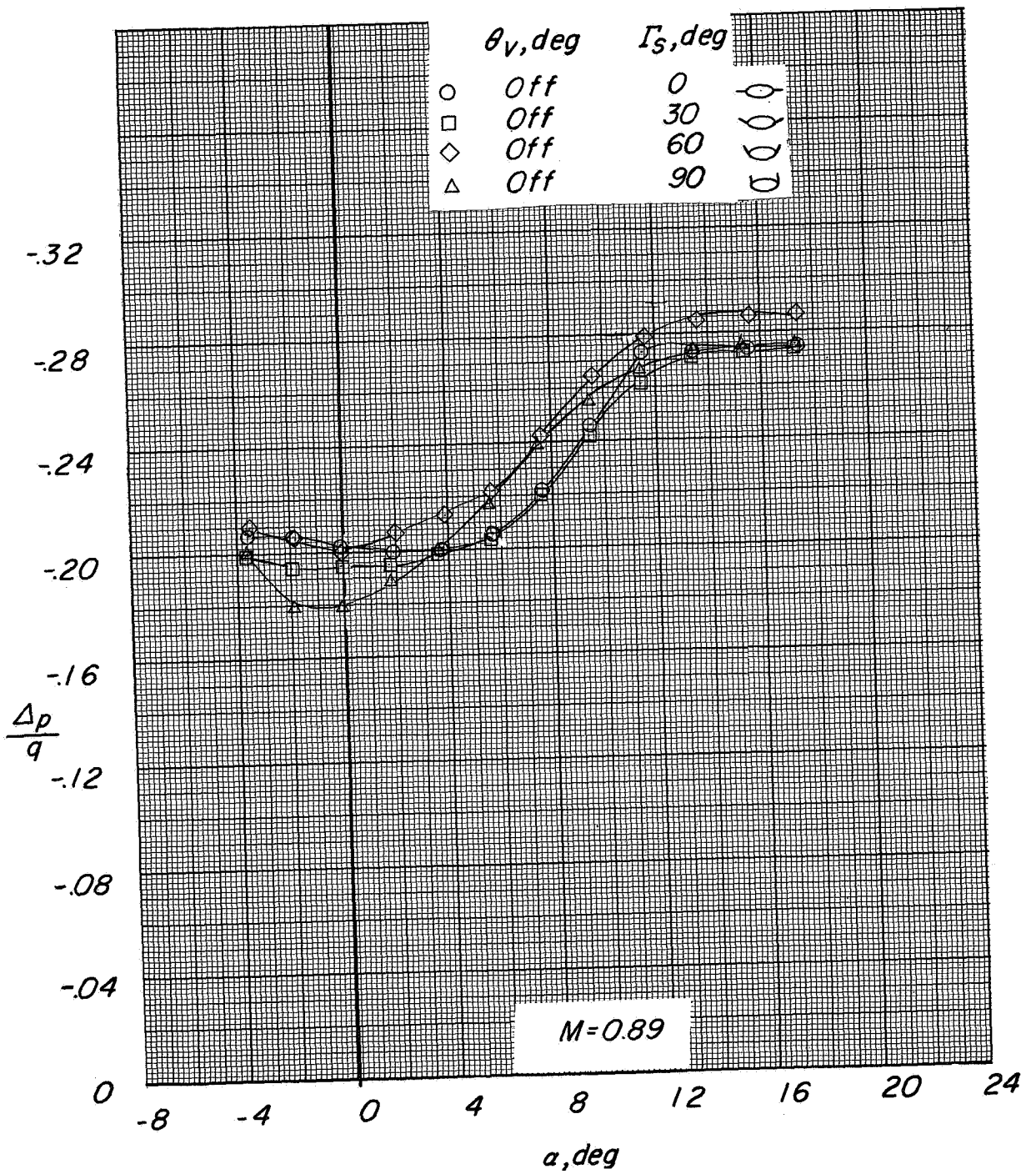

(b) Tails off; positive Γ_S.

Figure 2.- Continued.

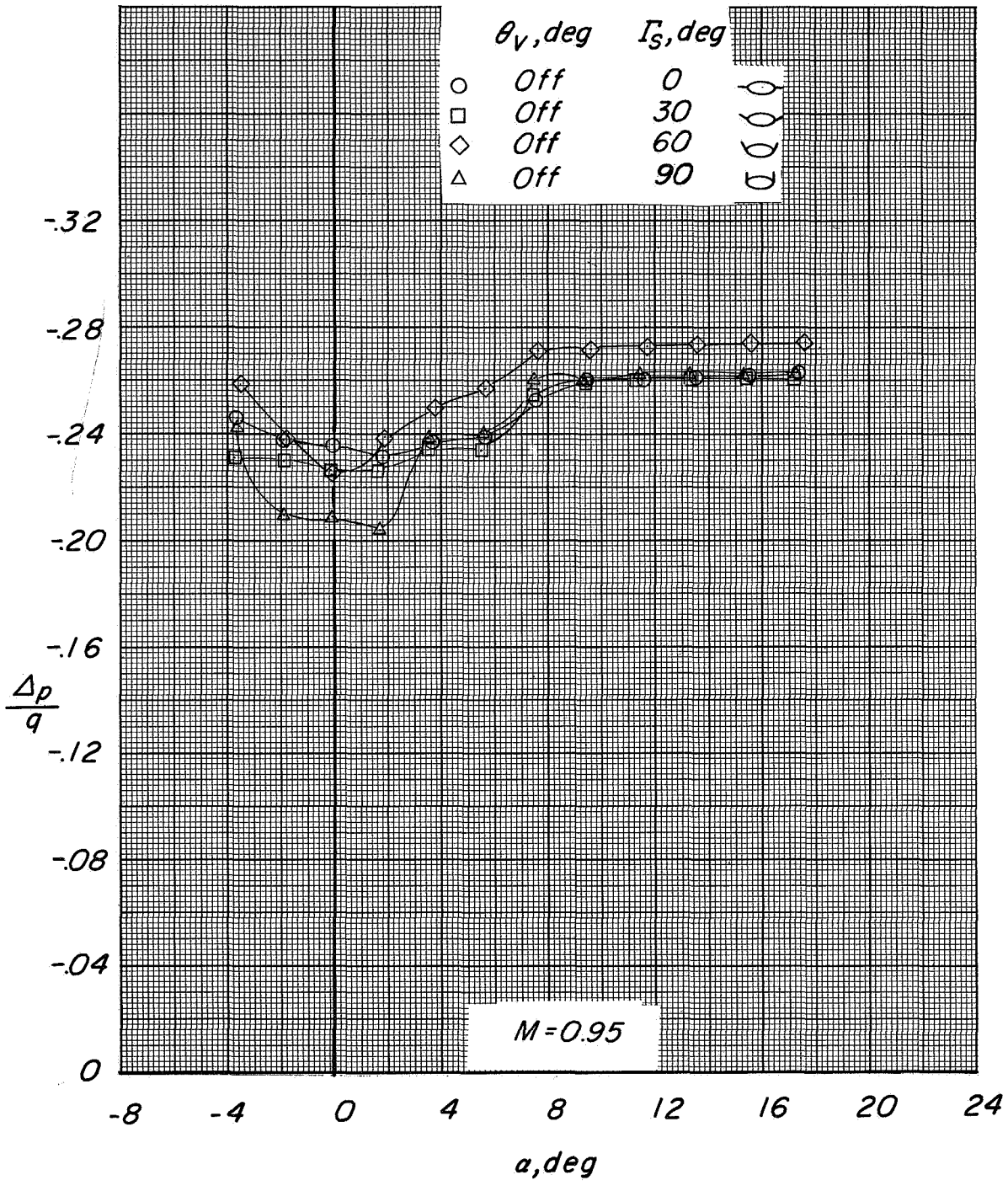

(b) Continued.

Figure 2.- Continued.

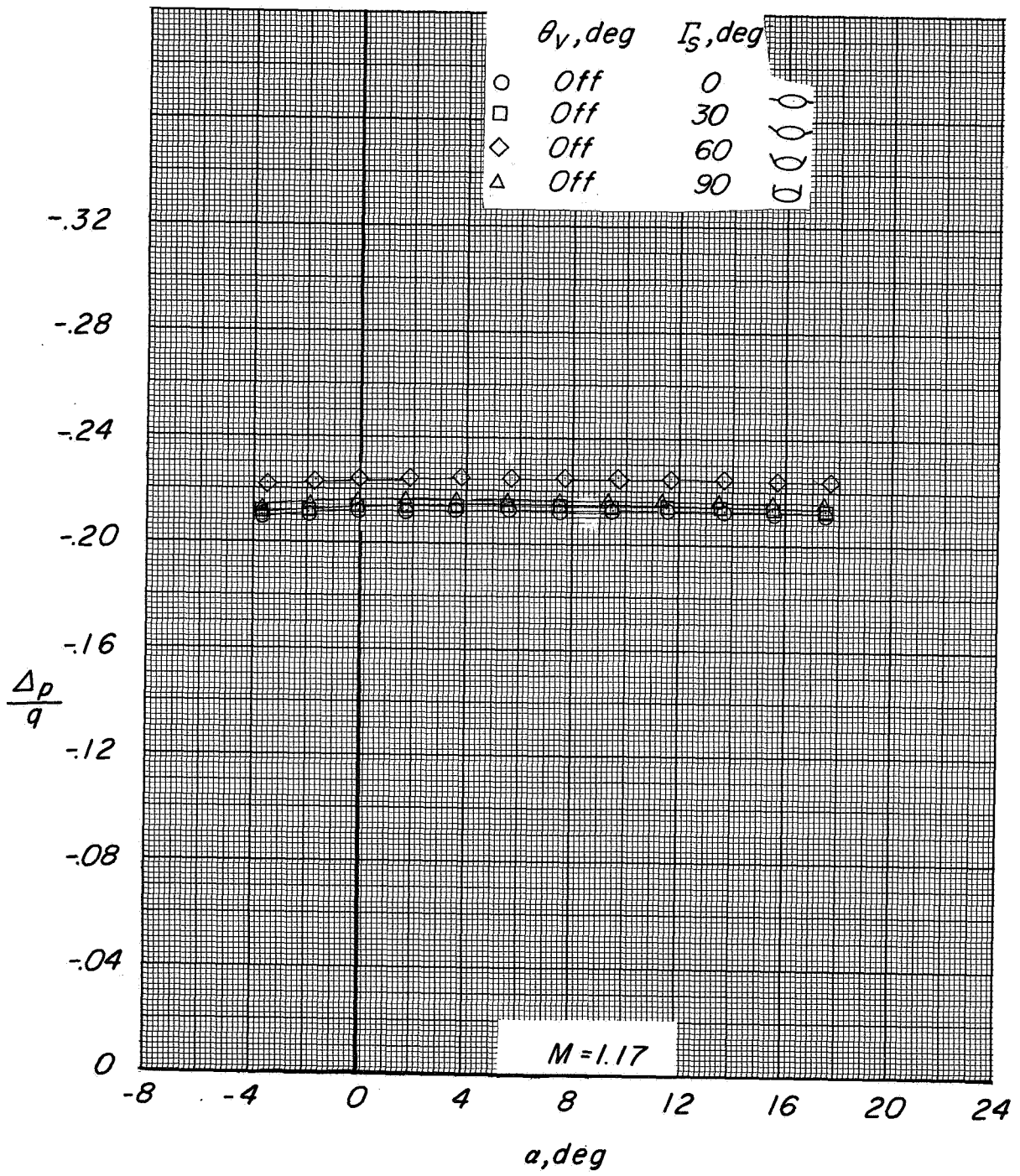

(b) Concluded.

Figure 2.- Continued.

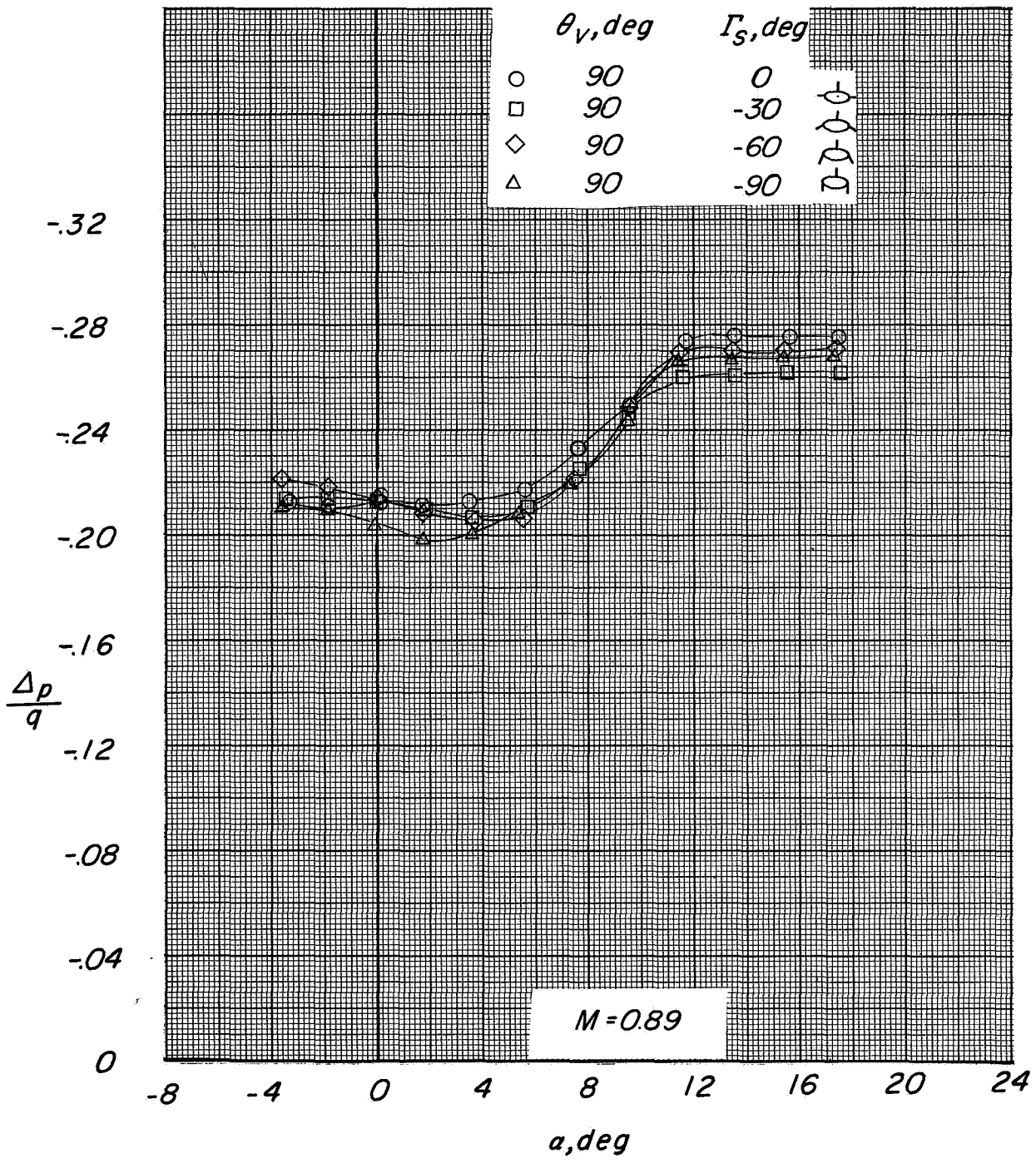

(c) $\theta_V = 90^0$; negative Γ_S.

Figure 2.- Continued.

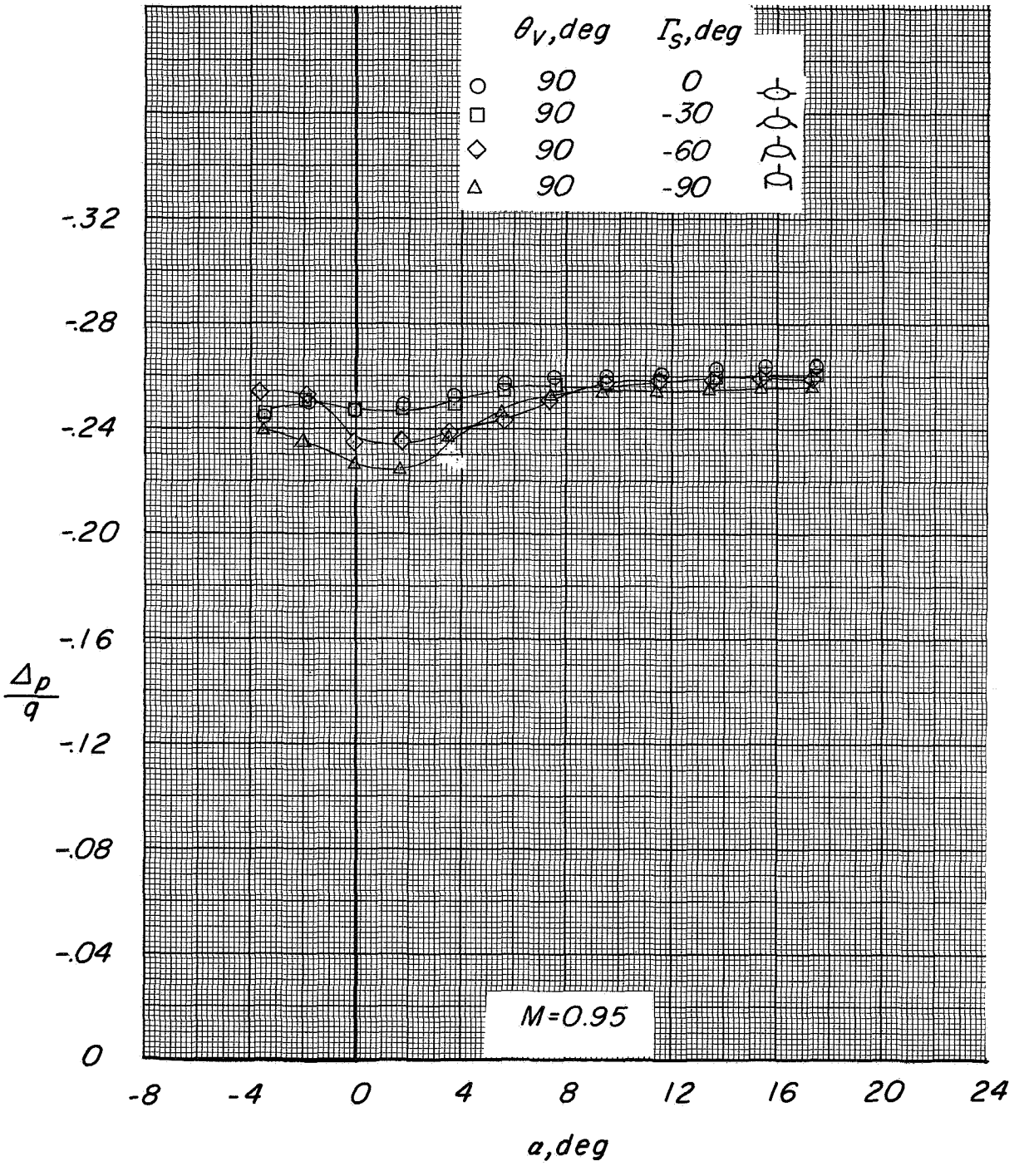

(c) Continued.

Figure 2.- Continued.

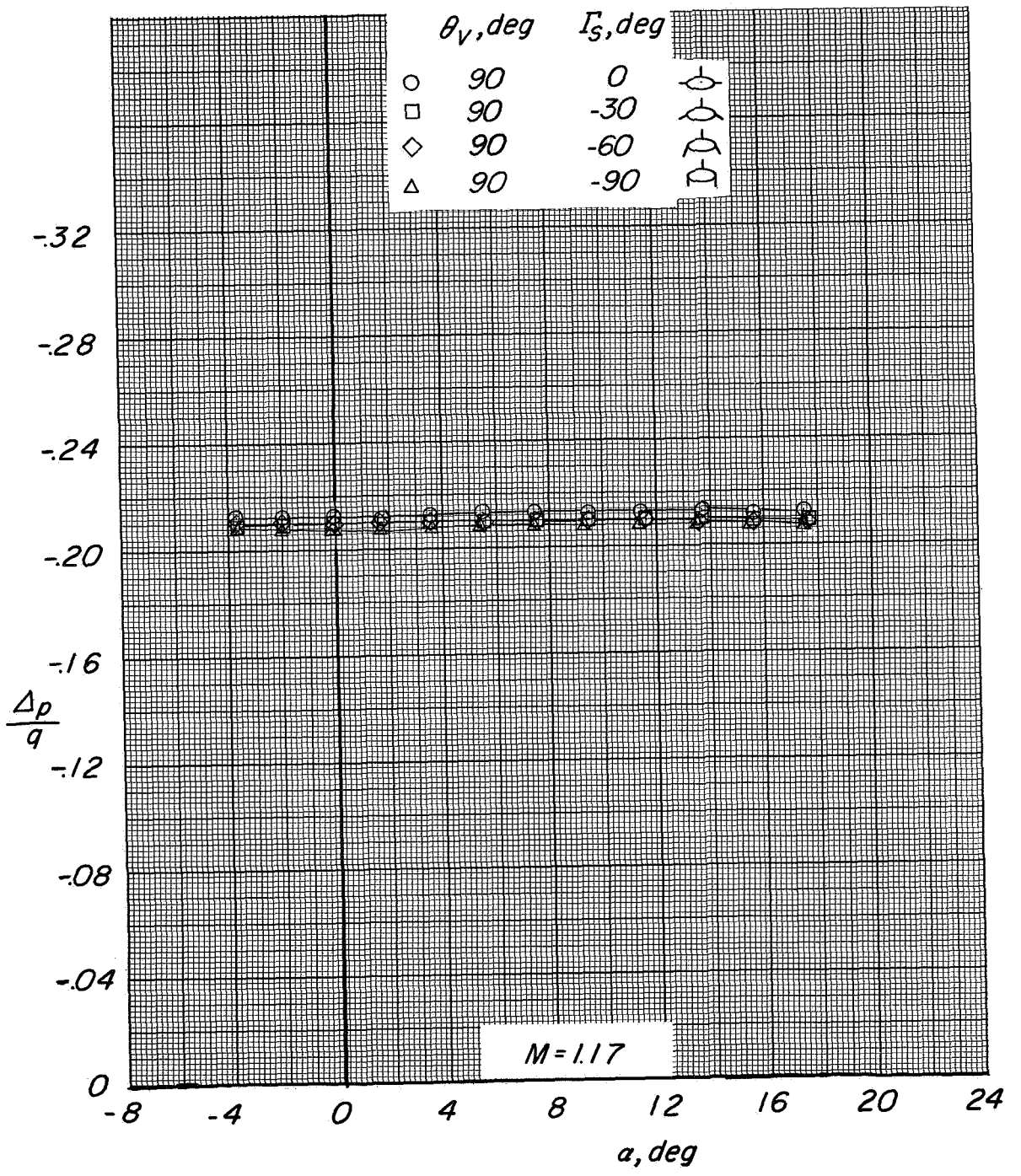

(c) Concluded.

Figure 2.- Continued.

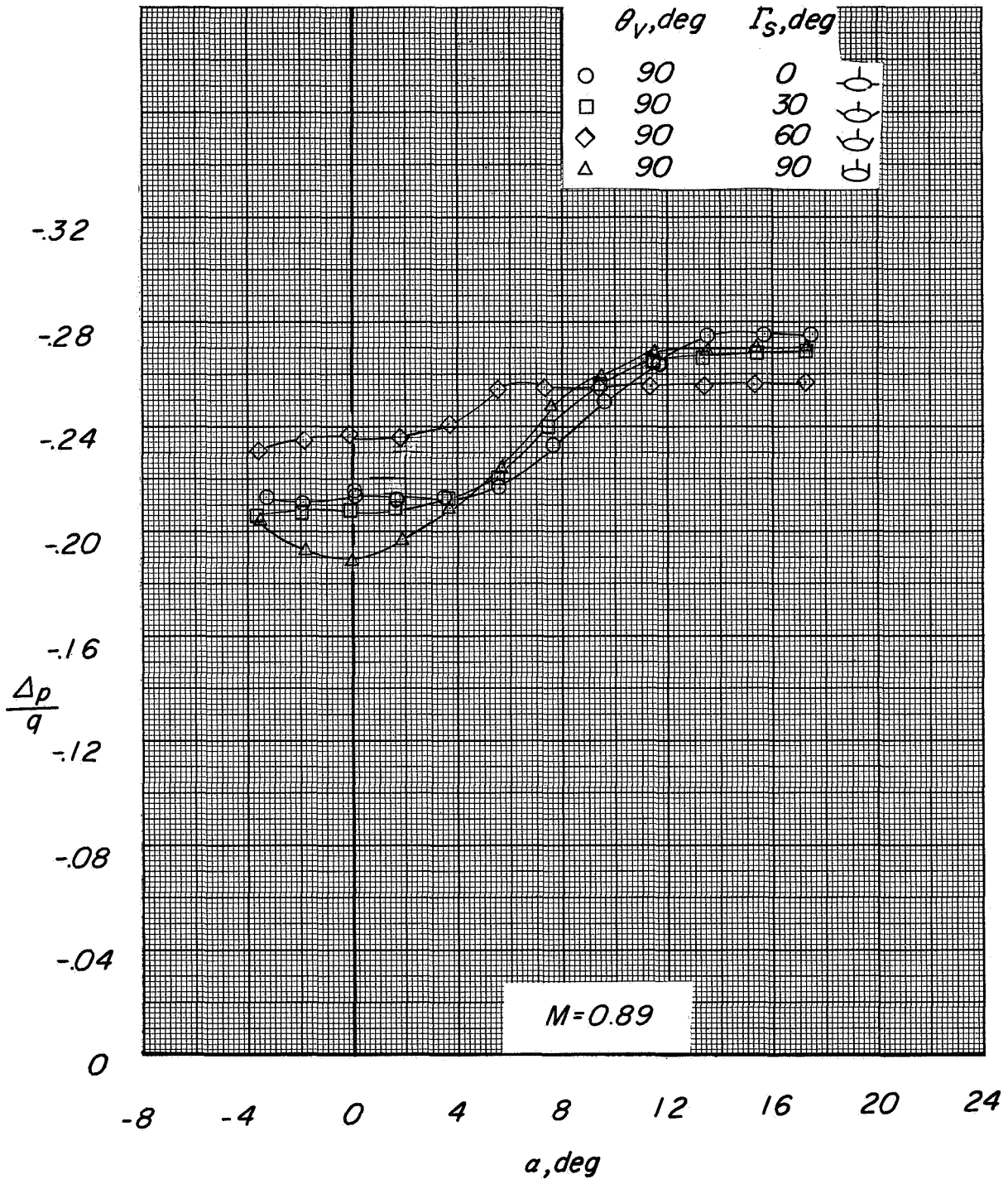

(d) $\theta_V = 90^0$; positive Γ_S.

Figure 2.- Continued.

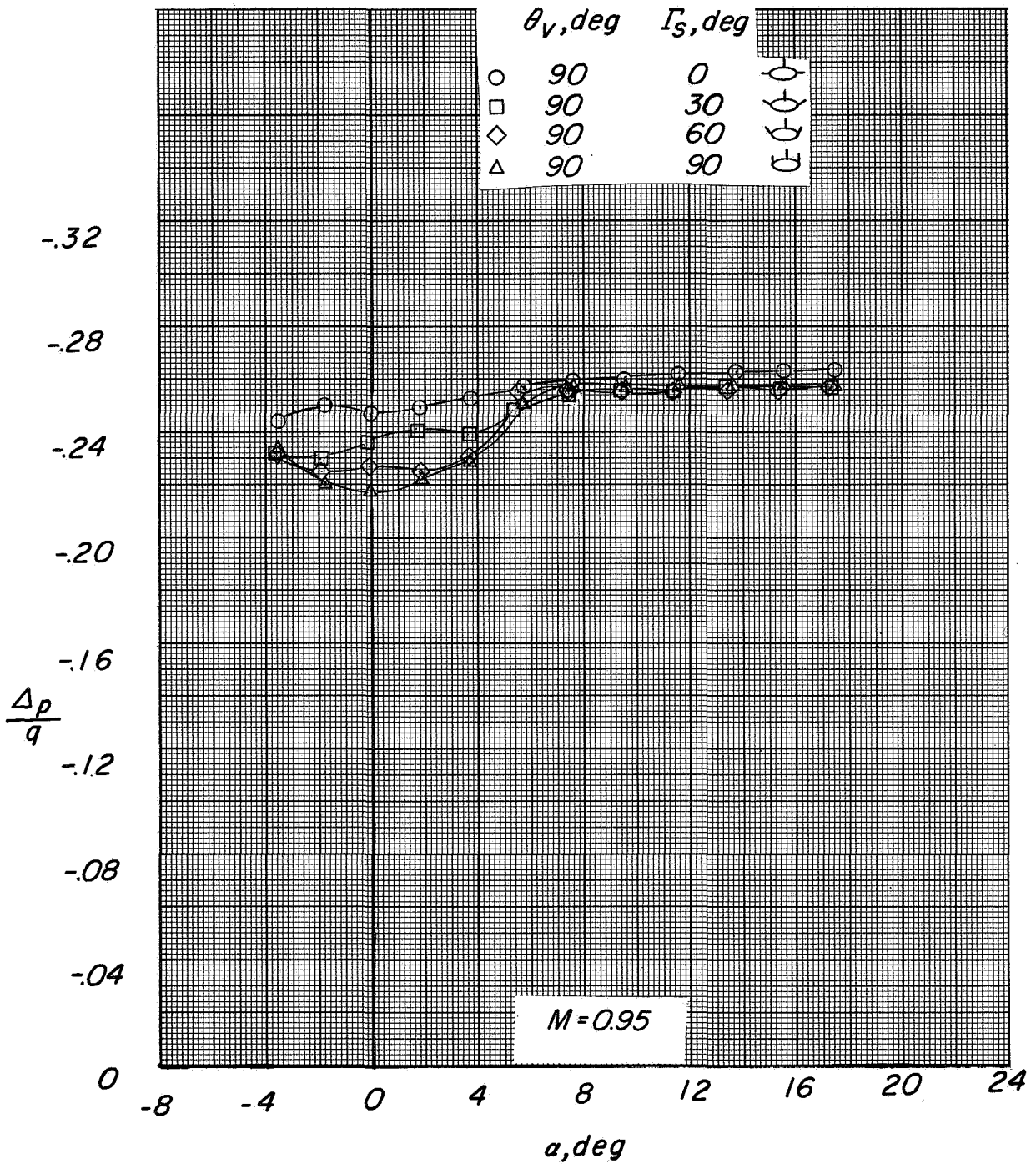

(d) Continued.

Figure 2.- Continued.

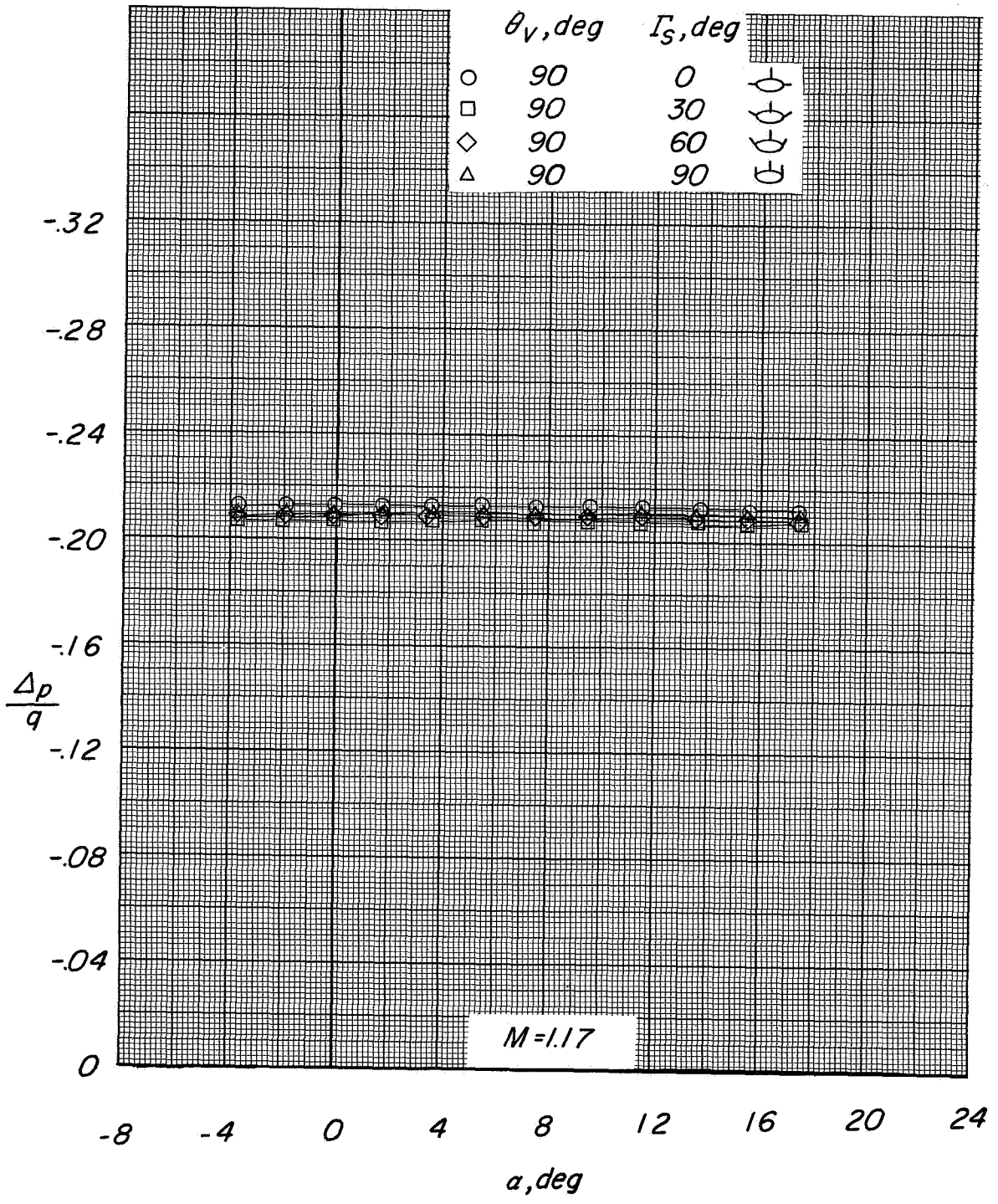

(d) Concluded.

Figure 2.- Continued.

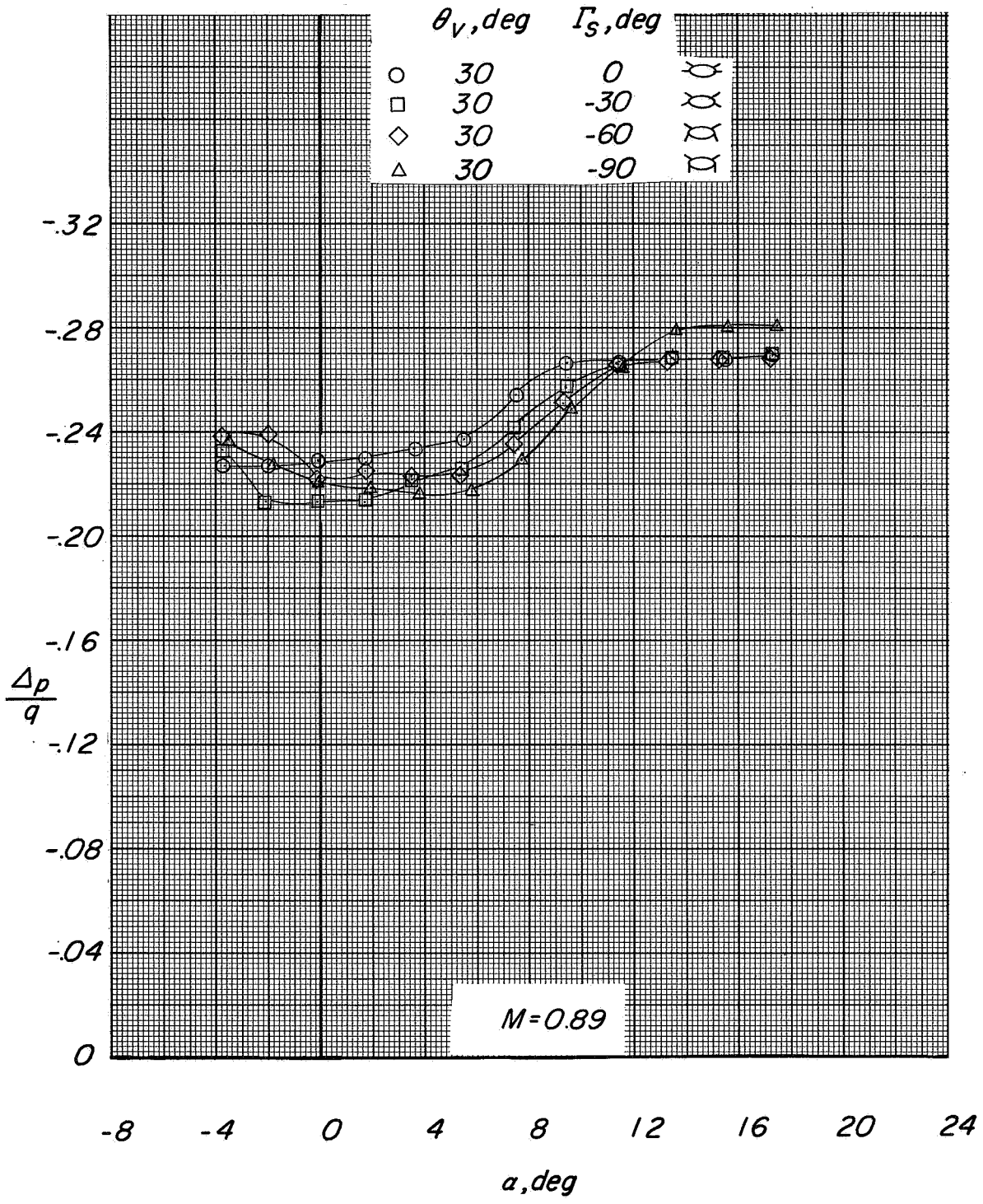

(e) $\theta_V = 30^0$; negative Γ_S.

Figure 2.- Continued.

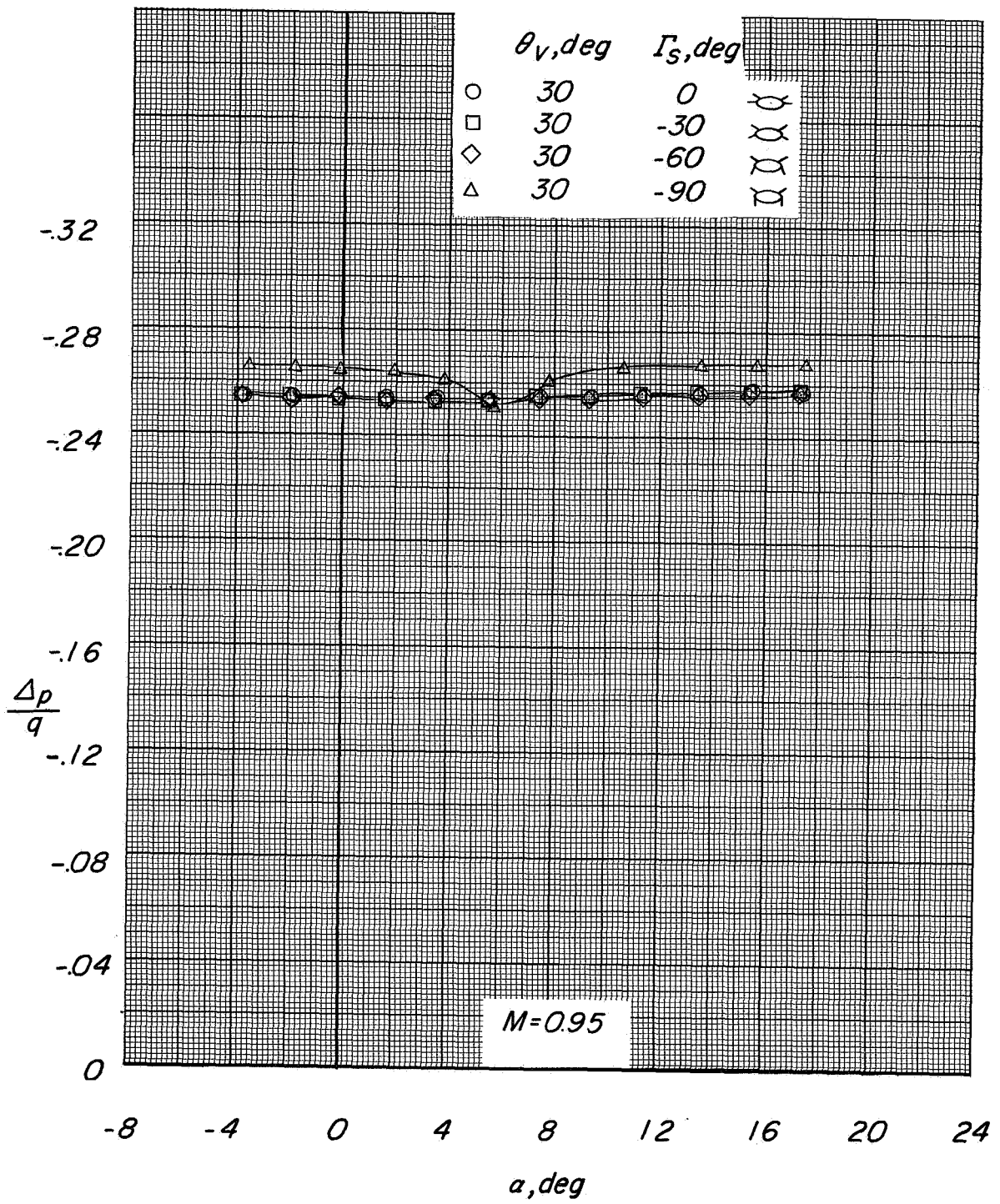

(e) Continued.

Figure 2.- Continued.

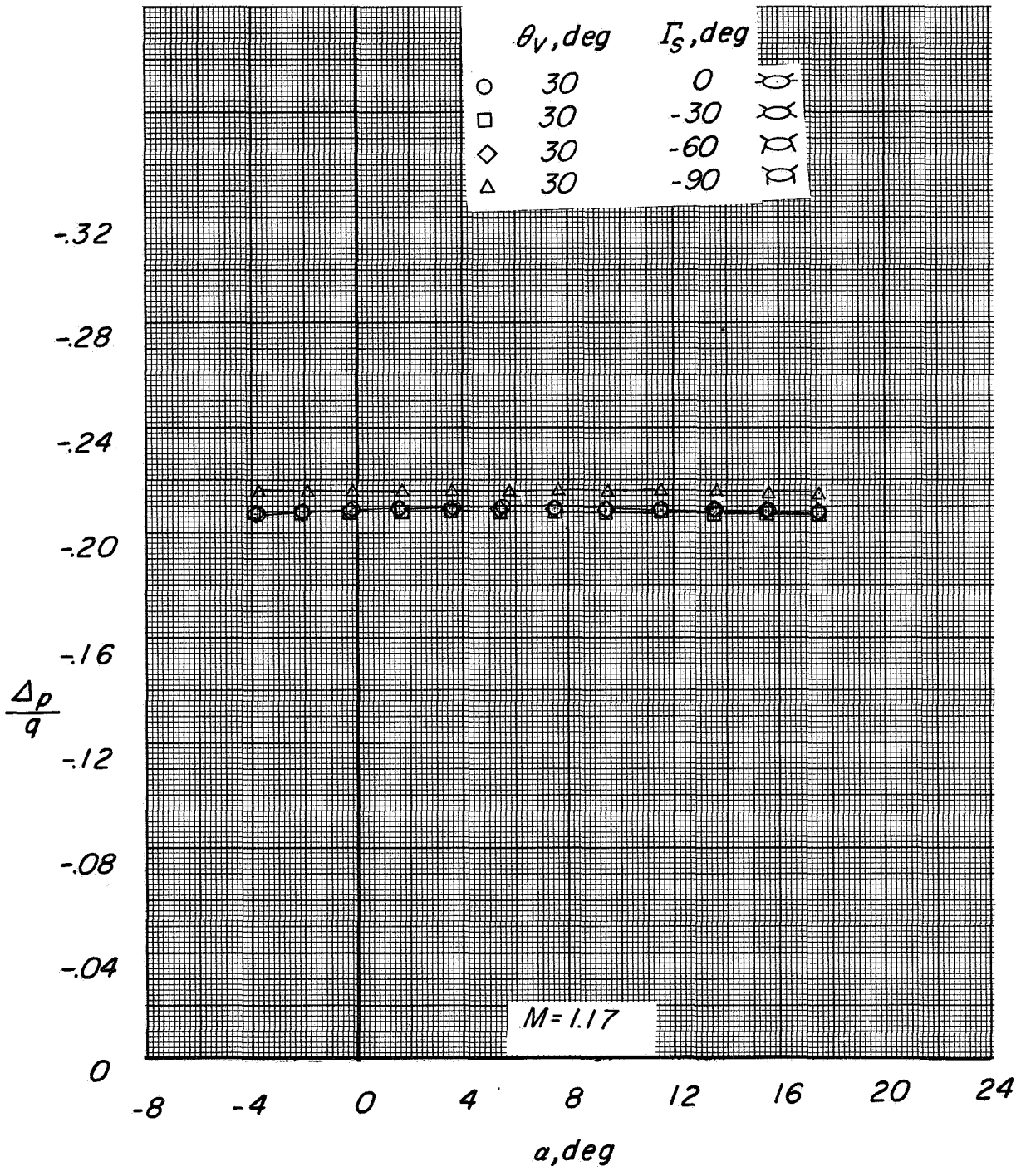

(e) Concluded.

Figure 2.- Concluded.

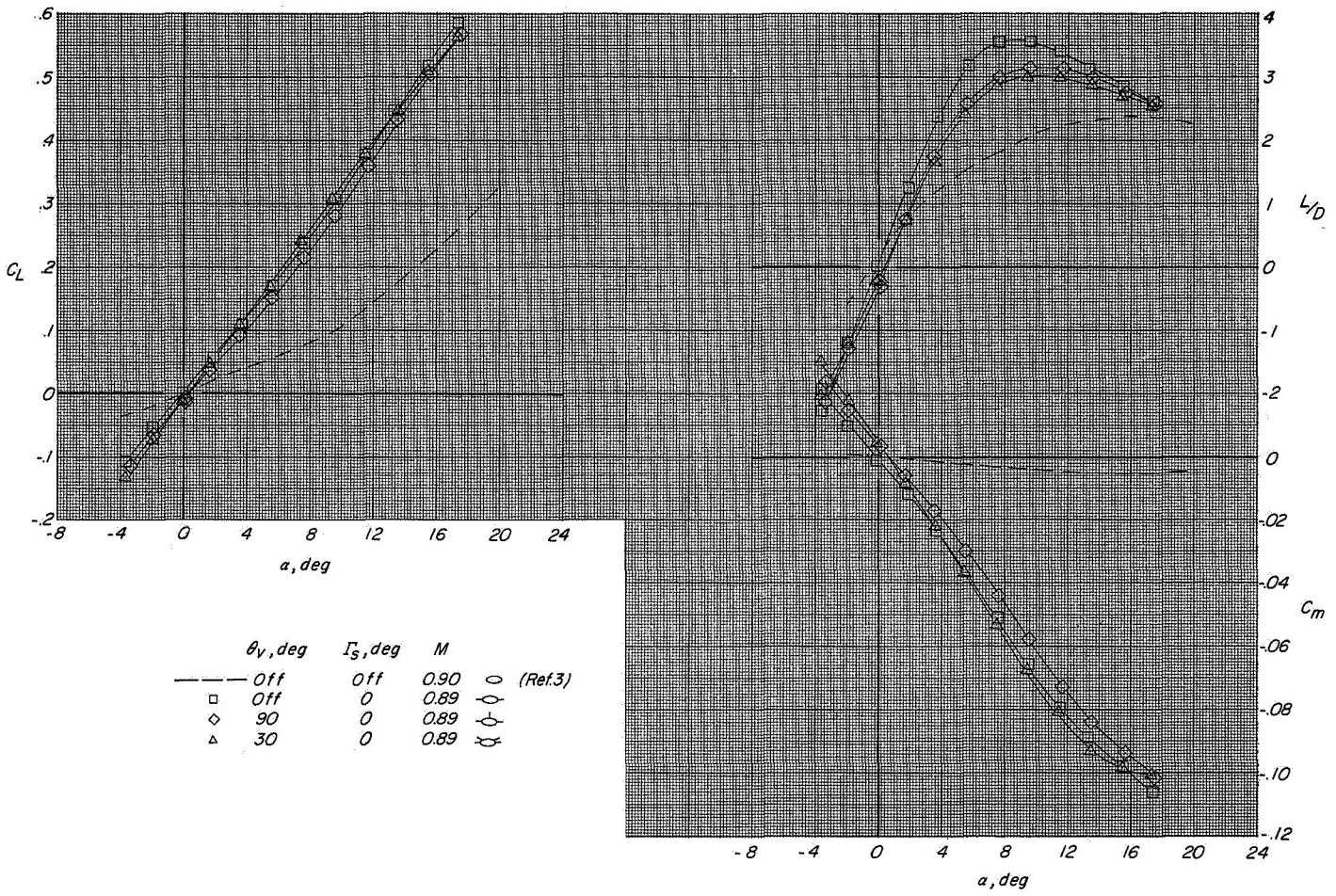

(a) M = 0.89.

Figure 3.- Comparison of selected longitudinal data with body-alone data of reference 3.

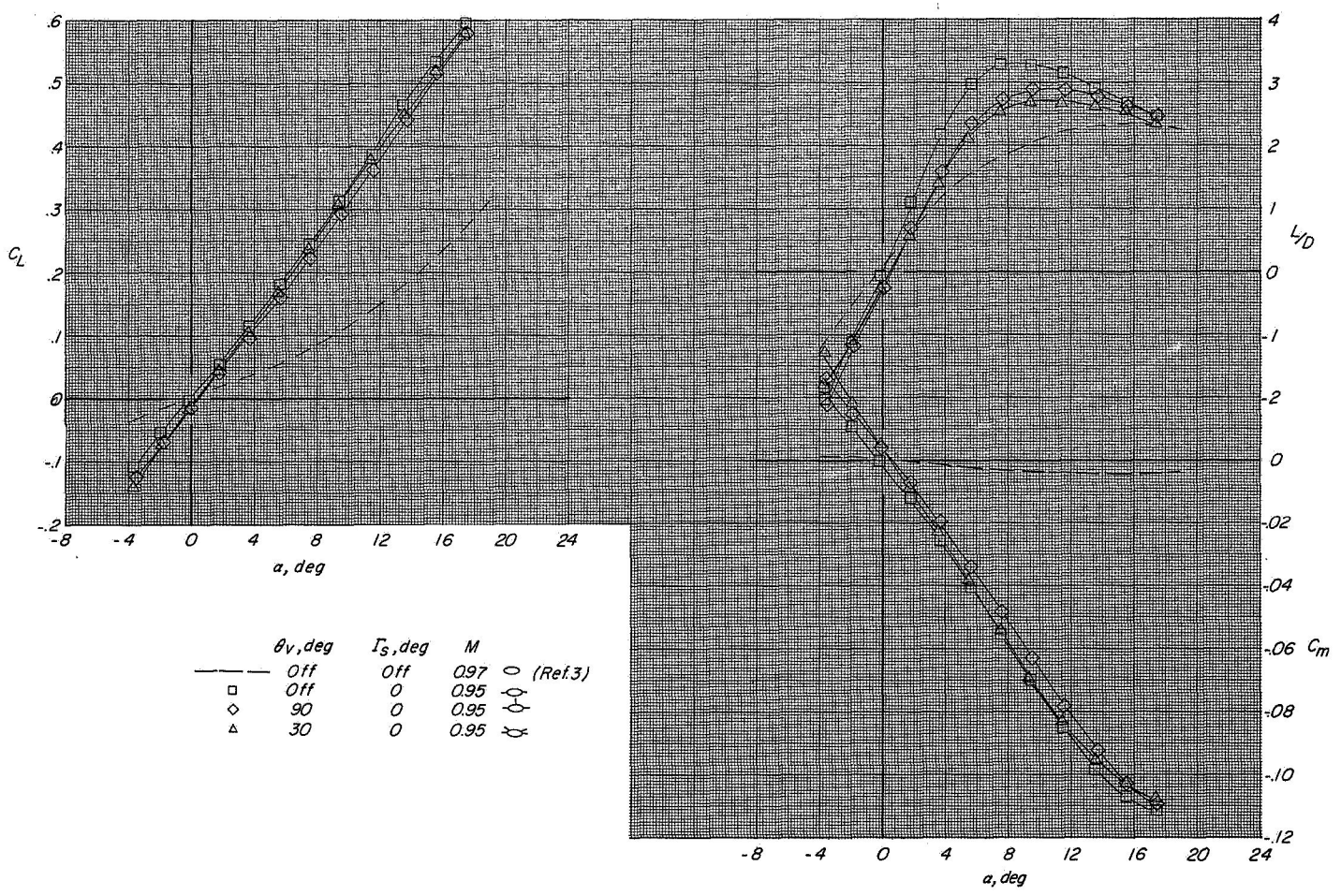

(b) M = 0.95.

Figure 3.- Continued.

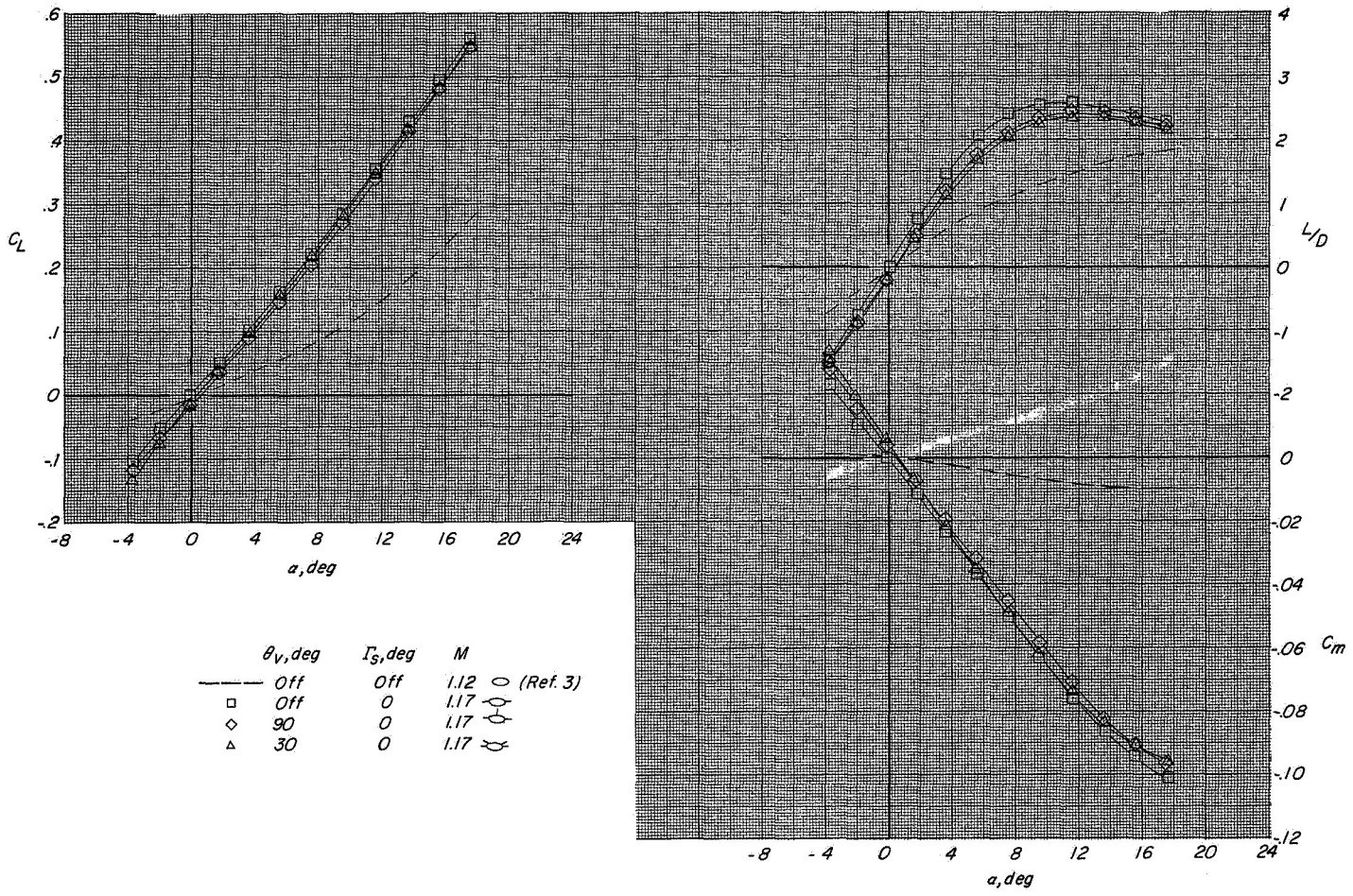

(c) M = 1.17.

Figure 3.- Concluded.

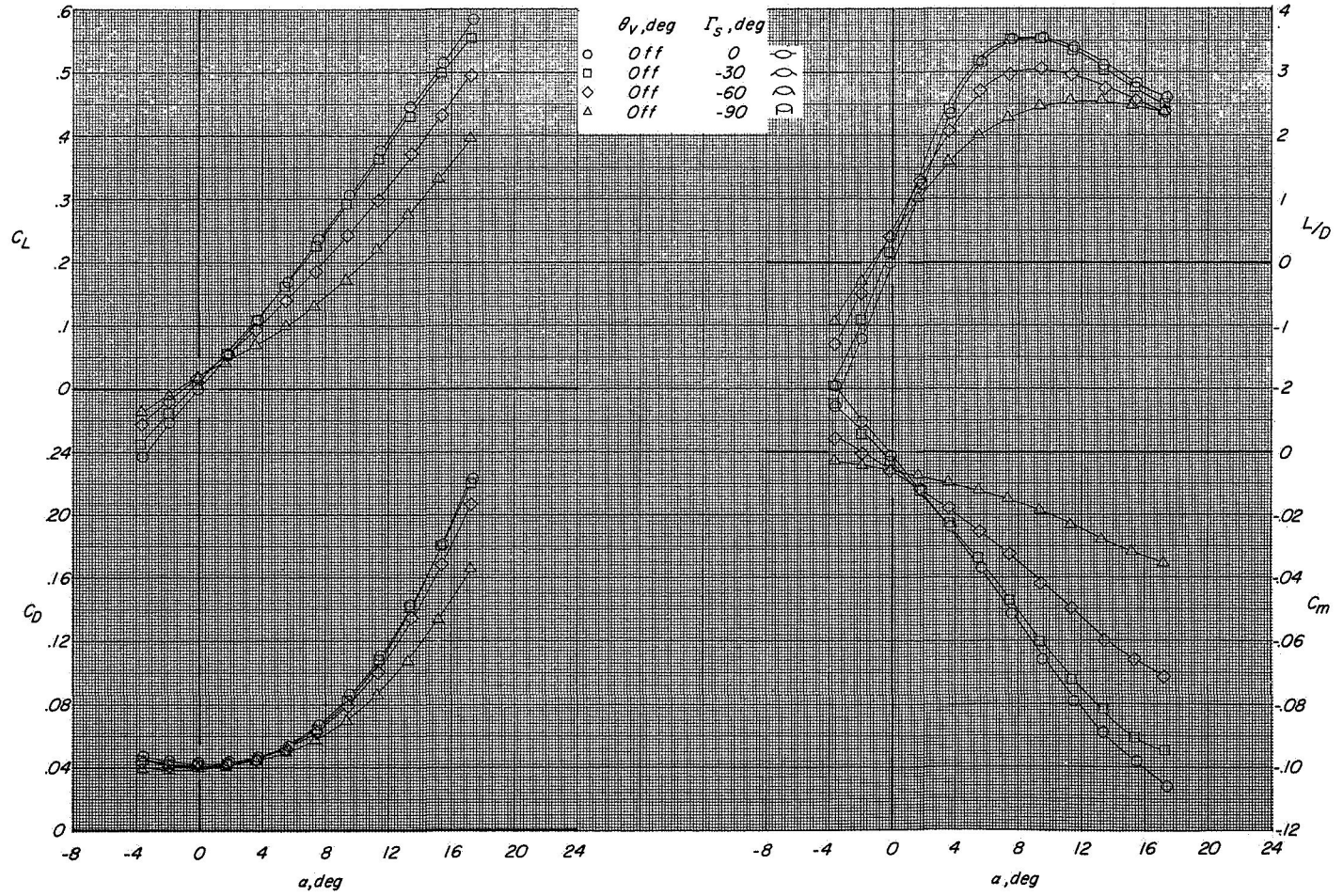

(a) M = 0.89.

Figure 4.- Effect of stabilizers at negative dihedral angles on longitudinal aerodynamic characteristics with tails off.

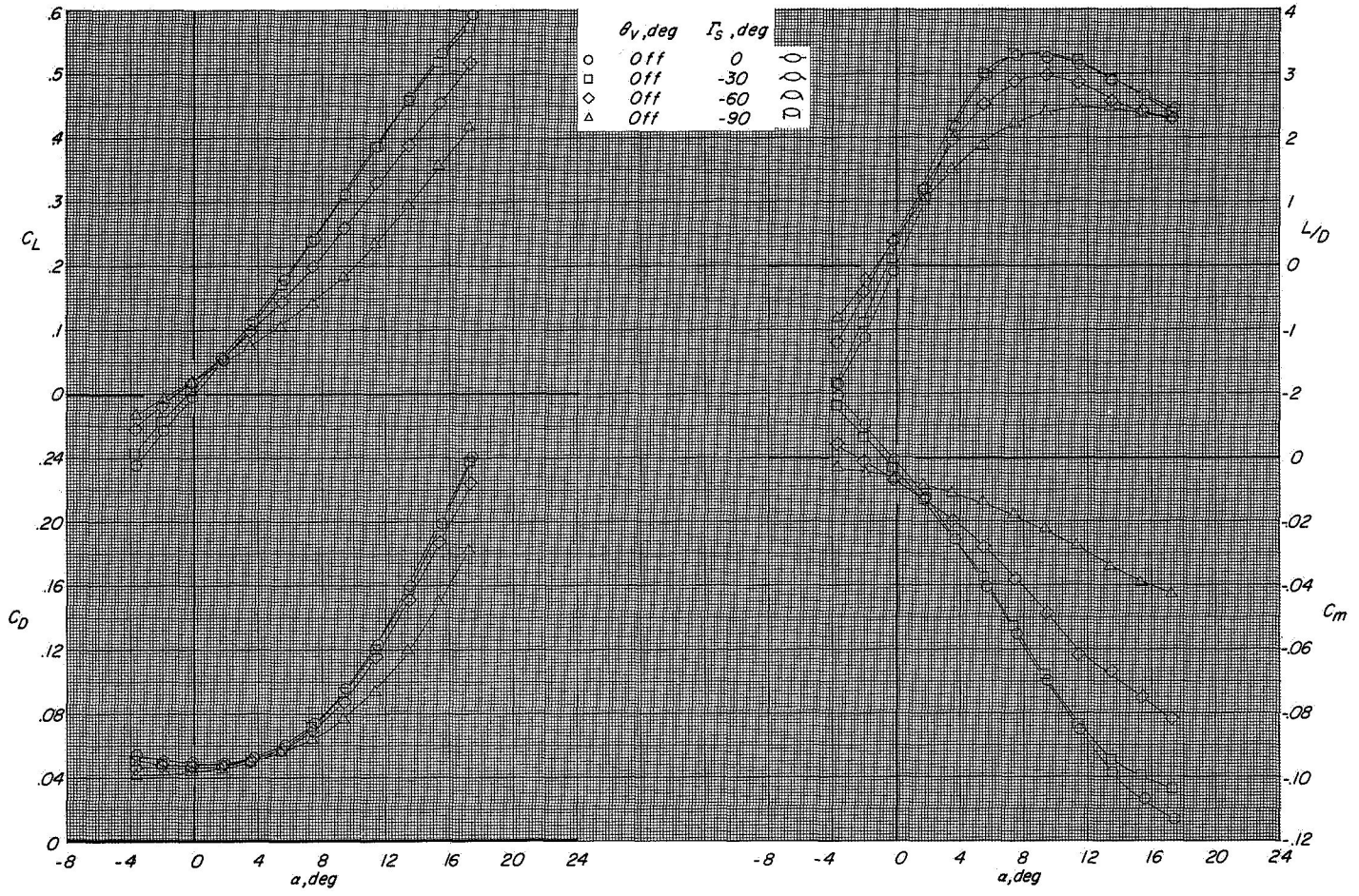

(b) M = 0.95.

Figure 4.- Continued.

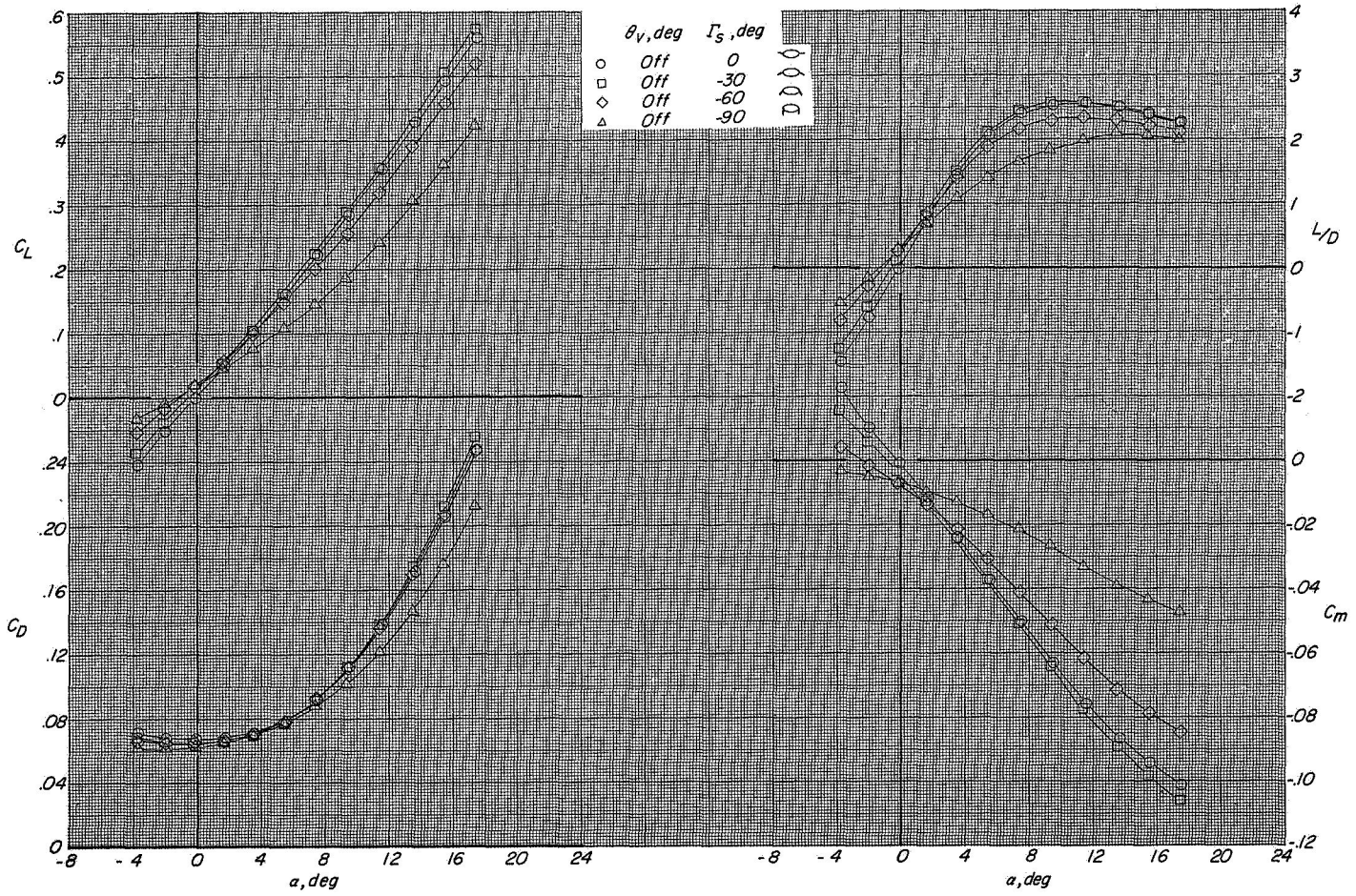

(c) M = 1.17.

Figure 4.- Concluded.

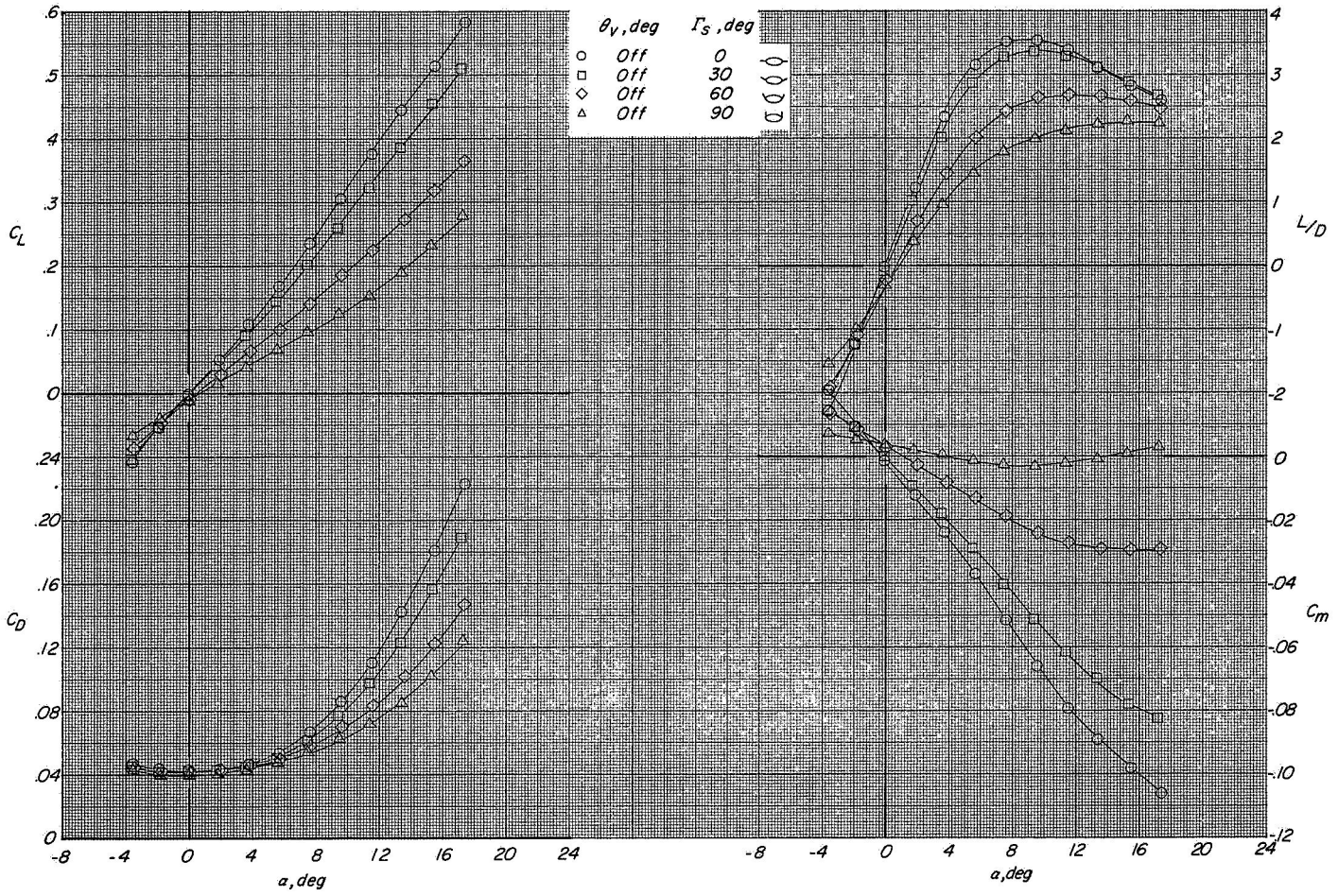

(a) M = 0.89.

Figure 5.- Effect of stabilizers at positive dihedral angles on longitudinal aerodynamic characteristics with tails off.

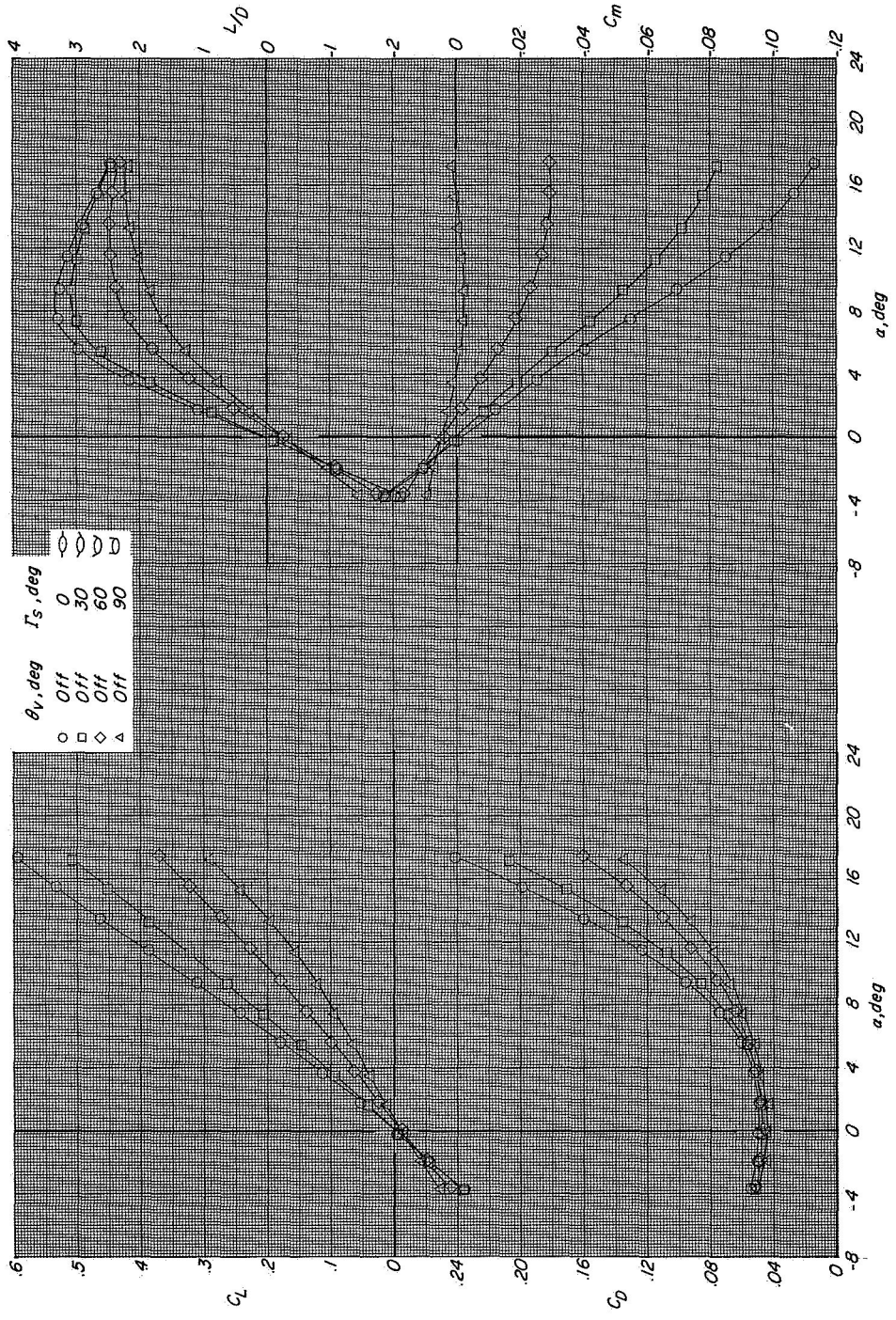

(b) M = 0.95.

Figure 5.- Continued.

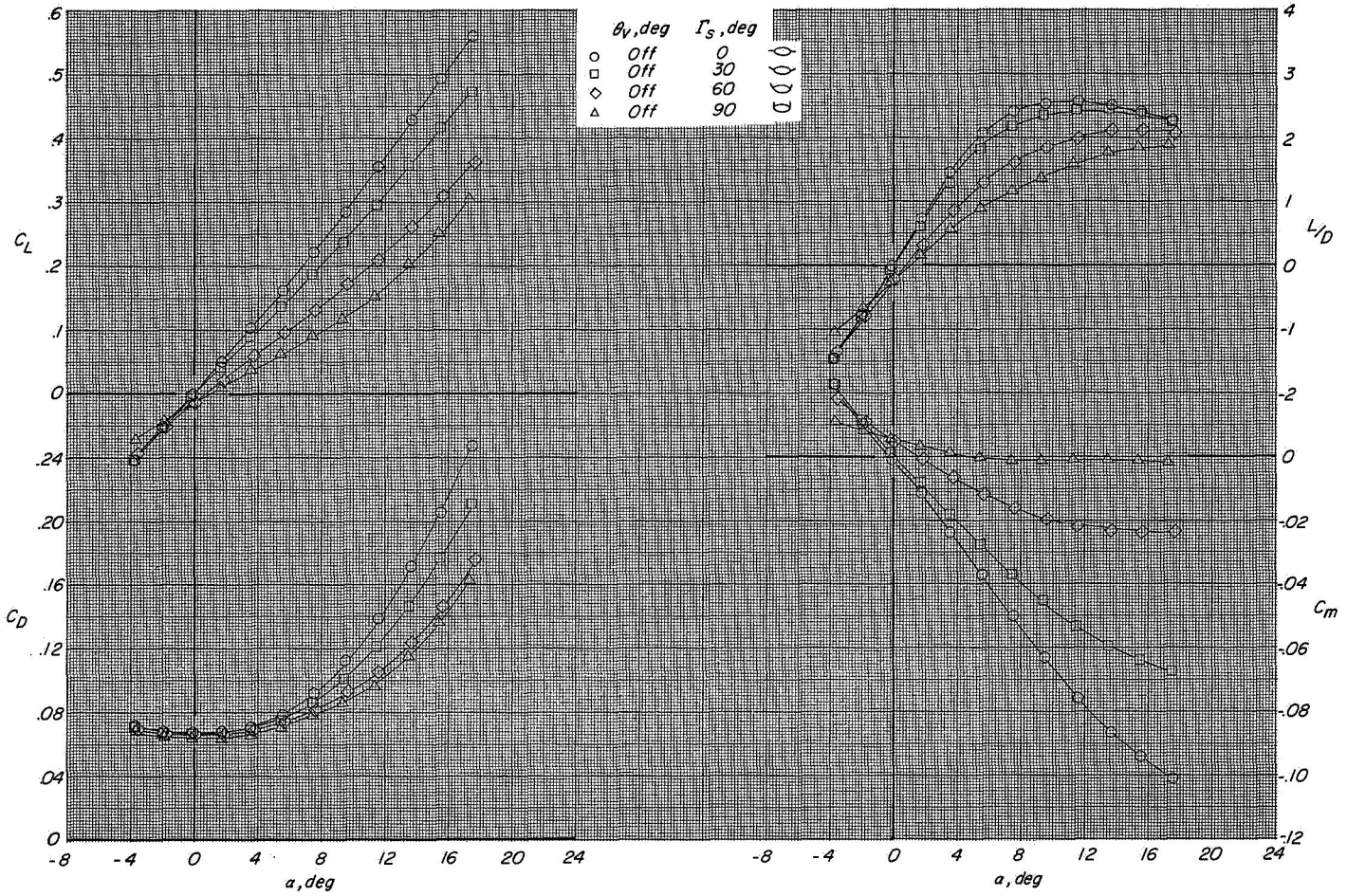

(c) M = 1.17.

Figure 5.- Concluded.

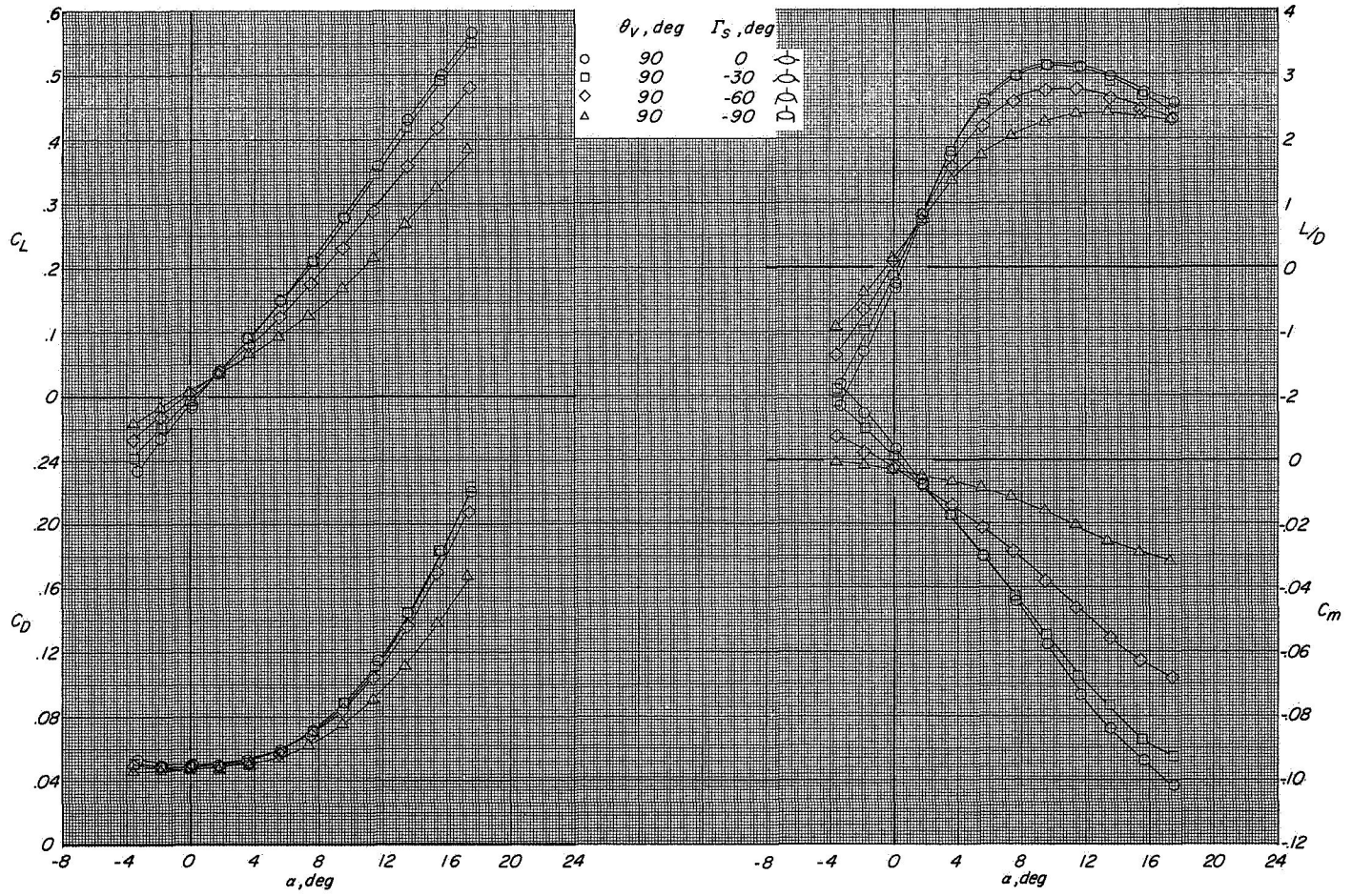

(a) M = 0.89.

Figure 6.- Effect of stabilizers at negative dihedral angles on longitudinal aerodynamic characteristics with vertical tails at $\theta_V = 90^o$.

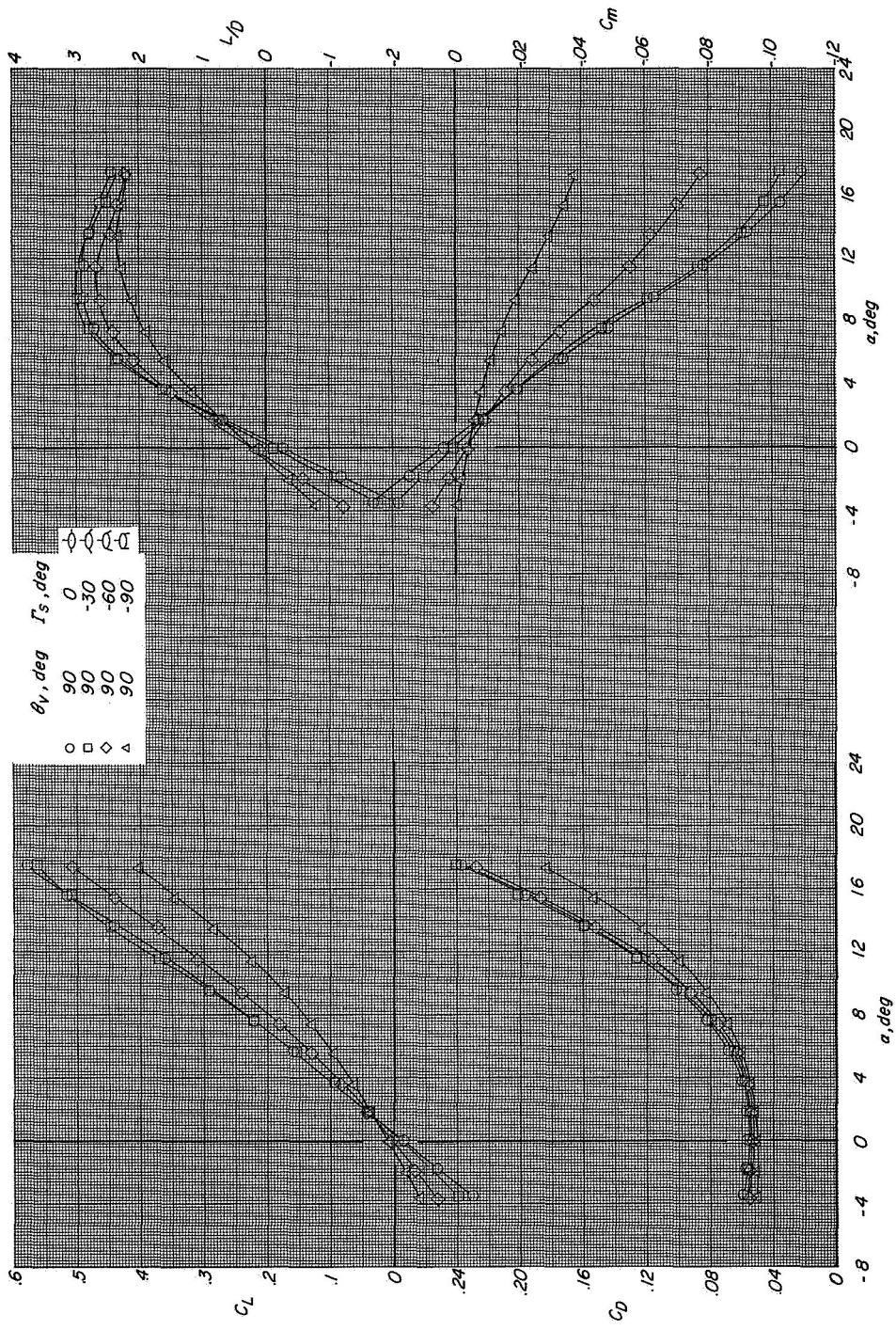

(b) M = 0.95.

Figure 6.- Continued.

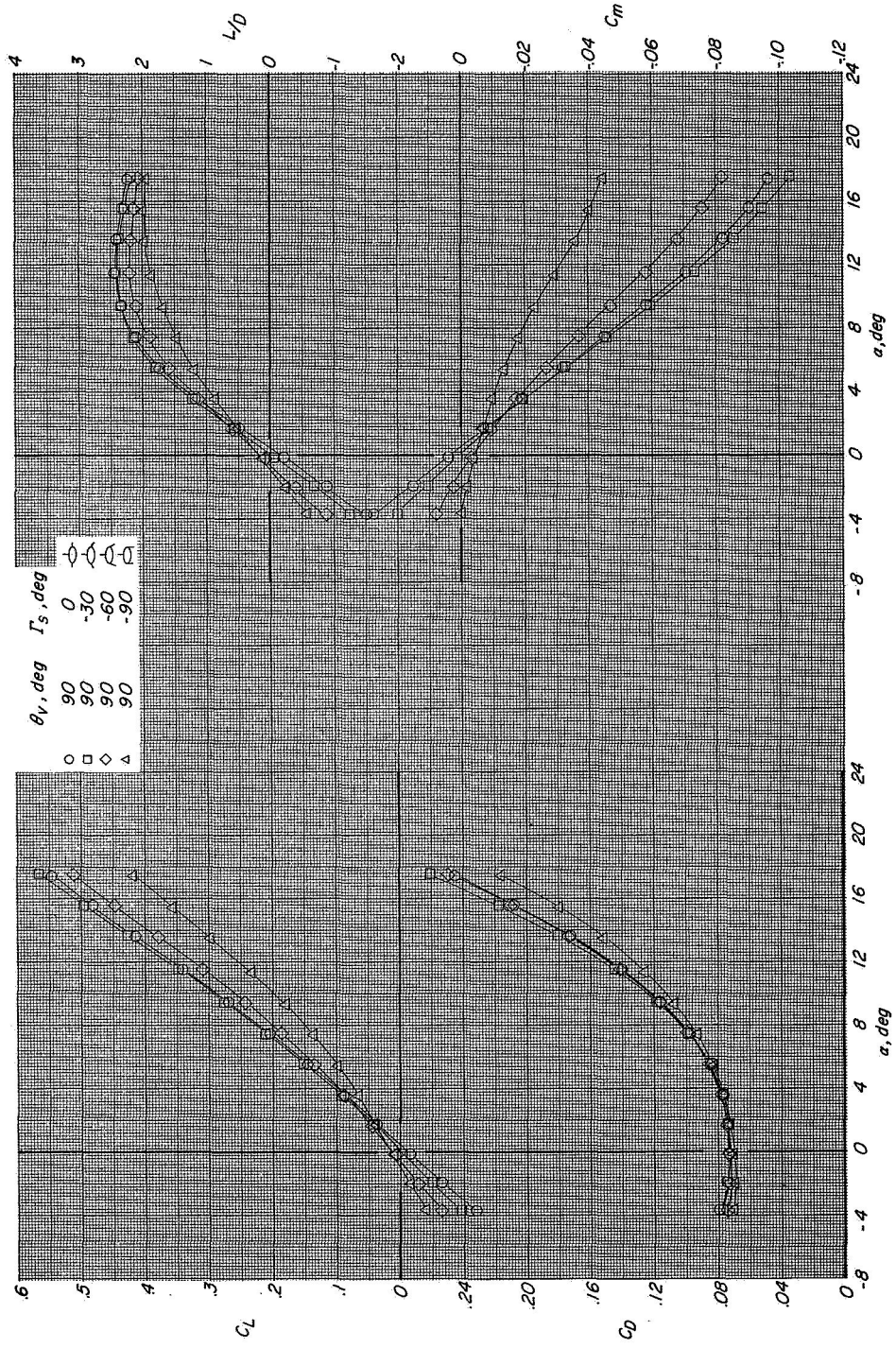

(c) M = 1.17.

Figure 6.- Concluded.

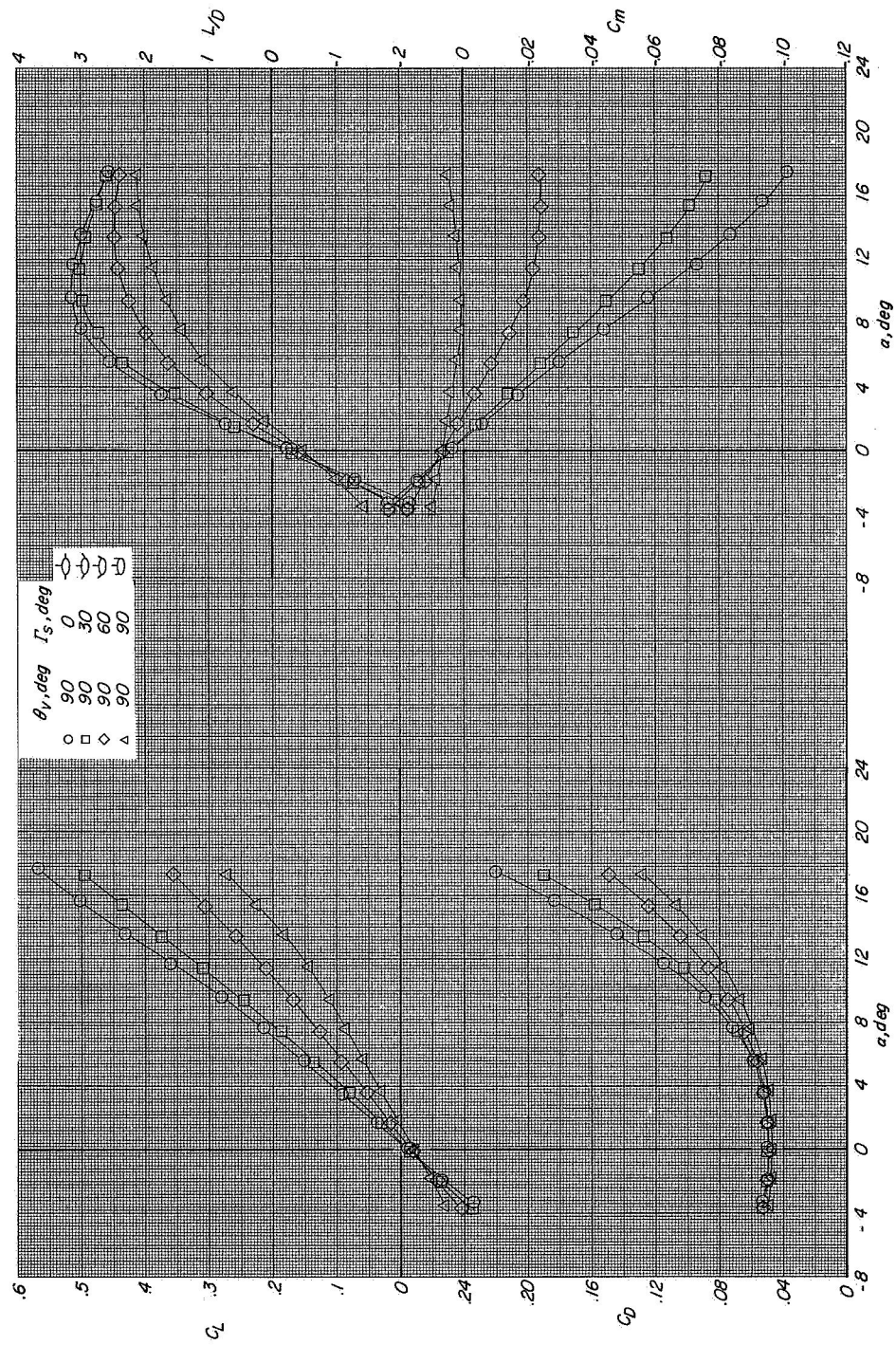

(a) M = 0.89.

Figure 7.- Effect of stabilizers at positive dihedral angles on longitudinal aerodynamic characteristics with vertical tails at $\theta_V = 90^0$.

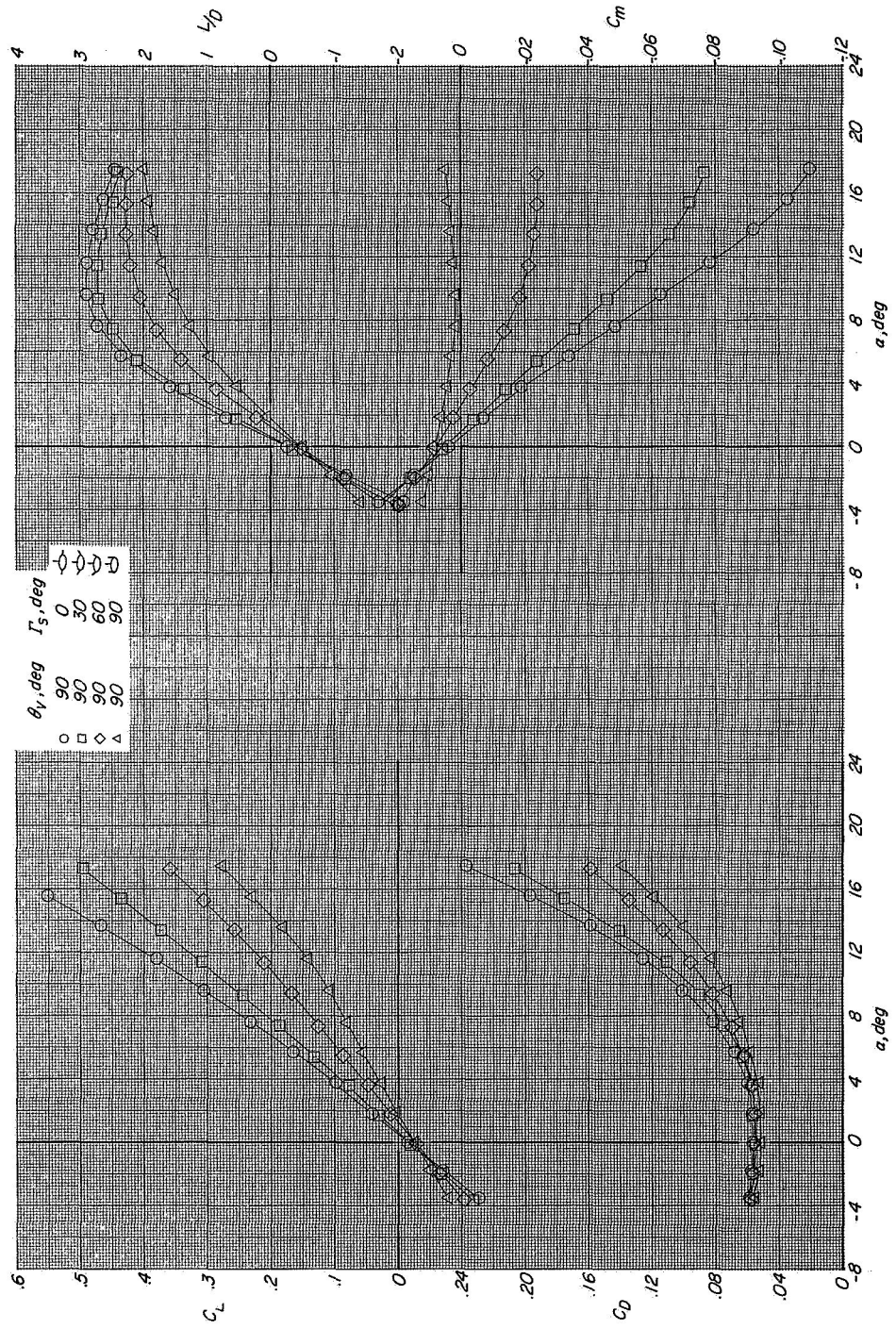

(b) M = 0.95.

Figure 7.- Continued.

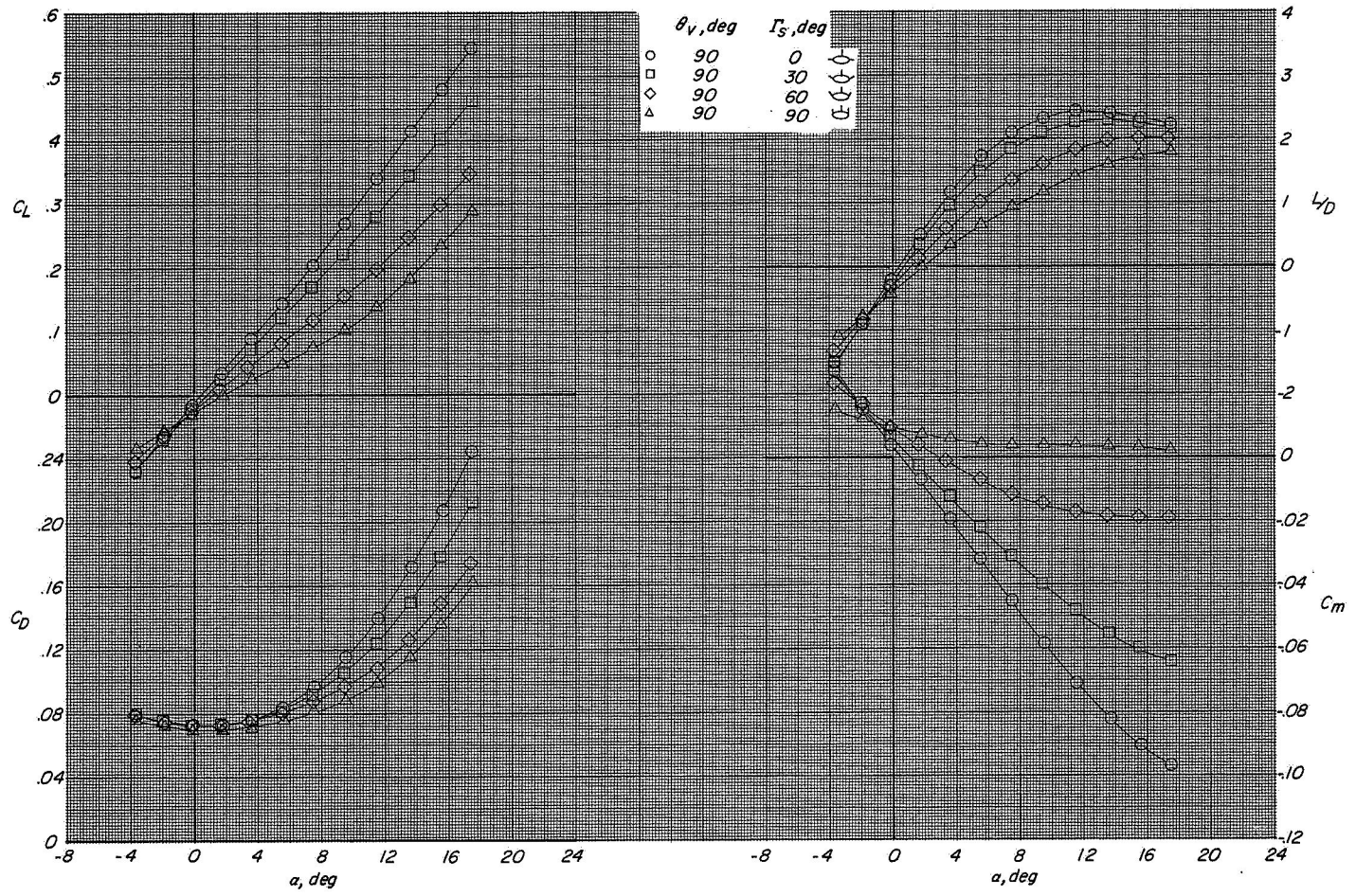

(c) M = 1.17.

Figure 7.- Concluded.

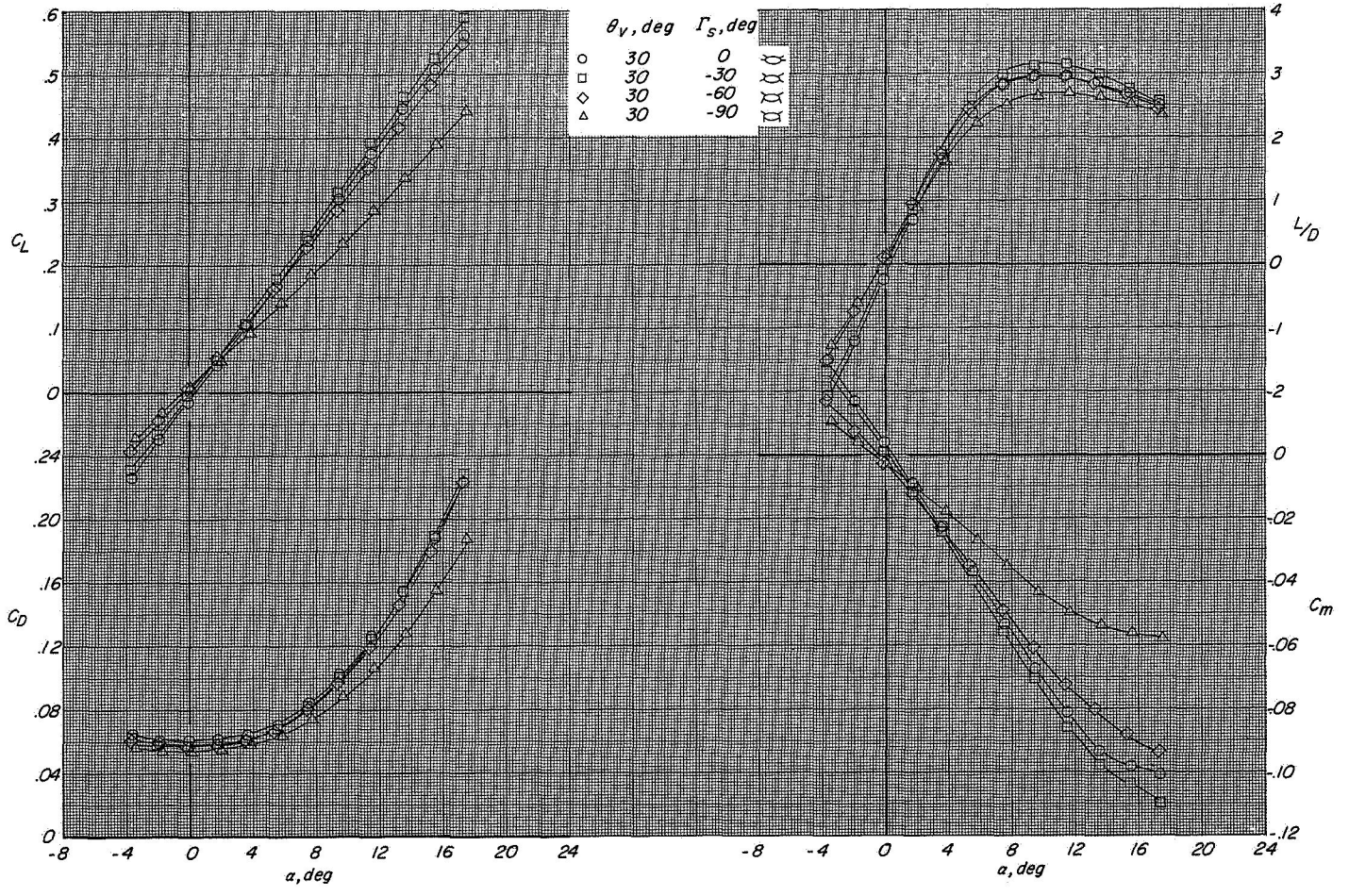

(a) M = 0.89.

Figure 8.- Effect of stabilizers at negative dihedral angles on longitudinal aerodynamic characteristics with vertical tails at $\theta_V = 30^0$.

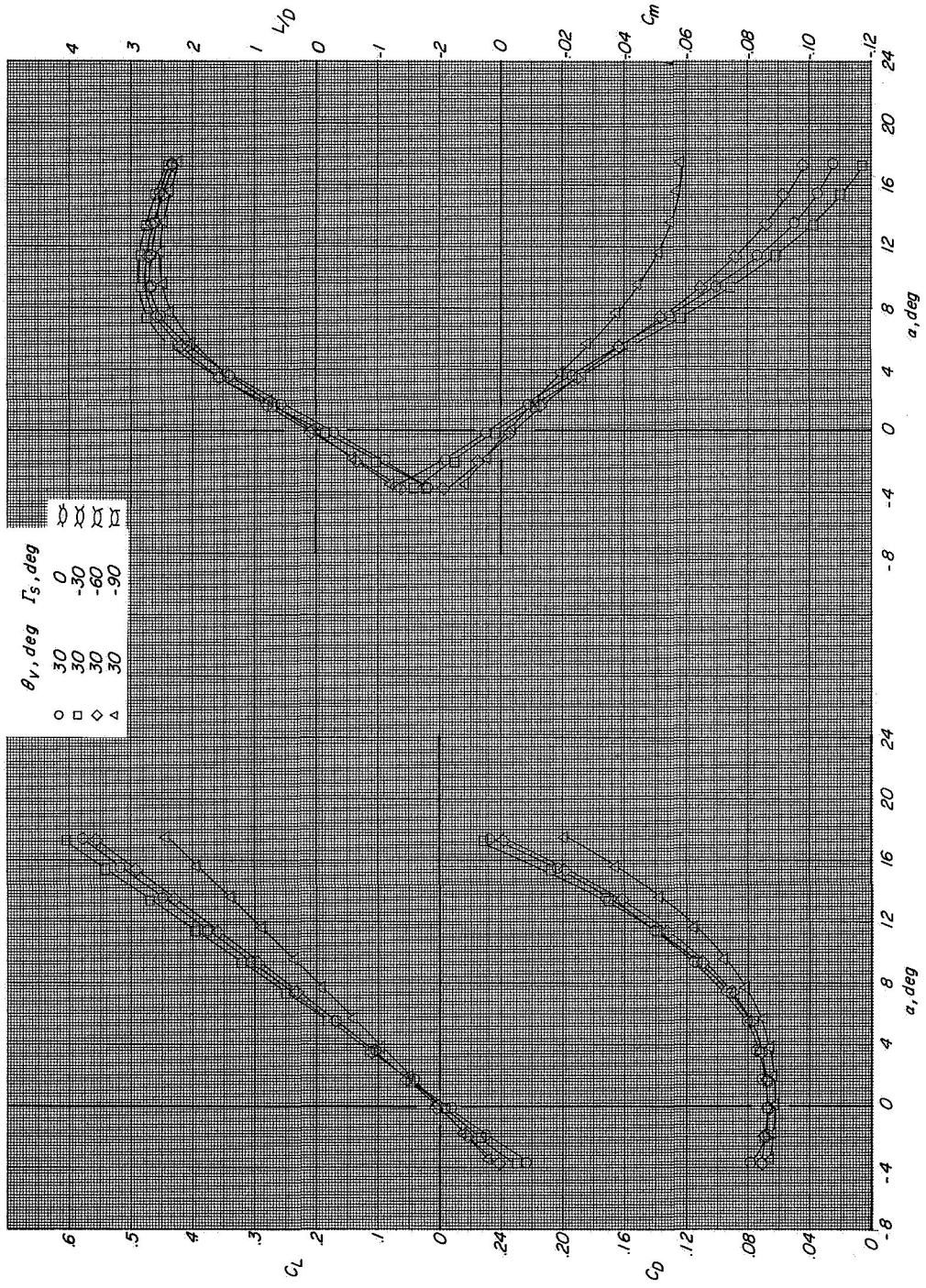

(b) M = 0.95.

Figure 8.- Continued.

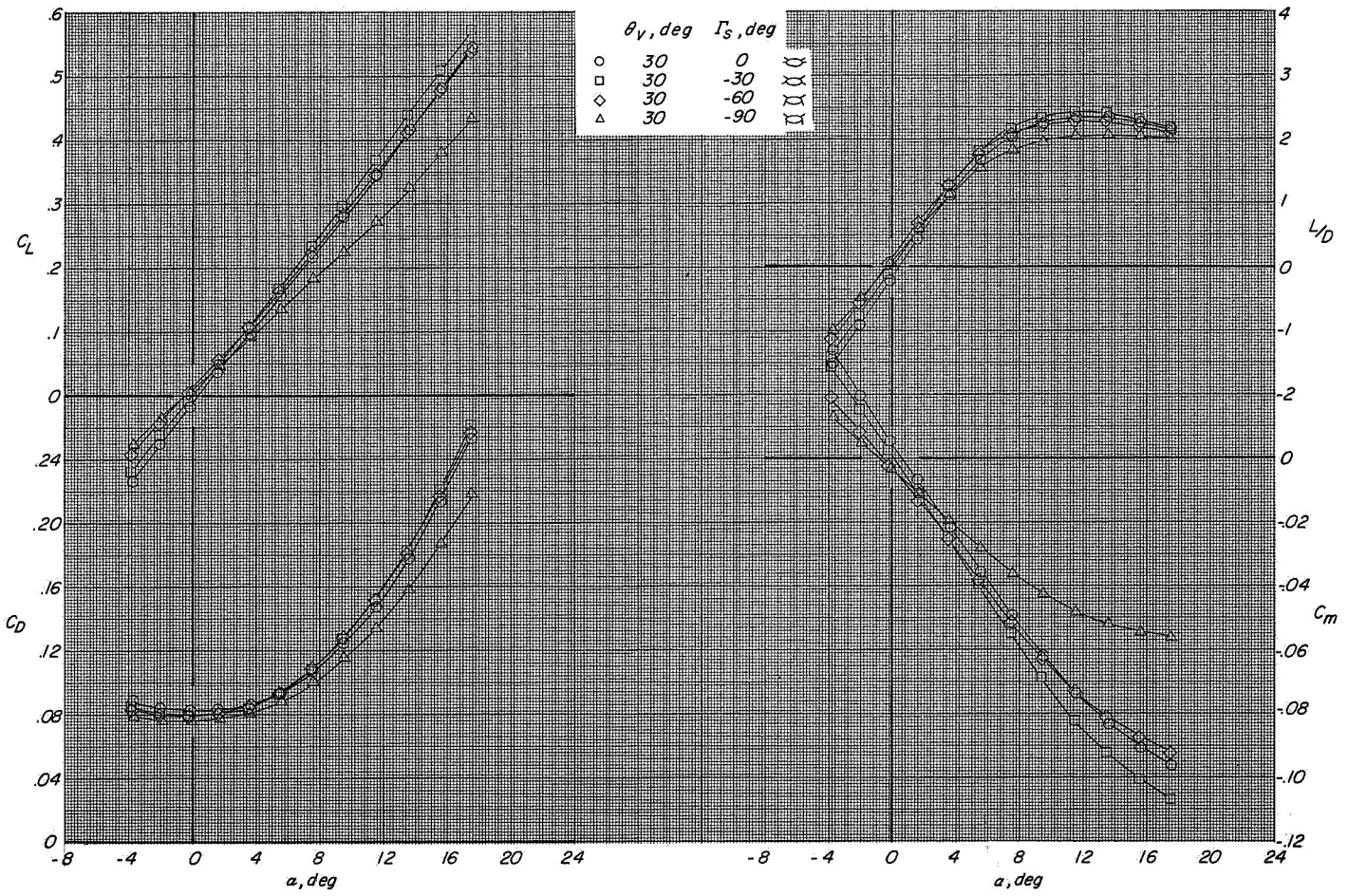

(c) M = 1.17.

Figure 8.- Concluded.

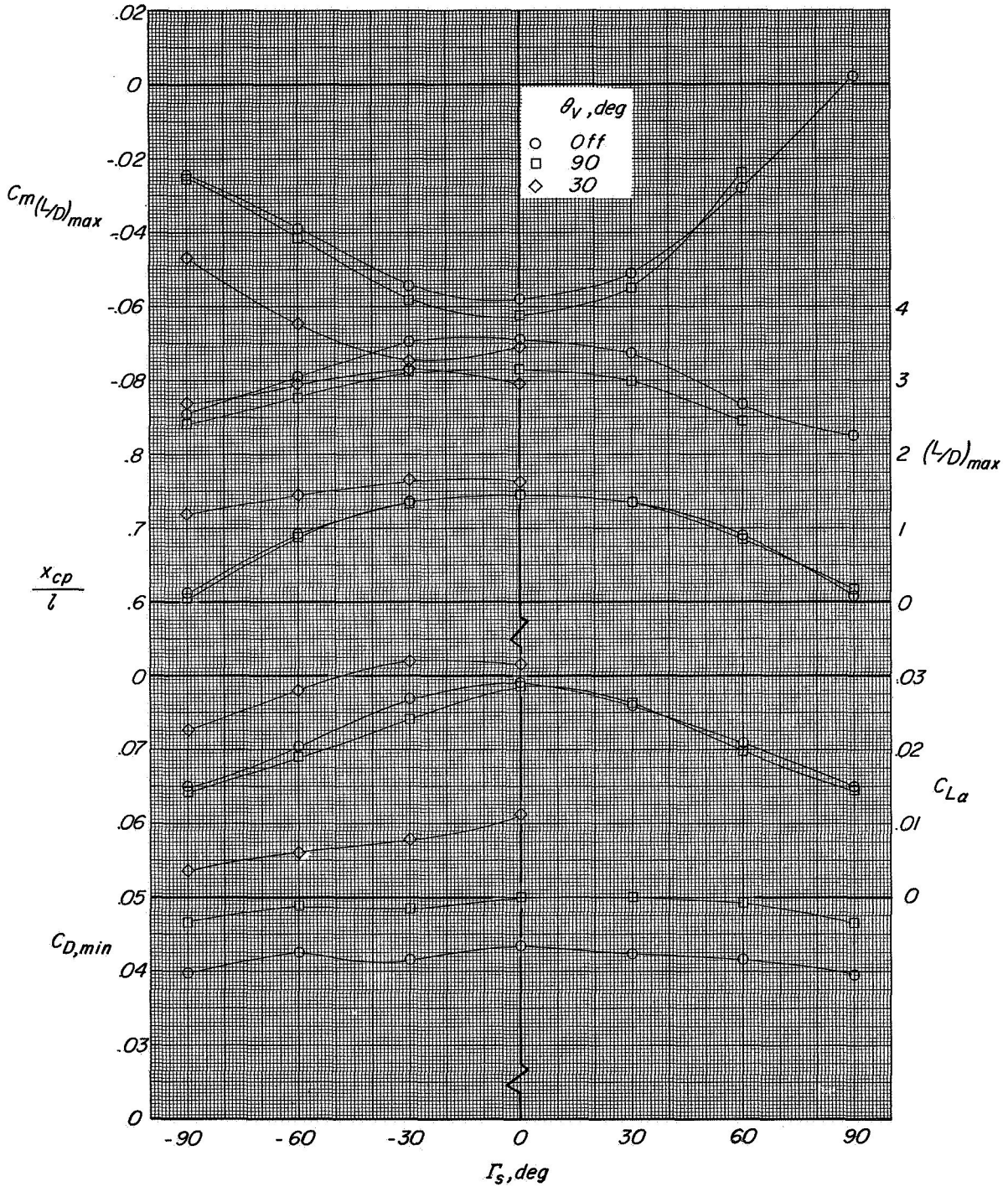

(a) M = 0.89.

Figure 9.- Summary of pertinent longitudinal characteristics of configurations tested.

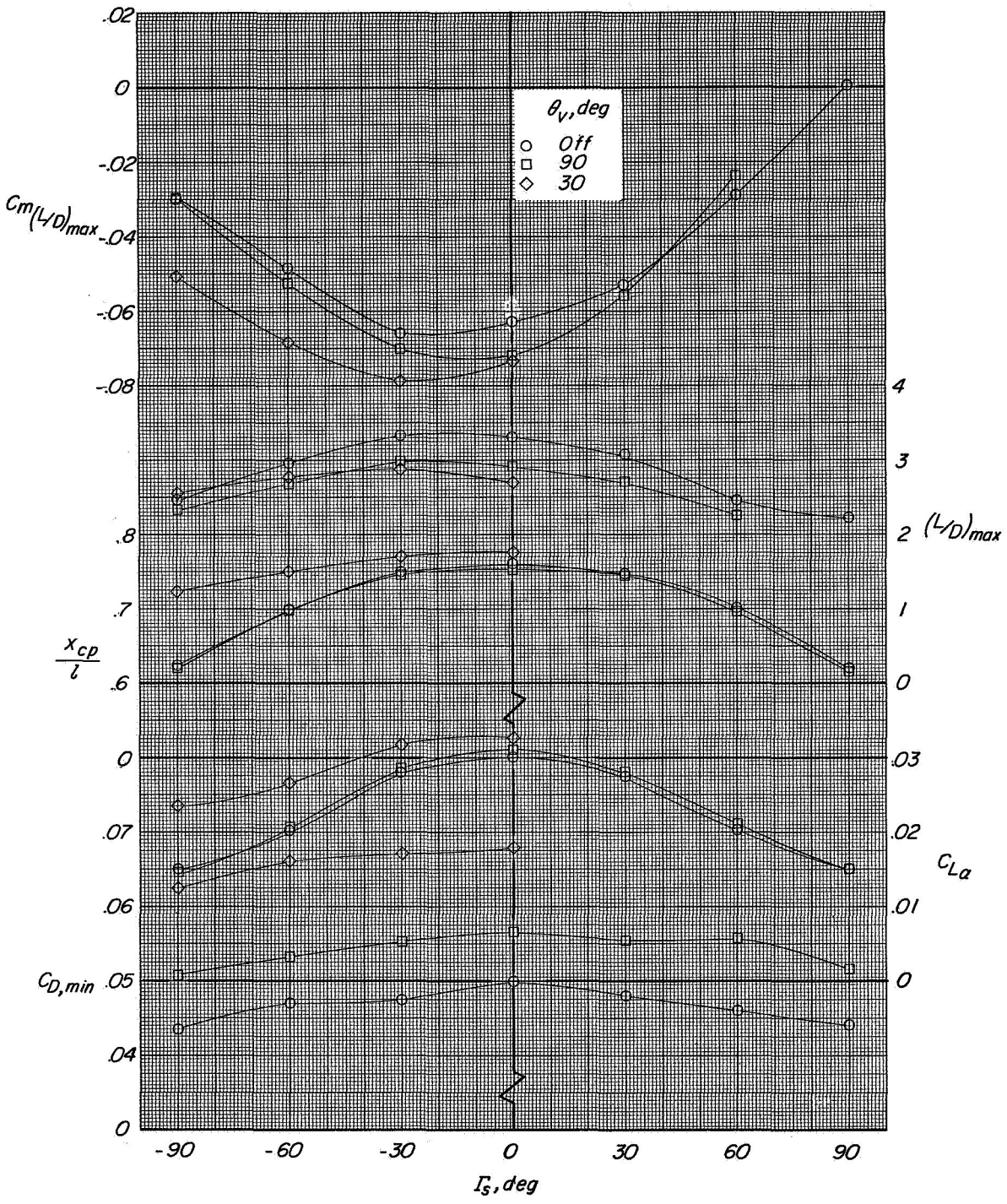

(b) M = 0.95.

Figure 9.- Continued.

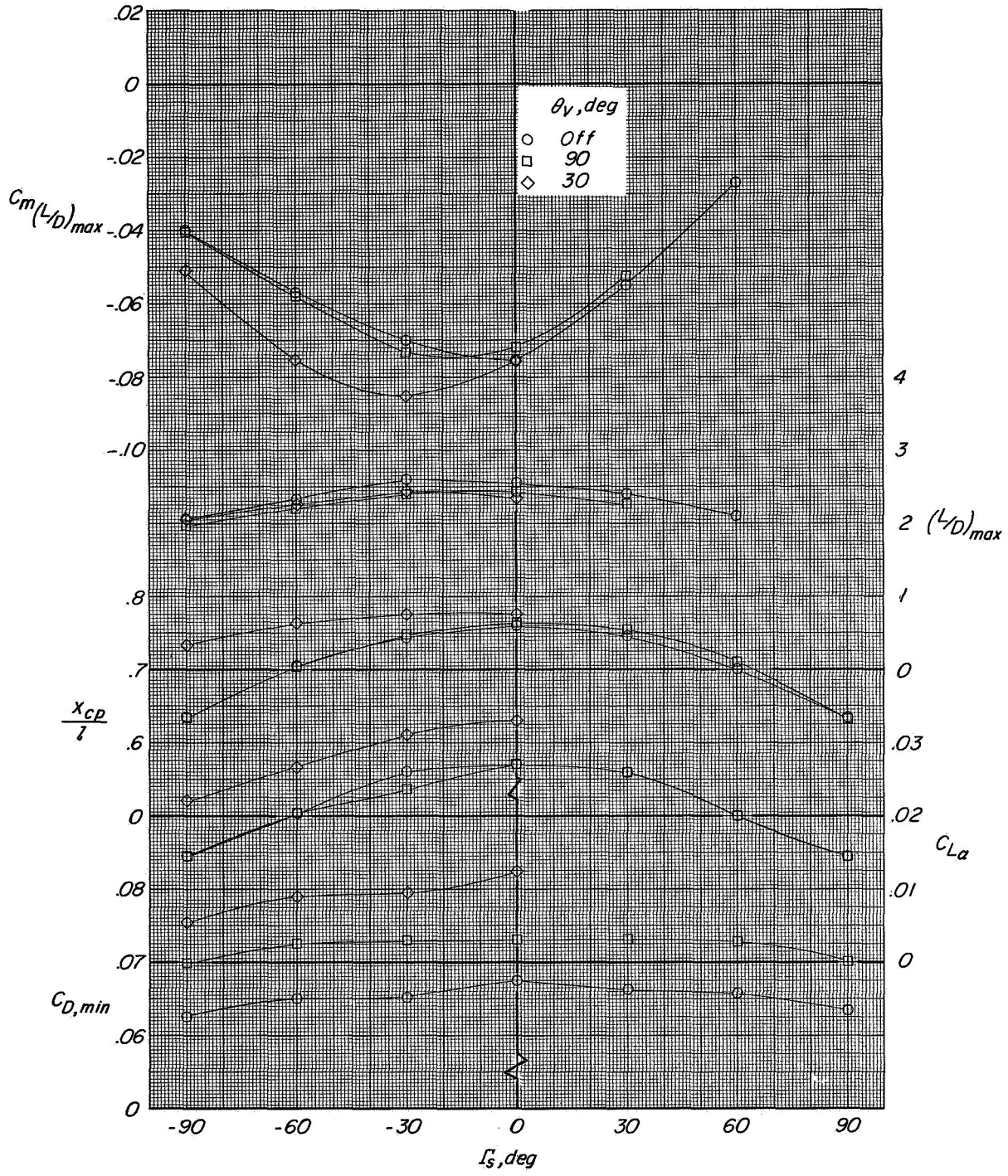

(c) M = 1.17.

Figure 9.- Concluded.

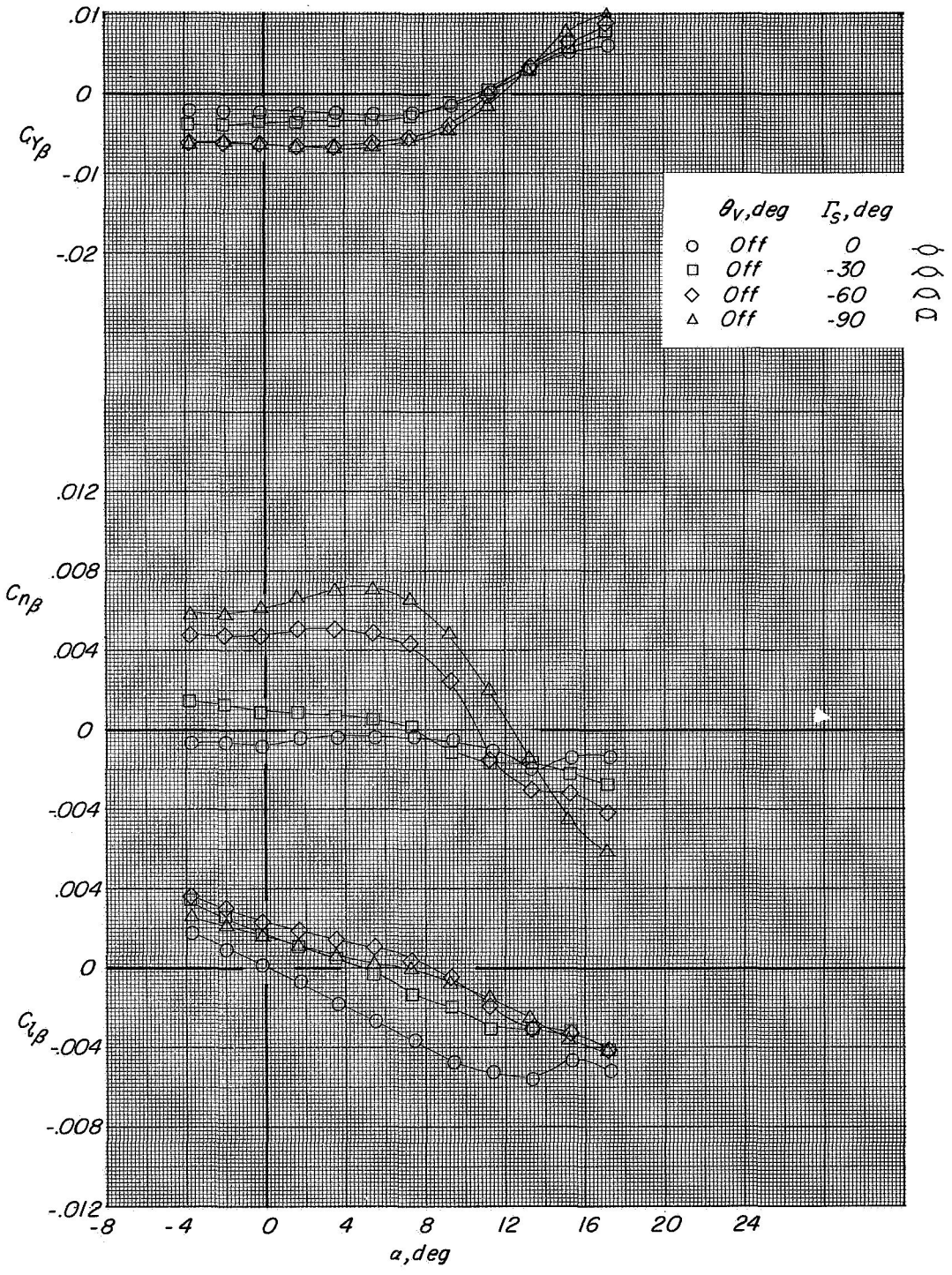

(a) M = 0.89.

Figure 10.- Effect of stabilizers at negative dihedral angles on lateral-directional characteristics with vertical tails off.

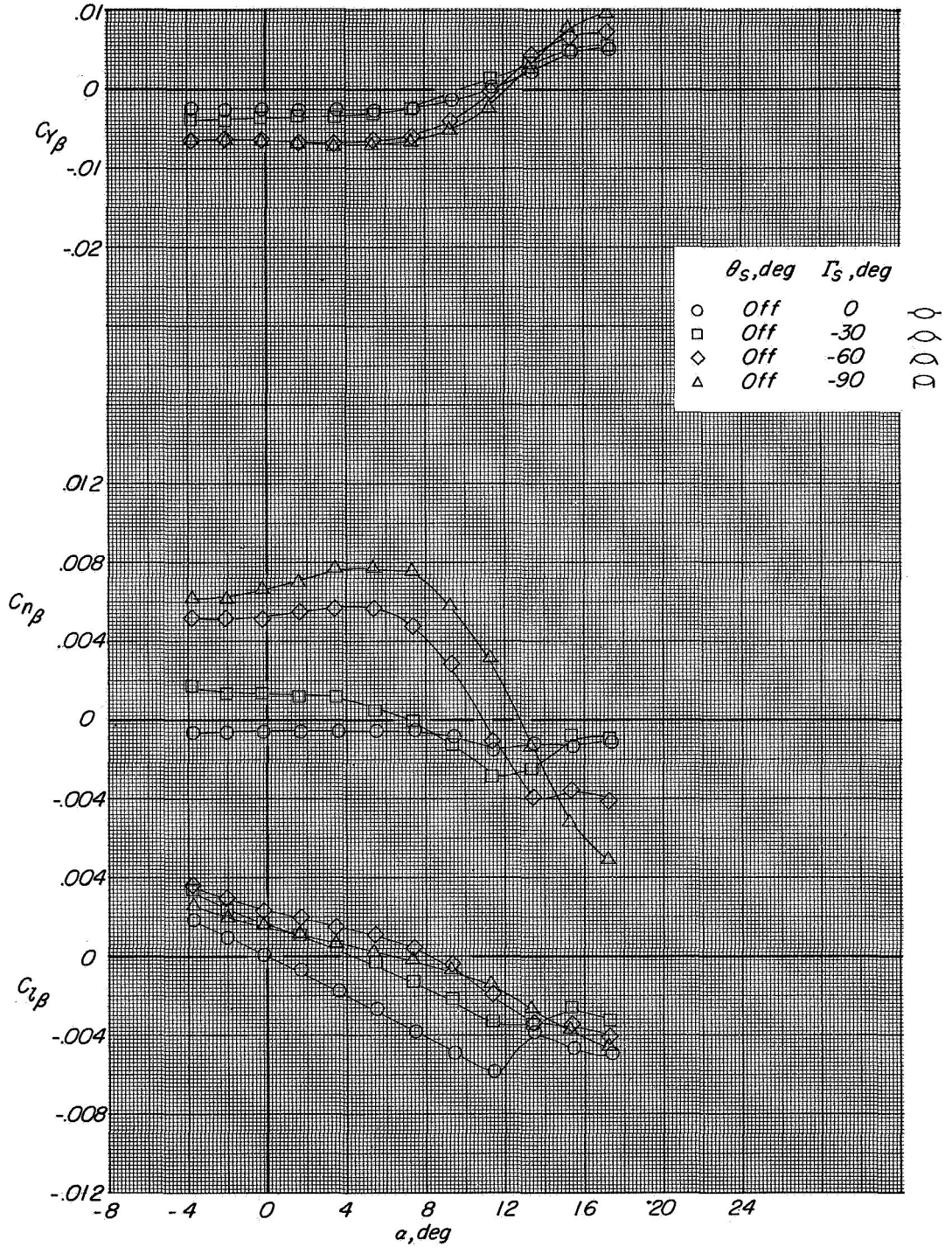

(b) M = 0.95.

Figure 10.- Continued.

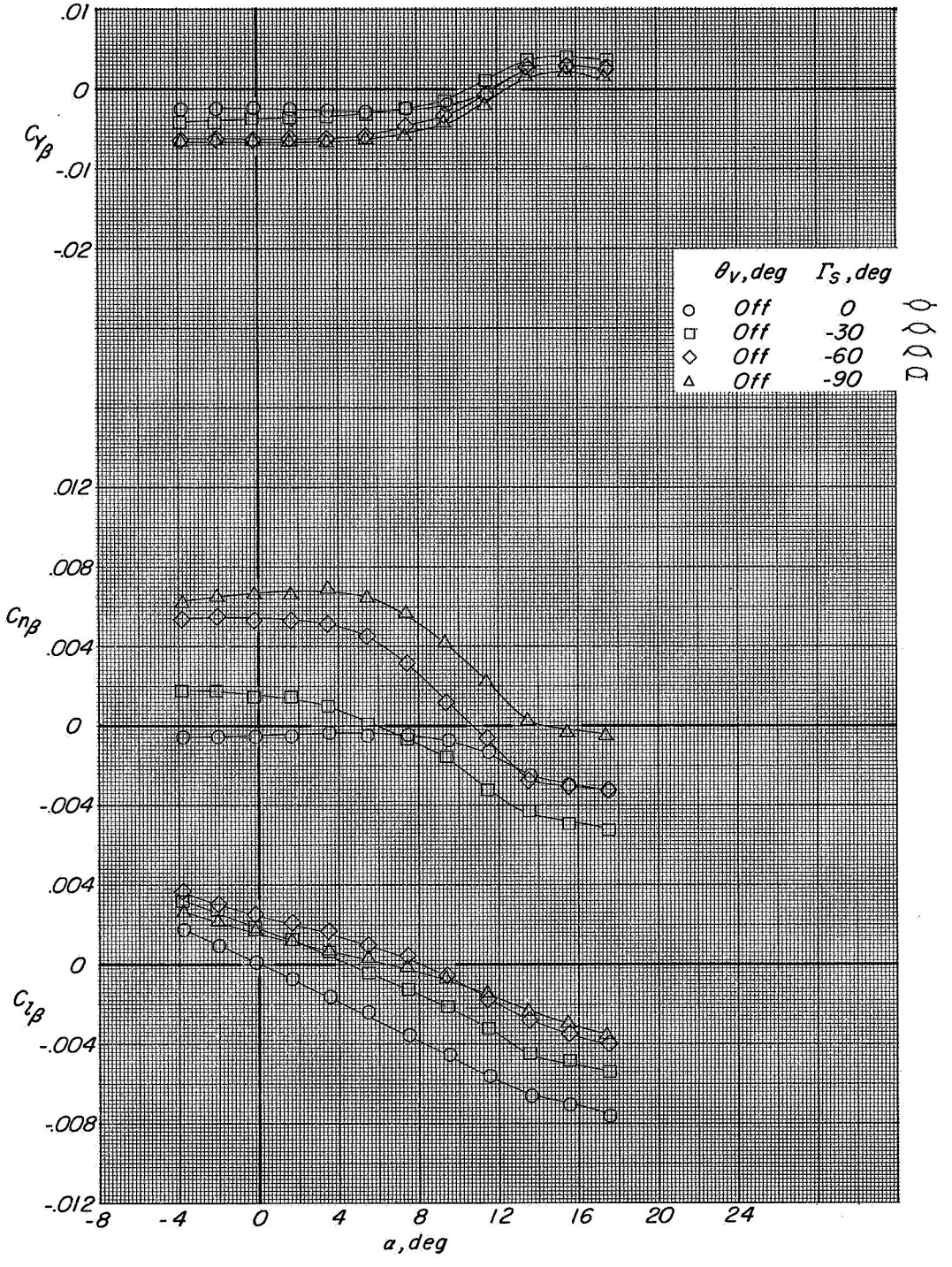

(c) M = 1.17.

Figure 10.- Concluded.

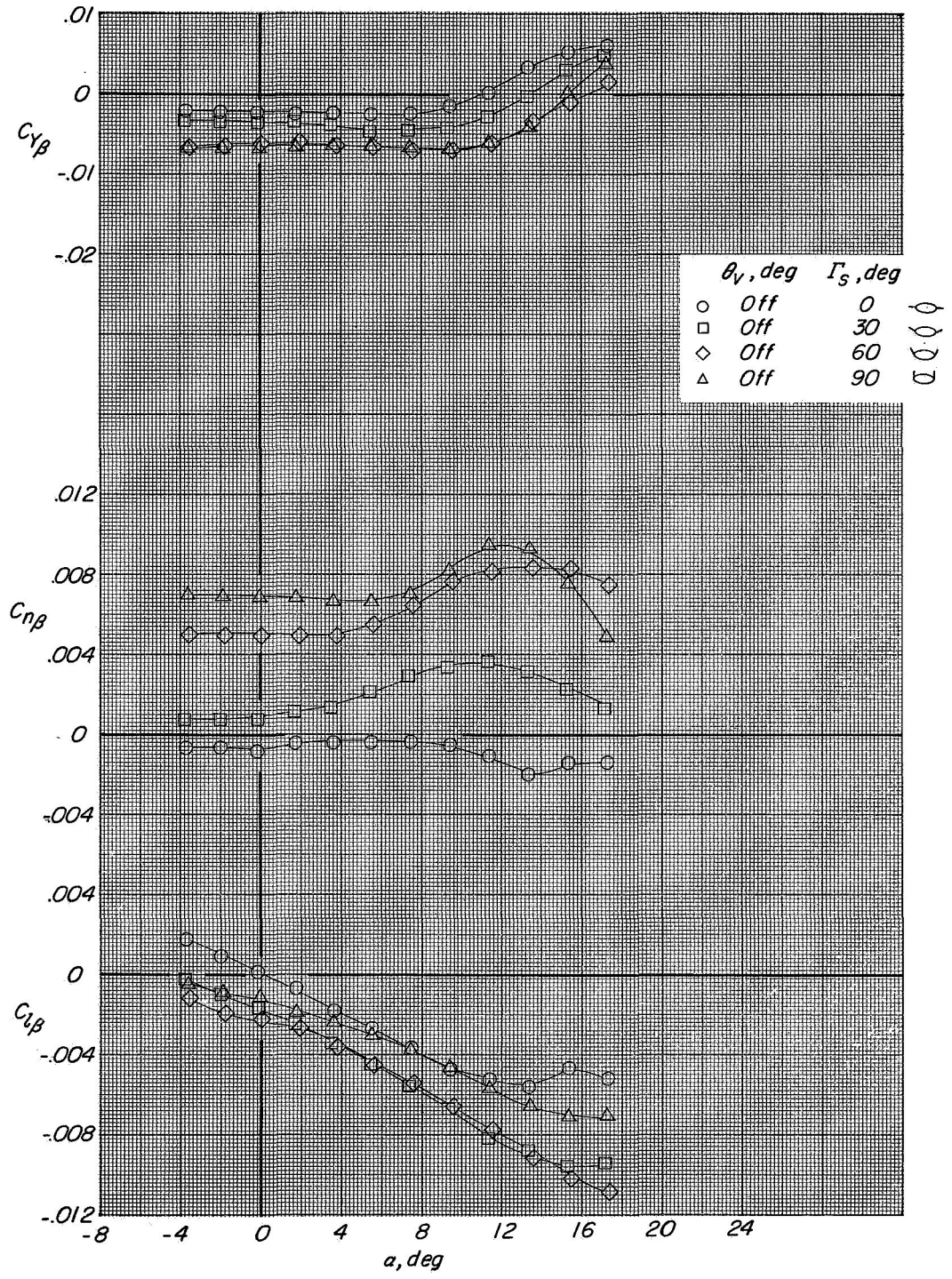

(a) M = 0.89.

Figure 11.- Effect of stabilizers at positive dihedral angles on lateral-directional characteristics with vertical tails off.

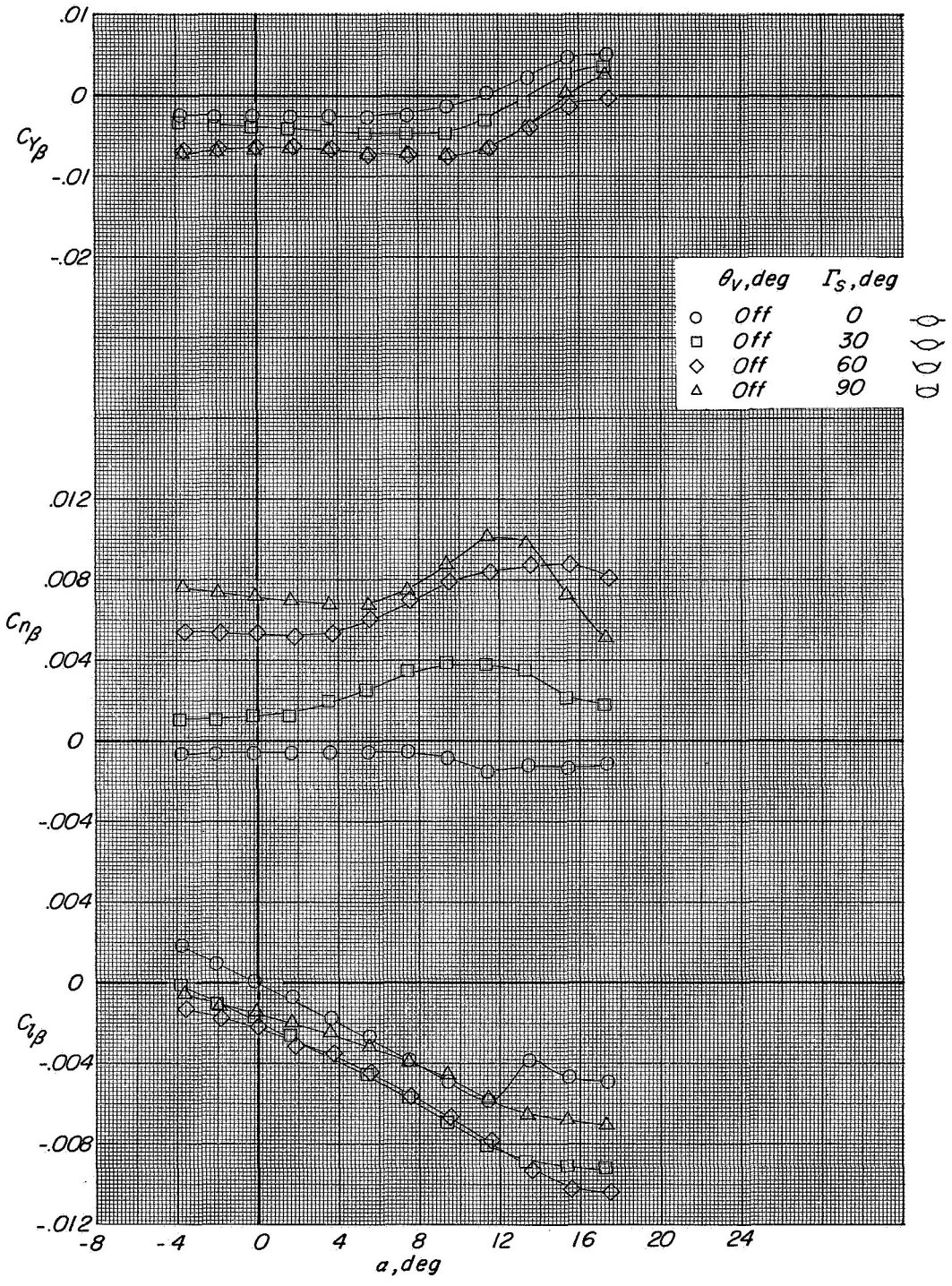

(b) M = 0.95.

Figure 11.- Continued.

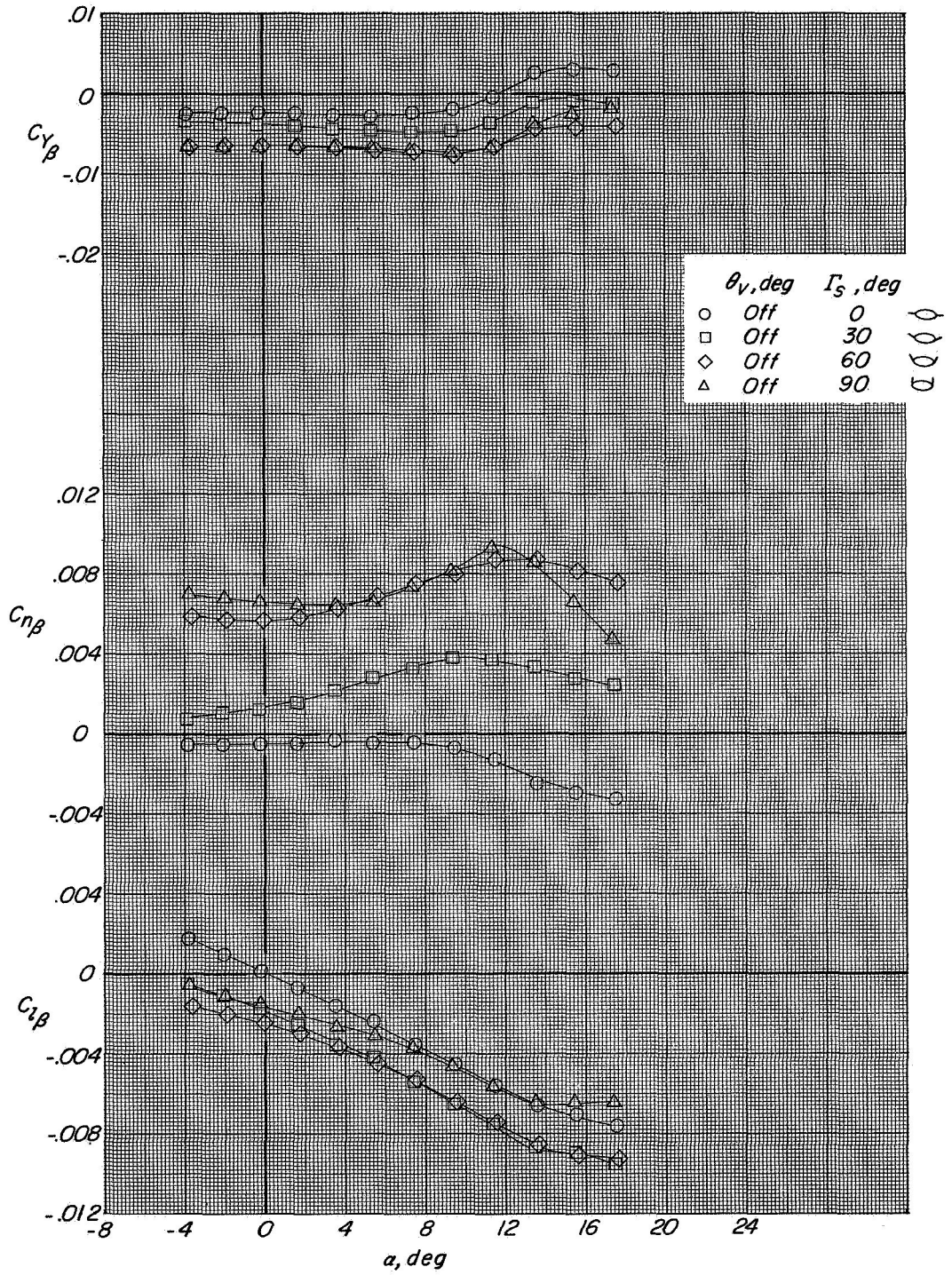

(c) M = 1.17.

Figure 11.- Concluded.

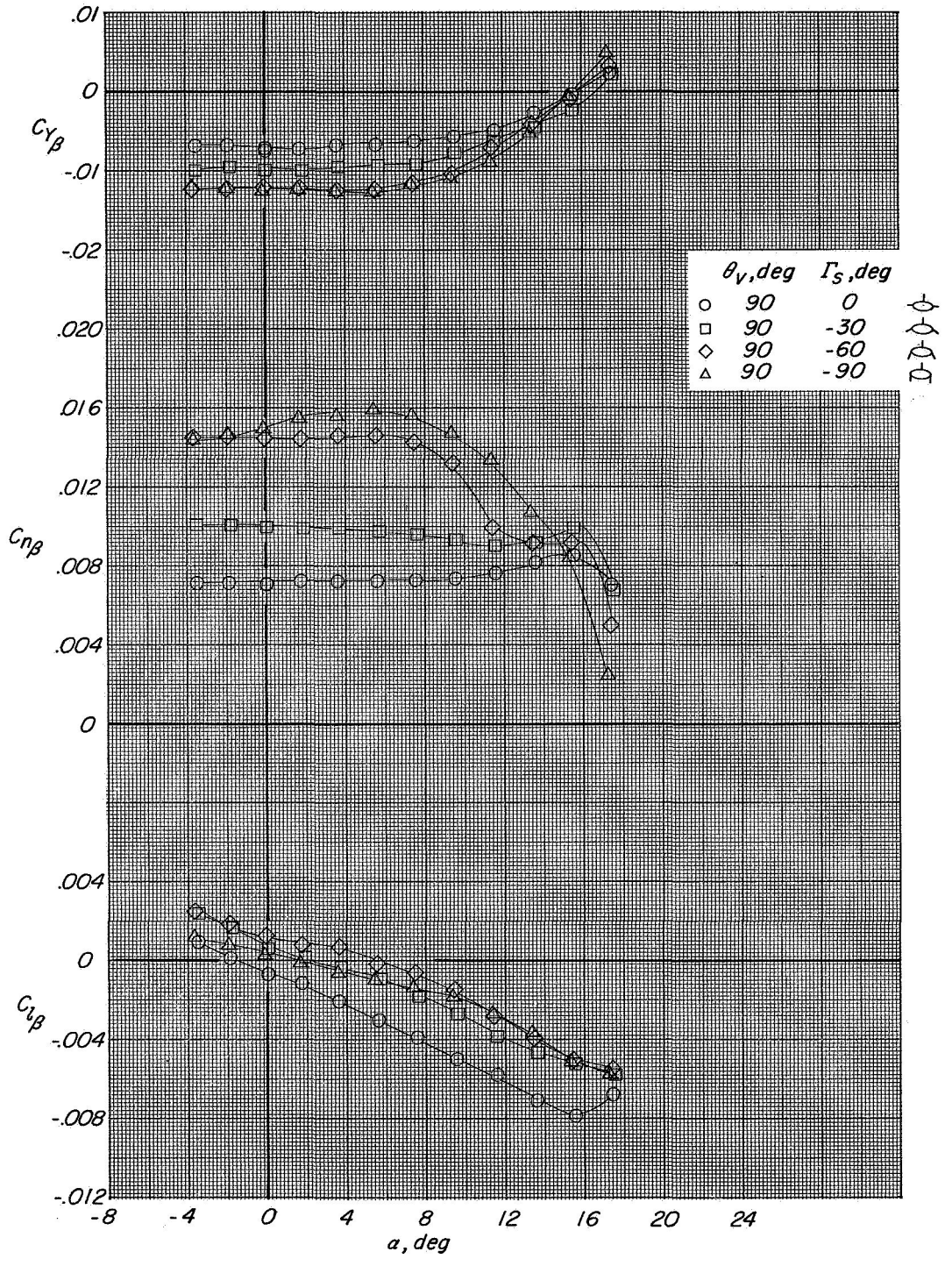

(a) M = 0.89.

Figure 12.- Effect of stabilizers at negative dihedral angles on lateral-directional characteristics with vertical tails at $\theta_V = 90^0$.

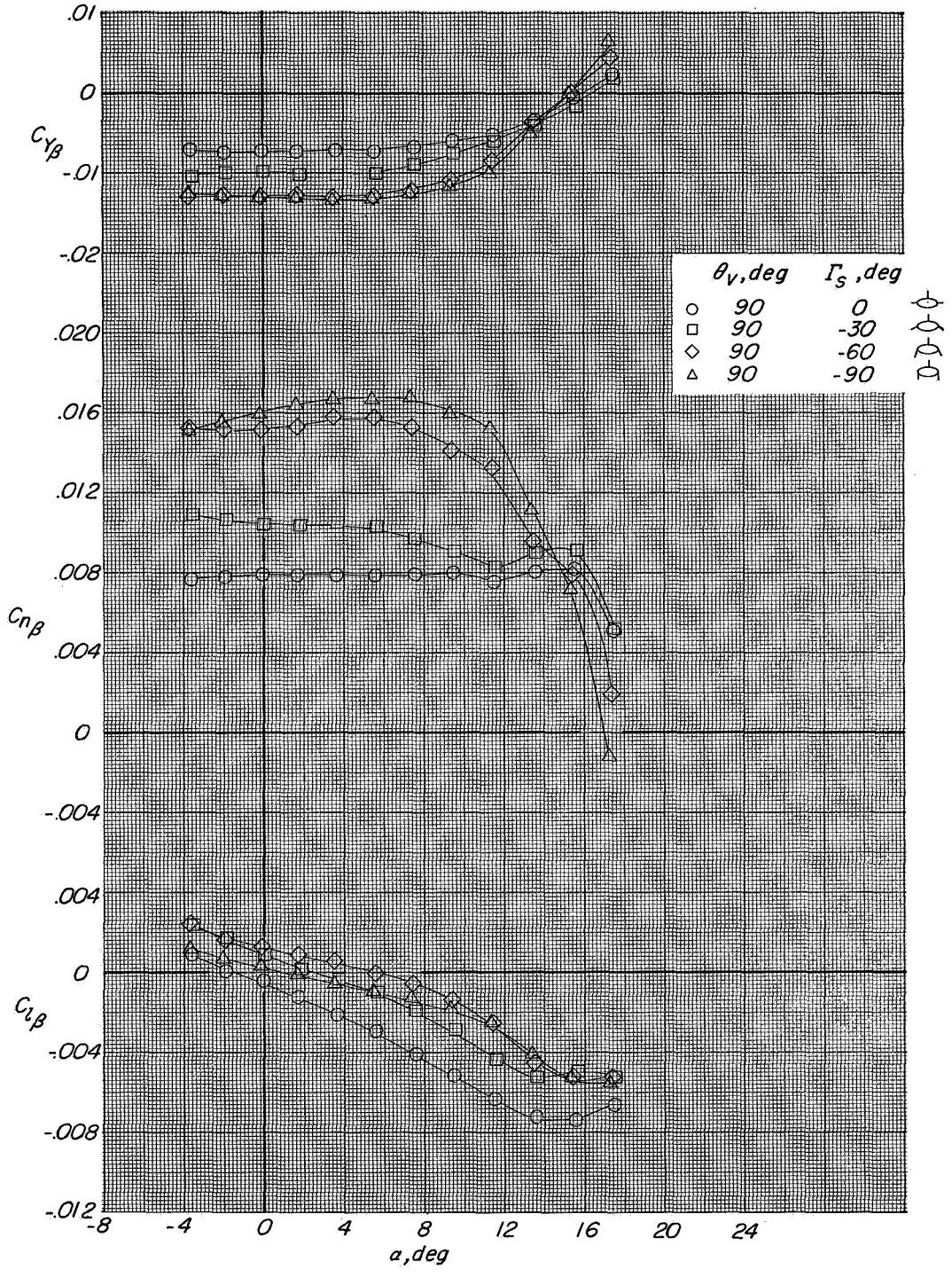

(b) M = 0.95.

Figure 12.- Continued.

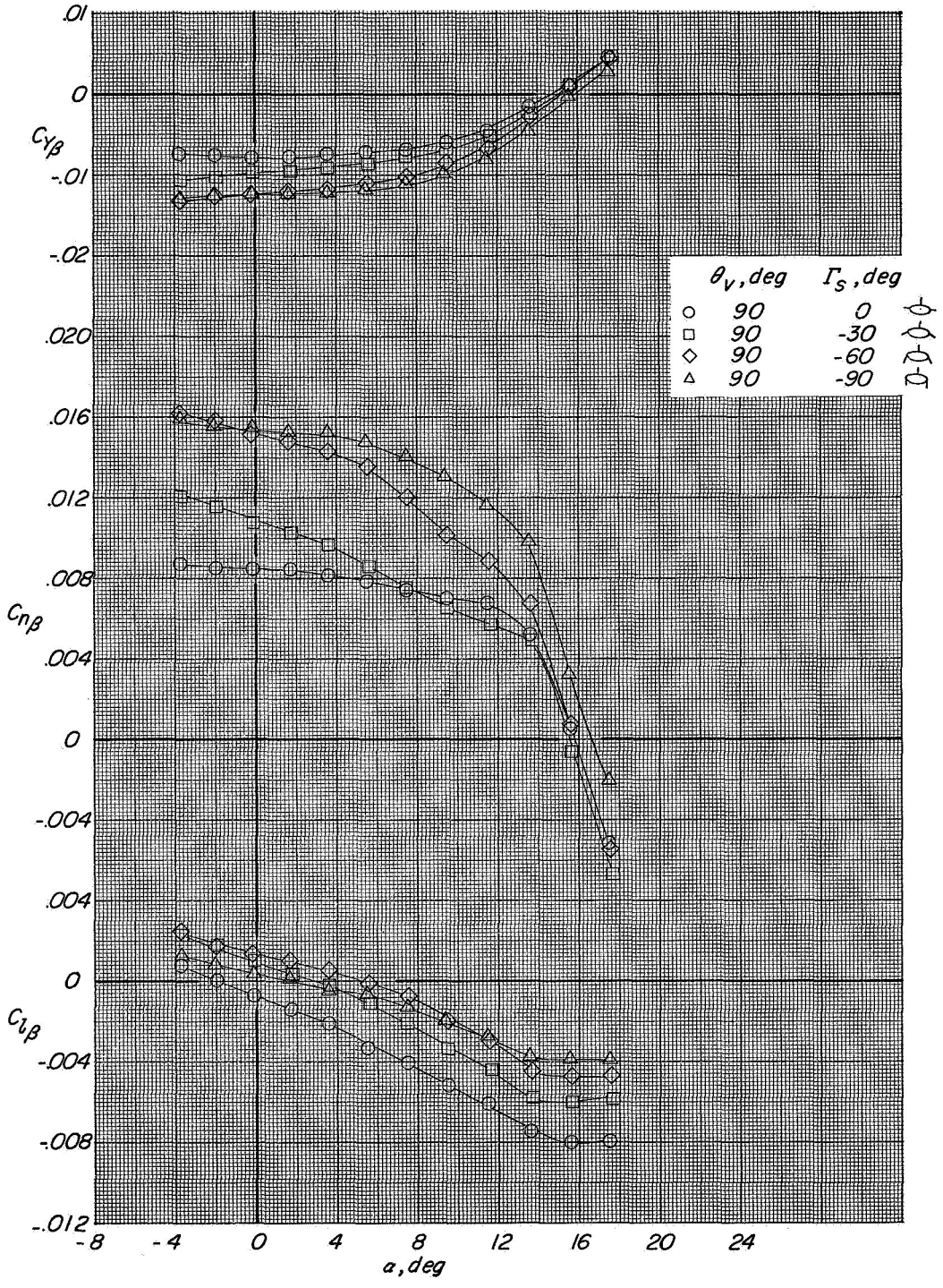

(c) M = 1.17.

Figure 12.- Concluded.

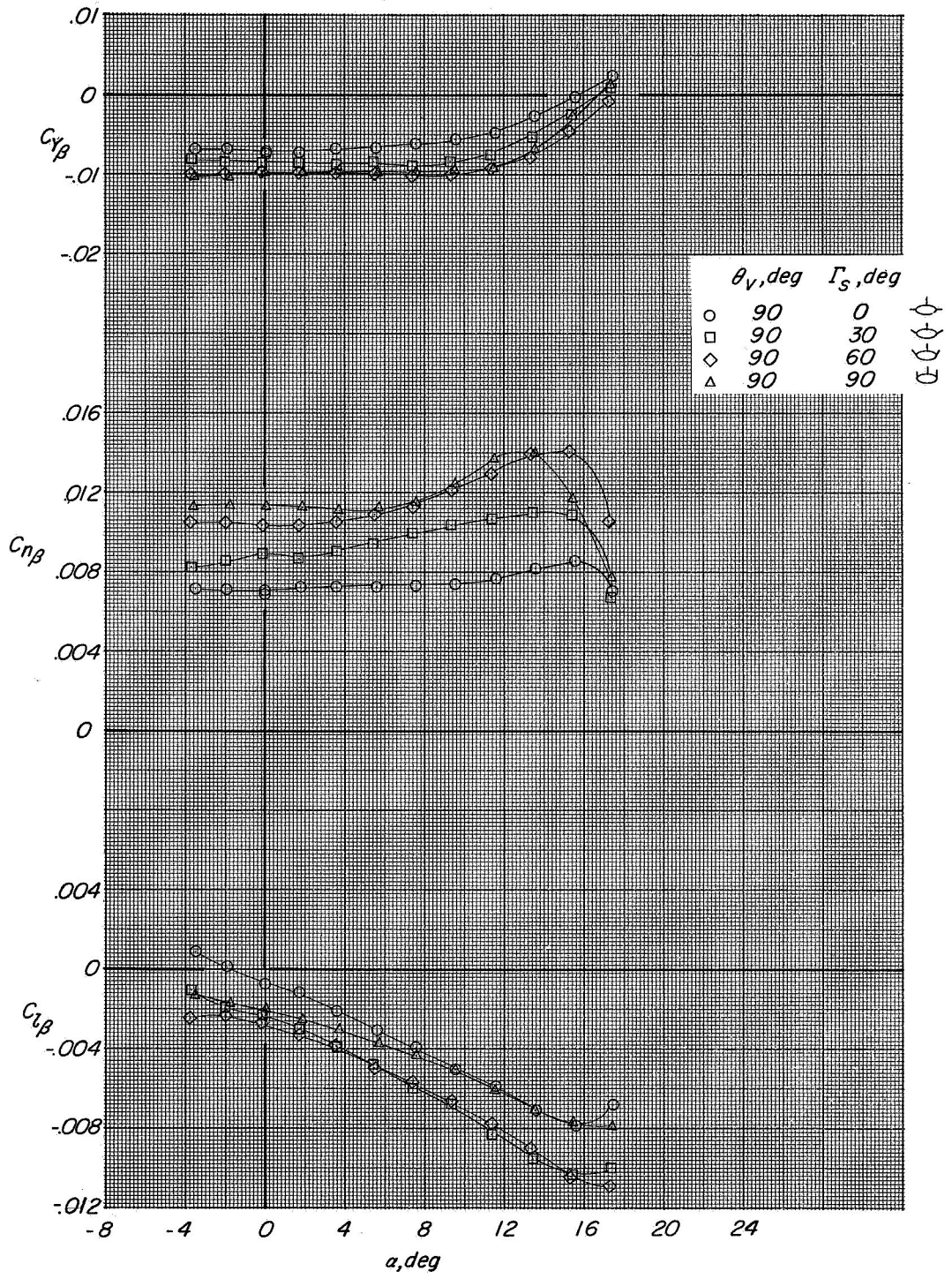

(a) M = 0.89.

Figure 13.- Effect of stabilizers at positive dihedral angles on lateral-directional characteristics with vertical tails at $\theta_V = 90^0$.

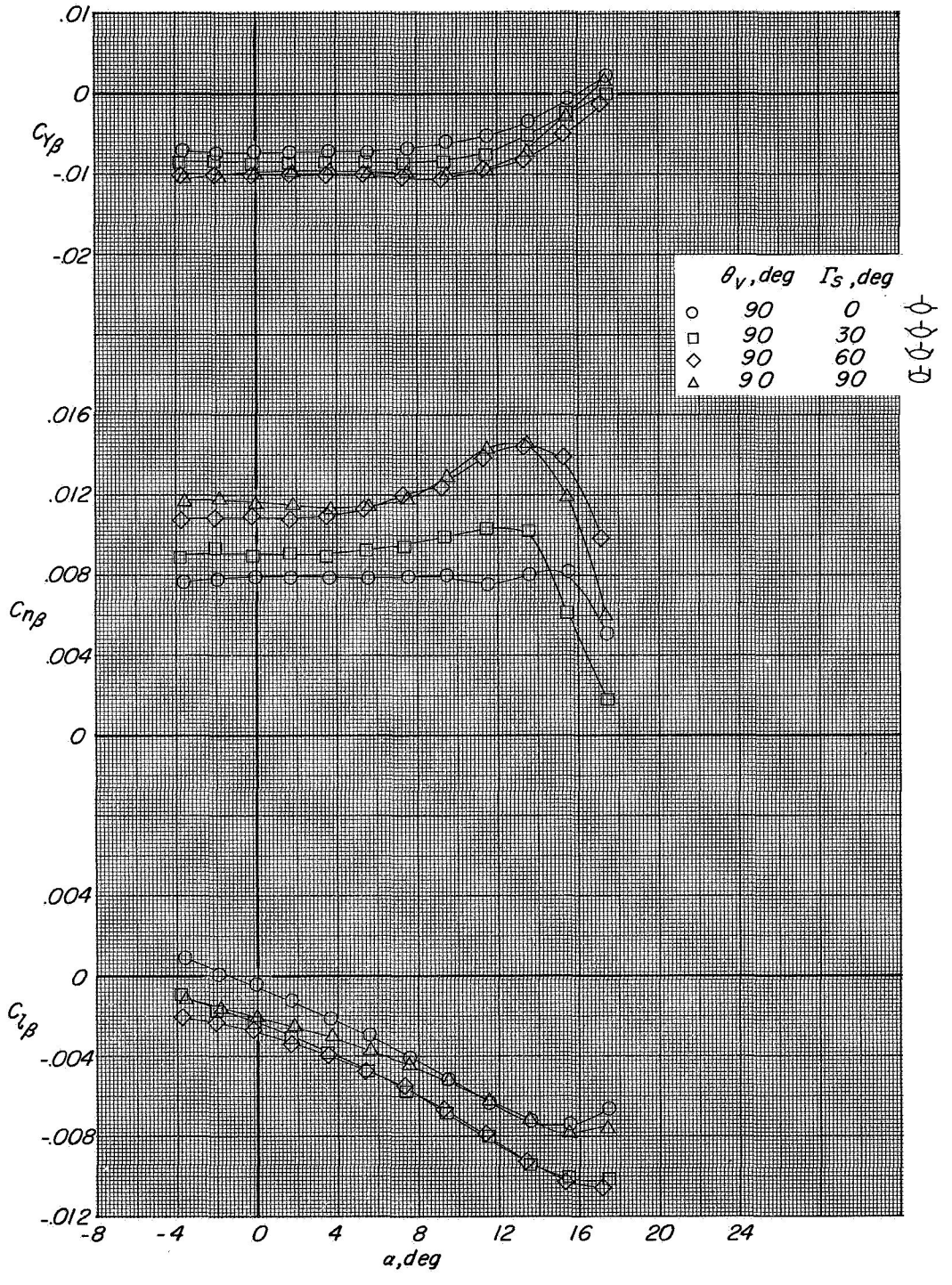

(b) M = 0.95.

Figure 13.- Continued.

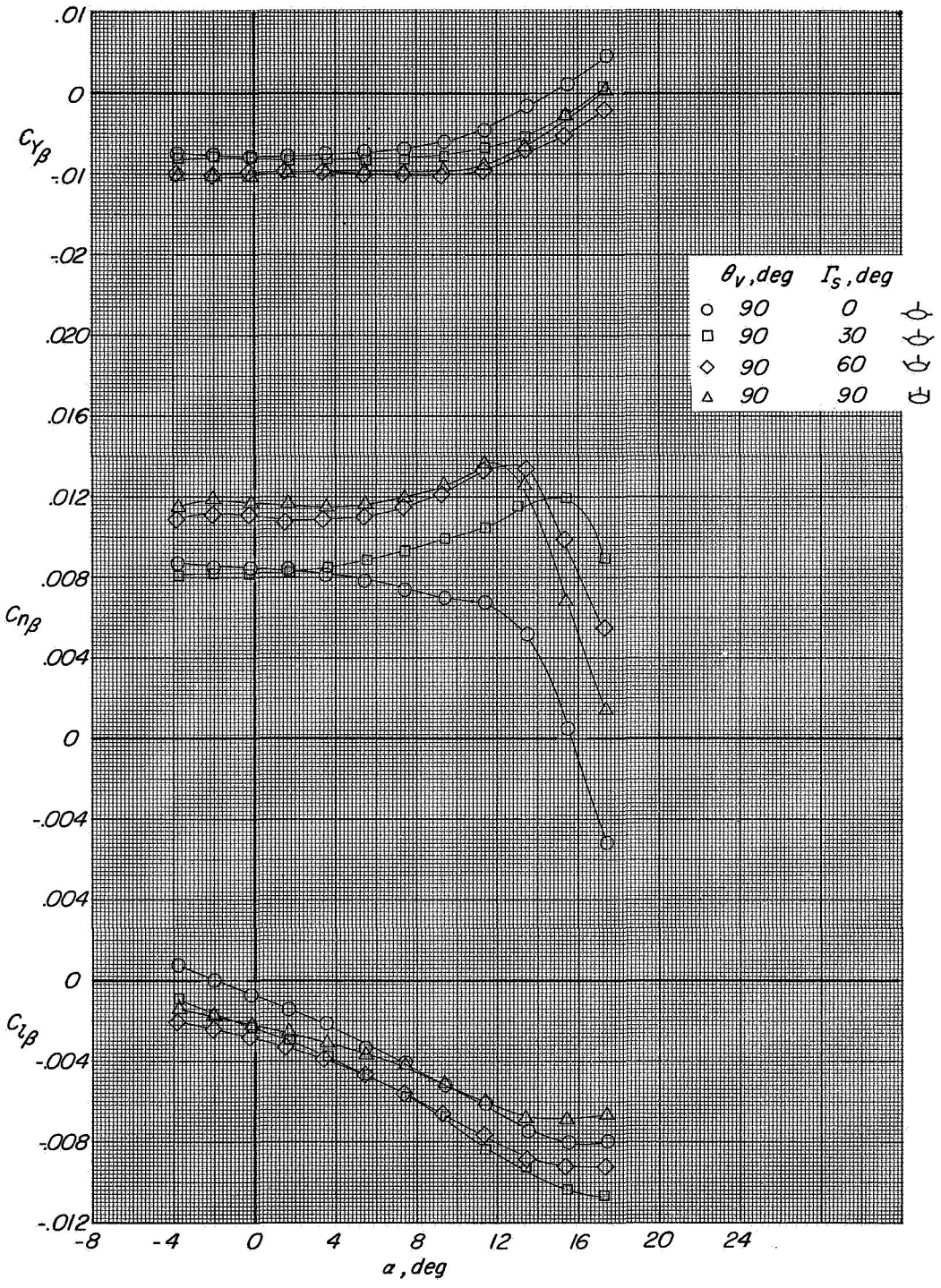

(c) M = 1.17.

Figure 13.- Concluded.

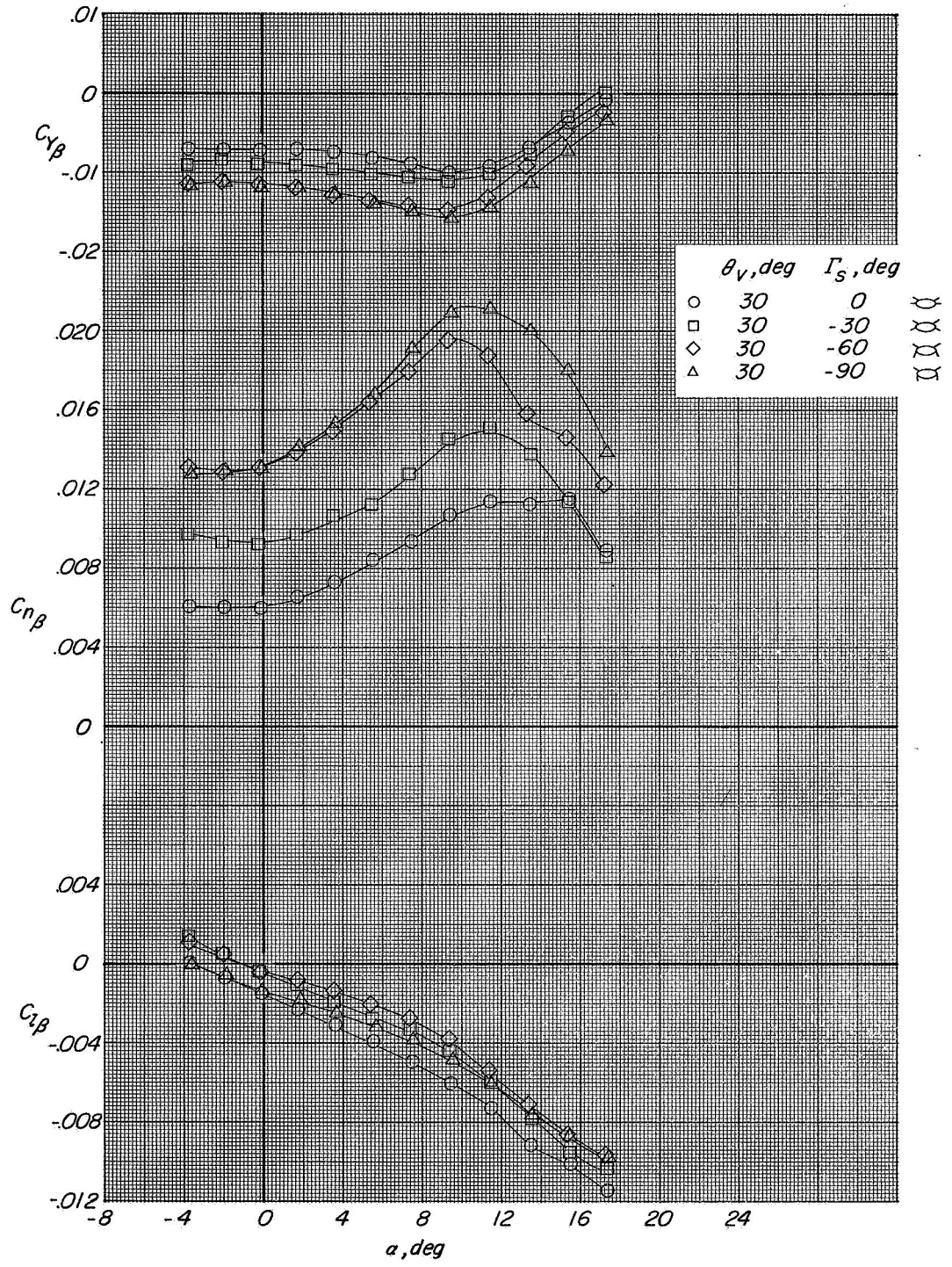

(a) M = 0.89.

Figure 14.- Effect of stabilizers at negative dihedral angles on lateral-directional characteristics with vertical tails at $\theta_V = 30^0$.

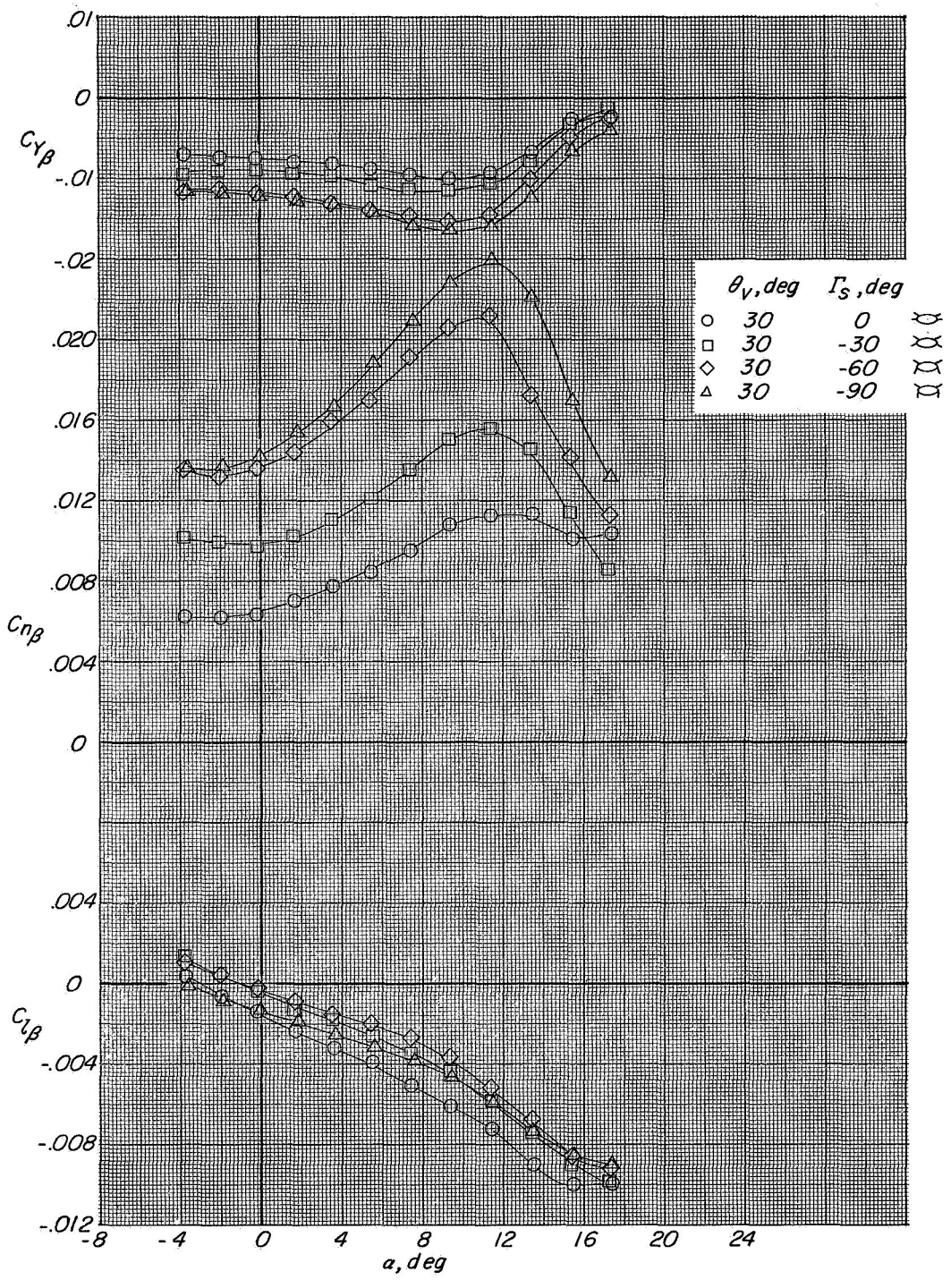

(b) M = 0.95.

Figure 14.- Continued.

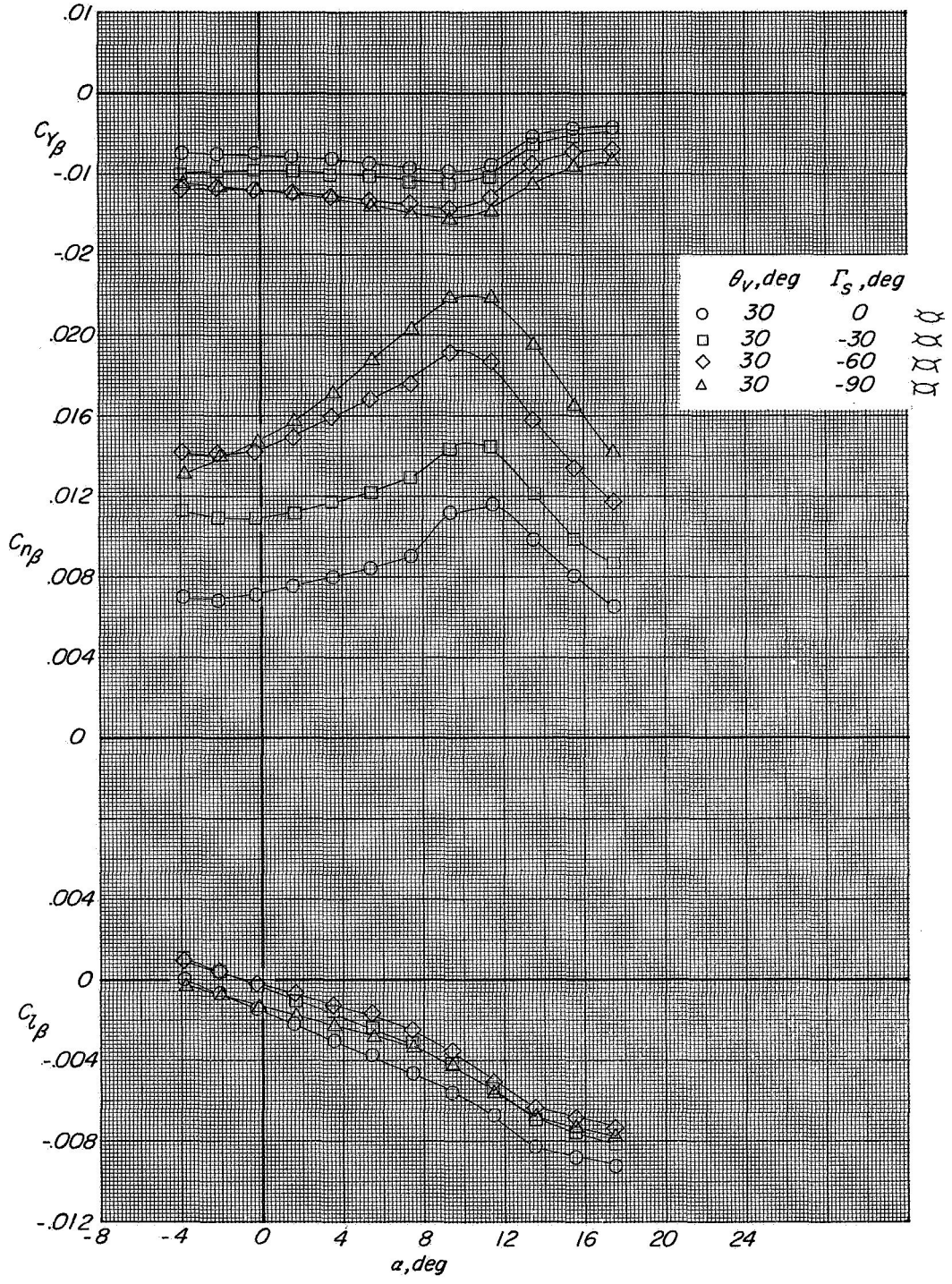

(c) M = 1.17.

Figure 14.- Concluded.

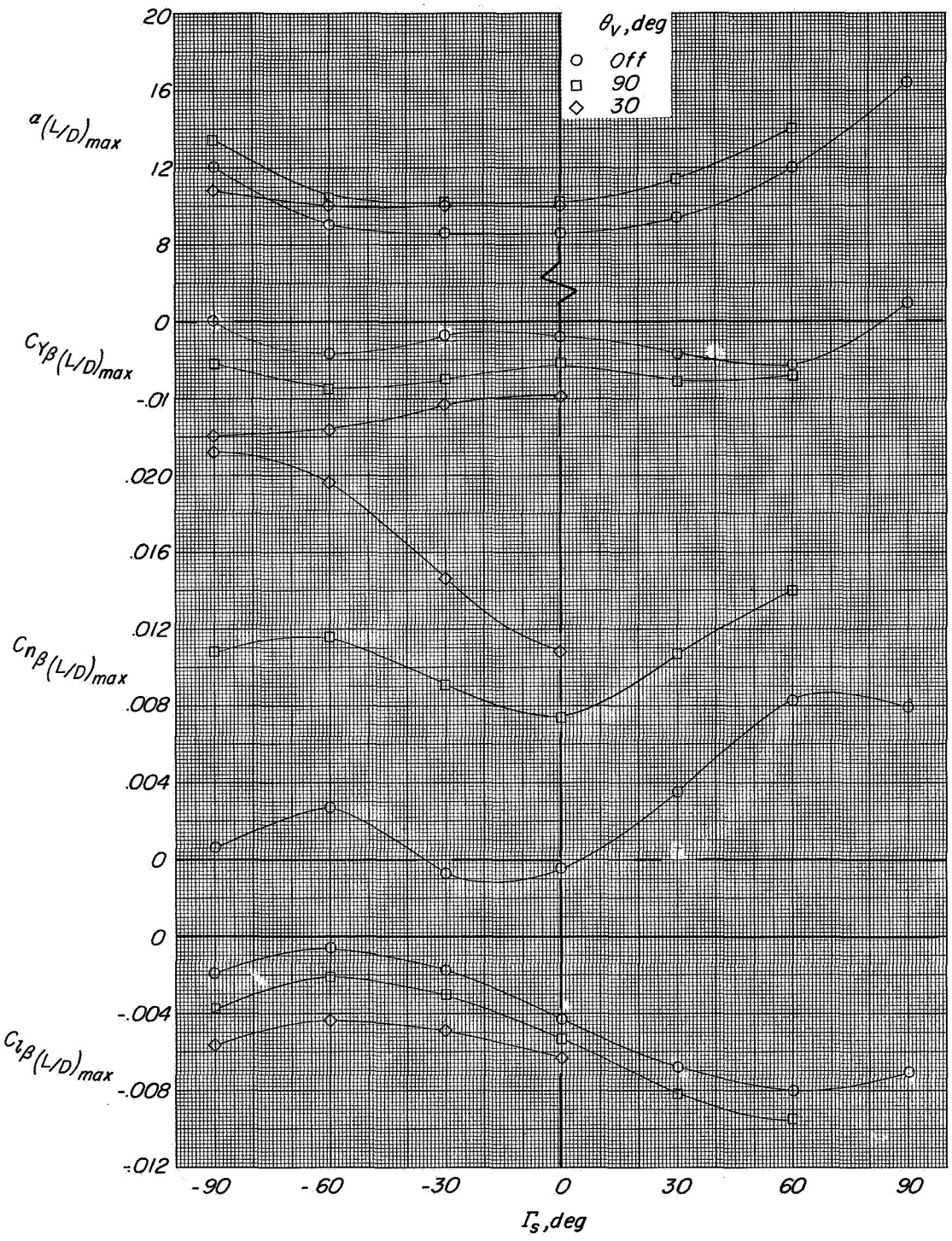

(a) M = 0.89.

Figure 15.- Summary of lateral and directional stability characteristics at $(L/D)_{max}$.

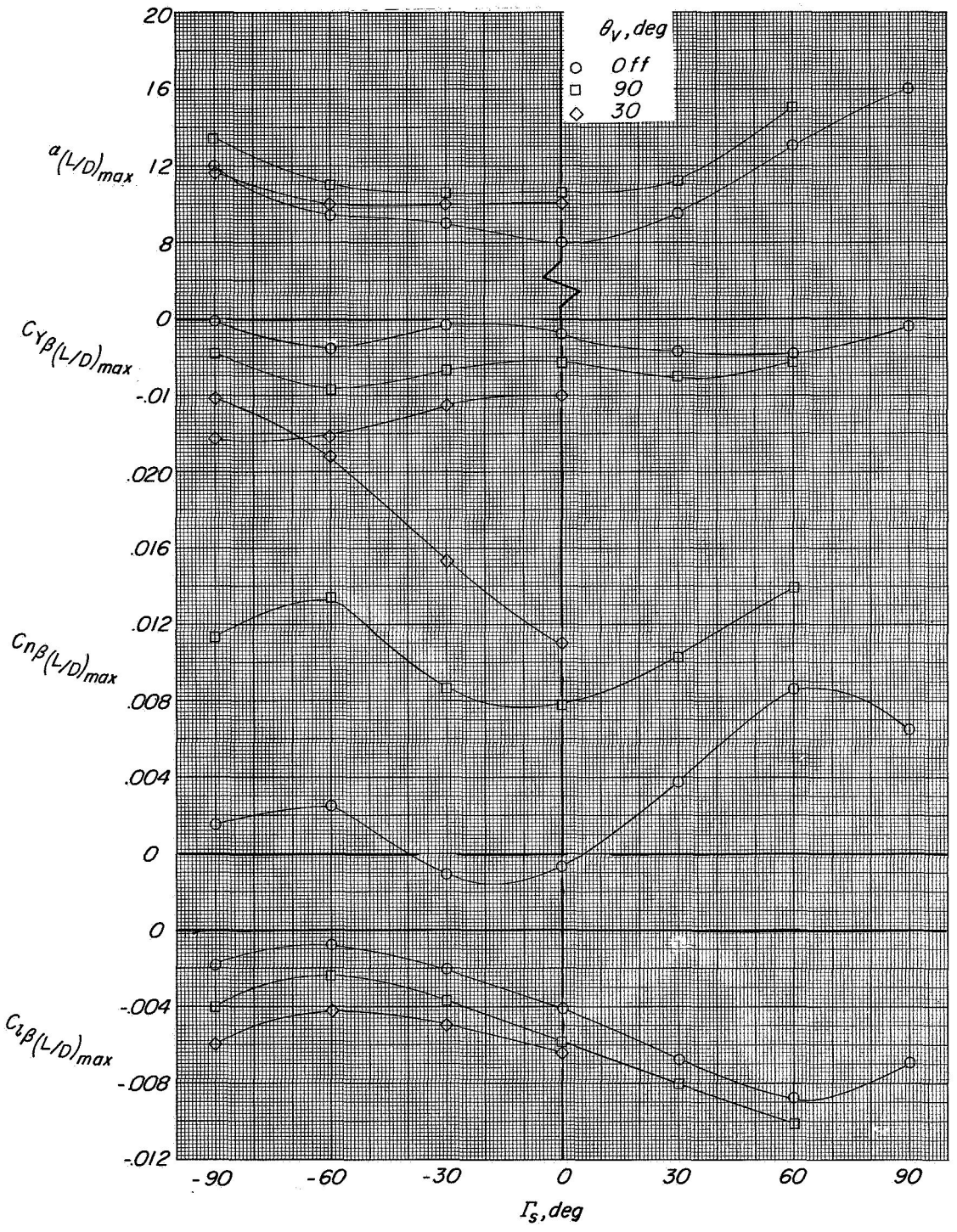

(b) M = 0.95.

Figure 15.- Continued.

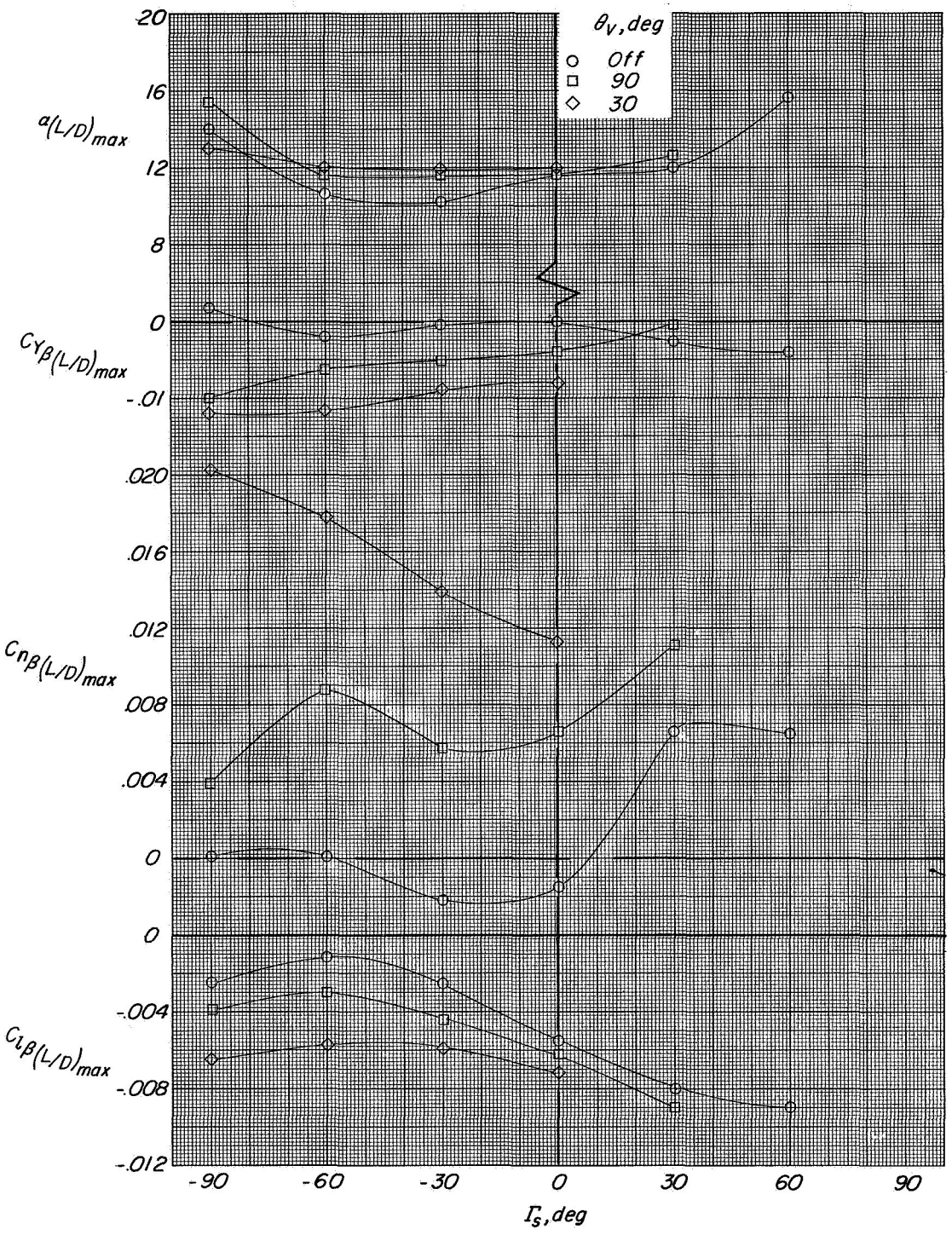

(c) M = 1.17.

Figure 15.- Concluded.

NASA-Langley, 1969 —— 1 L-6085

"The aeronautical and space activities of the United States shall be conducted so as to contribute . . . to the expansion of human knowledge of phenomena in the atmosphere and space. The Administration shall provide for the widest practicable and appropriate dissemination of information concerning its activities and the results thereof."

— NATIONAL AERONAUTICS AND SPACE ACT OF 1958

NASA SCIENTIFIC AND TECHNICAL PUBLICATIONS

TECHNICAL REPORTS: Scientific and technical information considered important, complete, and a lasting contribution to existing knowledge.

TECHNICAL NOTES: Information less broad in scope but nevertheless of importance as a contribution to existing knowledge.

TECHNICAL MEMORANDUMS: Information receiving limited distribution because of preliminary data, security classification, or other reasons.

CONTRACTOR REPORTS: Scientific and technical information generated under a NASA contract or grant and considered an important contribution to existing knowledge.

TECHNICAL TRANSLATIONS: Information published in a foreign language considered to merit NASA distribution in English.

SPECIAL PUBLICATIONS: Information derived from or of value to NASA activities. Publications include conference proceedings, monographs, data compilations, handbooks, sourcebooks, and special bibliographies.

TECHNOLOGY UTILIZATION PUBLICATIONS: Information on technology used by NASA that may be of particular interest in commercial and other non-aerospace applications. Publications include Tech Briefs, Technology Utilization Reports and Notes, and Technology Surveys.

Details on the availability of these publications may be obtained from:

SCIENTIFIC AND TECHNICAL INFORMATION DIVISION
NATIONAL AERONAUTICS AND SPACE ADMINISTRATION
Washington, D.C. 20546